Article

Aspartate signalling drives lung metastasis via alternative translation

https://doi.org/10.1038/s41586-024-08335-7

Received: 30 June 2023

Accepted: 1 November 2024

Published online: 01 January 2025

Check for updates

Ginevra Doglioni[1,2], Juan Fernández-García[1,2,22], Sebastian Igelmann[1,2,22], Patricia Altea-Manzano[1,2,20,22], Arnaud Blomme[3], Rita La Rovere[4], Xiao-Zheng Liu[1,2], Yawen Liu[1,2,5], Tine Tricot[1,2], Max Nobis[6,7,8], Ning An[3], Marine Leclercq[3], Sarah El Kharraz[1,2], Panagiotis Karras[9,10], Yu-Heng Hsieh[11], Fiorella A. Solari[11], Luiza Martins Nascentes Melo[12], Gabrielle Allies[12], Annalisa Scopelliti[1,2], Matteo Rossi[1,2], Ines Vermeire[1,2], Dorien Broekaert[1,2], Ana Margarida Ferreira Campos[1,2], Patrick Neven[13], Marion Maetens[14], Karen Van Baelen[13,14], H. Furkan Alkan[1,2,21], Mélanie Planque[1,2,15], Giuseppe Floris[16,17], Albert Sickmann[11,18], Alpaslan Tasdogan[12], Jean-Christophe Marine[9,10], Colinda L. G. J. Scheele[6,7], Christine Desmedt[14], Geert Bultynck[4], Pierre Close[3,19] & Sarah-Maria Fendt[1,2] ✉

Lung metastases occur in up to 54% of patients with metastatic tumours[1,2]. Contributing factors to this high frequency include the physical properties of the pulmonary system and a less oxidative environment that may favour the survival of cancer cells[3]. Moreover, secreted factors from primary tumours alter immune cells and the extracellular matrix of the lung, creating a permissive pre-metastatic environment primed for the arriving cancer cells[4,5]. Nutrients are also primed during pre-metastatic niche formation[6]. Yet, whether and how nutrients available in organs in which tumours metastasize confer cancer cells with aggressive traits is mostly undefined. Here we found that pulmonary aspartate triggers a cellular signalling cascade in disseminated cancer cells, resulting in a translational programme that boosts aggressiveness of lung metastases. Specifically, we observe that patients and mice with breast cancer have high concentrations of aspartate in their lung interstitial fluid. This extracellular aspartate activates the ionotropic *N*-methyl-D-aspartate receptor in cancer cells, which promotes CREB-dependent expression of deoxyhypusine hydroxylase (*DOHH*). DOHH is essential for hypusination, a post-translational modification that is required for the activity of the non-classical translation initiation factor eIF5A. In turn, a translational programme with TGFβ signalling as a central hub promotes collagen synthesis in lung-disseminated breast cancer cells. We detected key proteins of this mechanism in lung metastases from patients with breast cancer. In summary, we found that aspartate, a classical biosynthesis metabolite, functions in the lung environment as an extracellular signalling molecule to promote aggressiveness of metastases.

The lung is a frequent organ of metastasis across different cancers including breast cancer and pre-metastatic niche formation increases the aggressiveness of lung metastases. To investigate what promotes this aggressiveness, we performed single-cell RNA-sequencing (scRNA-seq) of metastases growing in healthy lungs and in lungs primed with tumour-secreted factors (TSFs) from 4T1 breast tumours, with the latter resulting in a more aggressive metastatic disease (Extended Data Fig. 1a–d).

Alternative translation promotes aggressivness

Focusing on the cancer cell populations, we found that several gene sets indicative of increased translation were enriched in metastases from TSF-treated mice (Fig. 1a and Extended Data Fig. 1e). After excluding an involvement of classical regulators of translation (Extended Data Fig. 1f,g), we therefore investigated non-classical activators of translation. We found increased activity of the translation initiation/elongation factor eIF5A[7] based on its hypusination—an activating post-translational modification that is exclusive to eIF5A[8] (Extended Data Fig. 1h)—in aggressive 4T1 and EMT6.5 lung metastases from TSF-treated mice and in spontaneous 4T1 metastases compared with control (Fig. 1b–d). To investigate whether eIF5A activity drives metastasis aggressiveness, we reduced eIF5A hypusination by targeting the first enzymatic step of hypusination, catalysed by deoxyhypusine synthase (DHPS) (Extended Data Fig. 1h,i). Indeed, silencing *Dhps* in 4T1 and EMT6.5 breast cancer cells abrogated the metastasis aggressiveness induced by TSFs and impaired spontaneous metastasis growth (Fig. 1e–h). Thus, we concluded that the aggressiveness of lung metastases is mediated by eIF5A hypusination.

A list of affiliations appears at the end of the paper.

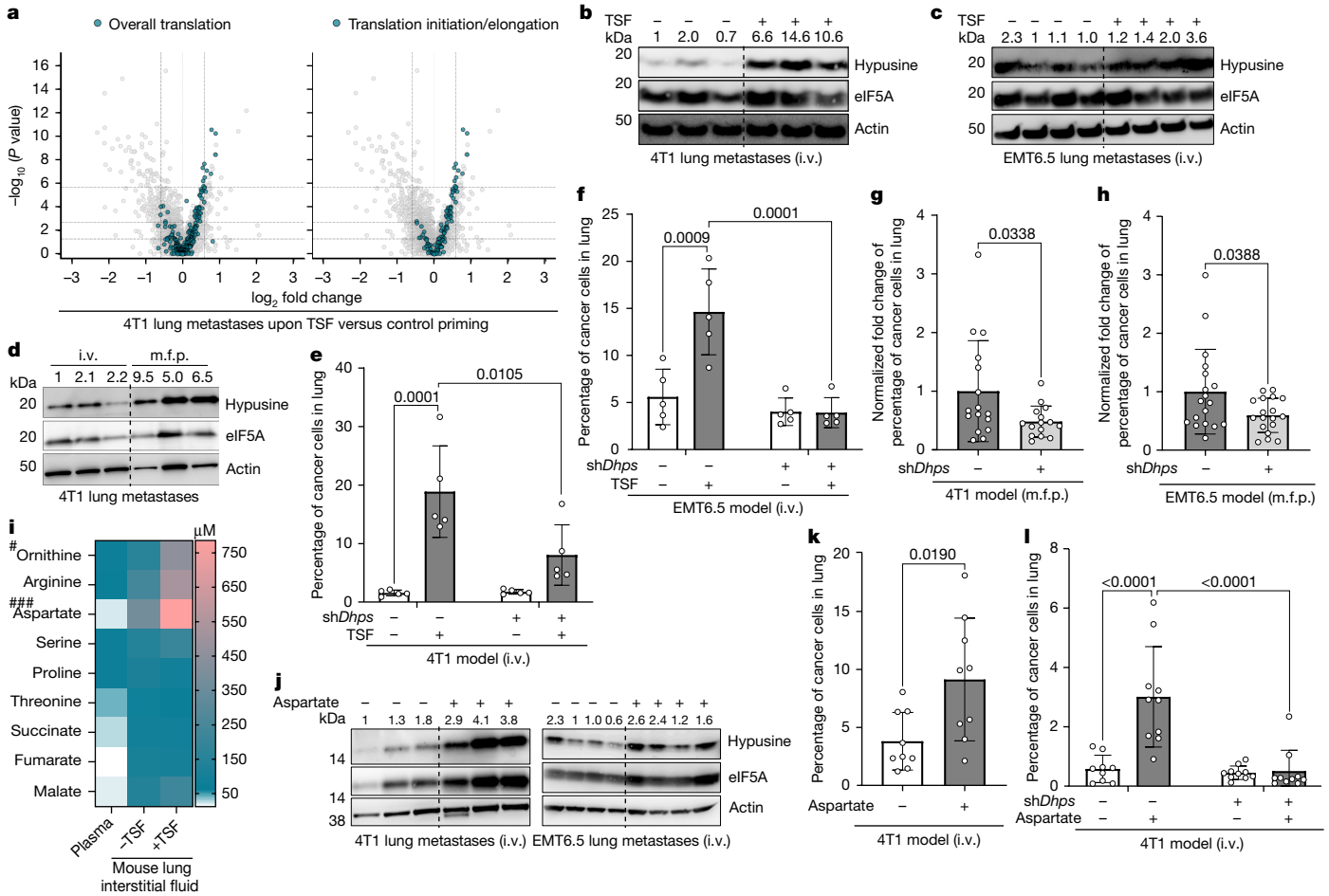

Fig. 1 | Aspartate promotes the aggressiveness of lung metastases by inducing eIF5A hypusination. a, Volcano plots based on single-cell differential expression analysis comparing cancer cells from 4T1 lung metastases pre-treated with control or TSFs. Genes related to overall translation (left) and translation initiation/elongation (right) are highlighted in blue. Horizontal lines correspond to raw (bottom), Benjamini–Hochberg-adjusted (middle) and Bonferroni-adjusted (top) *P* values of 0.05. Vertical lines correspond to absolute fold changes of 1.5. **b**,**c**, Western blot showing hypusine detection in 4T1 (**b**) or EMT6.5 (**c**) metastases in mice pre-treated with TSFs or control ($n = 3$ (4T1) or 4 (EMT6.5) per group). **d**, Hypusine detection in 4T1 lung metastases transplanted into mice intravenously (i.v.; $n = 3$) or by injection into the mammary fat pad (m.f.p.; $n = 3$). **e**,**f**, Percentage of CD90.1$^+$ 4T1 (**e**) or EMT6.5 (**f**) cells treated with short hairpin RNA (shRNA) targeting *Dhps* (sh*Dhps*) or scramble shRNA ($n = 5$ per group) in mice pre-treated with TSFs or control. **g**,**h**, Fold change of the percentage of CD90.1$^+$ 4T1 (**g**) or EMT6.5 (**h**) cells treated with sh*Dhps* ($n = 15$, 4T1; $n = 18$, EMT6.5) or scramble shRNA ($n = 16$, 4T1; $n = 18$ EMT6.5), normalized by weight of the primary tumour. Data from three (4T1) or two (EMT6.5) independent experiments, and normalized relative to each scramble shRNA group average. **i**, Average metabolite concentrations in plasma and lung interstitial fluid in mice pre-treated with TSFs or control ($n \geq 5$ per group). $^{###}P = 0.0006$, $^{\#}P = 0.053$. **j**, Hypusine detection in 4T1 (left, $n = 3$ per group) or EMT6.5 (right, $n = 4$ per group) metastases in mice pre-treated with aspartate or PBS. **k**, Percentage of CD90.1$^+$ 4T1 cells expressing scramble shRNA ($n = 9$ per group) in mice pre-treated with aspartate or PBS. **l**, Percentage of CD90.1$^+$ 4T1 cells treated with sh*Dhps* or scramble shRNA ($n = 9$ scramble + PBS, $n = 10$ for all other groups) in mice pre-treated with aspartate or PBS. **b**–**d**,**j**, Hypusine quantification relative to total eIF5A is shown at the top of each lane. Wilcoxon rank-sum test implementation in Seurat (**a**); two-way analysis of variance (ANOVA) with Tukey's multiple-comparison tests (**e**,**f**,**l**); unpaired two-tailed *t*-test with Welch's correction (**g**–**i**,**k**). Data are mean ± s.d. unless indicated otherwise.

Aspartate induces eIF5A hypusination

To identify the trigger of eIF5A hypusination in aggressive metastases, we analysed the nutrient concentrations in lung interstitial fluid from TSF-primed versus control mice. Most nutrient concentrations did not change significantly (Fig. 1i). An exception was aspartate, an amino acid that is present at very low levels in blood plasma and that is mostly synthesized de novo in cancer cells and used in the biosynthesis of nucleotides and proteins. In TSF-primed mice or in the presence of a primary breast tumour, lung aspartate increased to almost millimolar levels (Fig. 1i and Extended Data Fig. 1j,k). This increase did not occur in other organs or in mice with non-metastatic primary breast tumours (Extended Data Fig. 1k–m). Next, we investigated whether aspartate induces eIF5A hypusination and lung metastasis aggressiveness. We pre-treated mice with aspartate or PBS (vehicle; intraperitoneal injection) for 10 days, which resulted in a similar increase in aspartate in lung interstitial fluid to that seen with TSF treatment, without changing circulating aspartate (Extended Data Fig. 1n–p). Subsequently, we injected the mice with 4T1 or EMT6.5 cancer cells. Metastases from mice pre-treated with aspartate displayed increased eIF5A hypusination (Fig. 1j and Extended Data Fig. 1q) and increased metastasis aggressiveness based on the total number of cancer cells detected in the lung (Fig. 1k). Moreover, decreasing eIF5A hypusination by silencing *Dhps* abrogated aspartate-induced metastasis aggressiveness (Fig. 1l and Extended Data Fig. 1r). We thus concluded that lung aspartate triggers eIF5A hypusination and promotes the aggressiveness of lung metastases.

Lung-like medium promotes aggressiveness

To assess the in vivo findings in cultured cells, we grew tumour spheroids from mouse 4T1 and human MCF10A HRAS^{V12} breast cancer

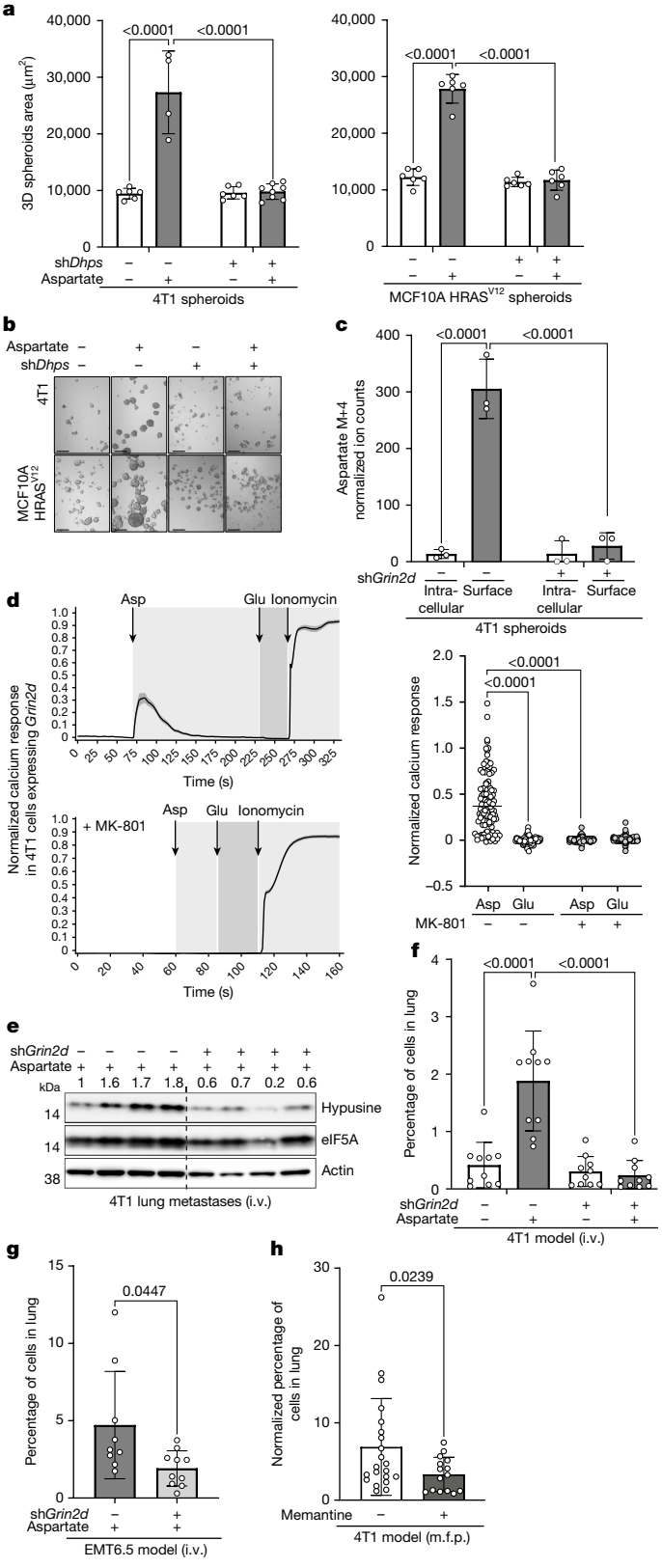

Fig. 2 | Aspartate triggers NMDA receptor activity. a, Total spheroid areas for 4T1 (left) and MCF10A HRAS^{V12} (right) cells treated with sh*Dhps* ($n = 6$ 4T1 or MCF10A HRAS^{V12} without aspartate, $n = 8$ 4T1 plus aspartate, $n = 6$ MCF10A HRAS^{V12} plus aspartate) or scramble shRNA ($n = 6$ 4T1 or MCF10A HRAS^{V12} without aspartate, $n = 4$ 4T1 plus aspartate, $n = 6$ MCF10A HRAS^{V12} plus aspartate) in LLM with or without aspartate. **b**, Representative images from **a**. Scale bars, 250 µm. **c**, Intracellular and cell-surface levels of ^{13}C-aspartate in 4T1 spheroids treated with shRNA targeting *Grin2d* (sh*Grin2d*) or scramble shRNA ($n = 3$ per group) and supplemented with $^{13}C_4$-aspartate in LLM. **d**, Left, average ionomycin-normalized calcium response traces with (bottom) or without (top) MK-801 treatment in 4T1 cells overexpressing *Grin2d*. The shaded regions around the traces show the s.e.m. and arrows indicate sequential addition of aspartate, glutamate and ionomycin. One representative experiment ($n = 39$ without MK-801 and $n = 73$ with MK-801) out of four independent experiments is shown. Right, ionomycin-normalized calcium response in 4T1 cells overexpressing *Grin2d* without ($n = 106$) or with ($n = 219$) MK-801 treatment from four independent experiments. Two-way ANOVA with Šídák's multiple-comparison tests considering all independent cells. **e**, Hypusine detection in 4T1 lung metastases treated with sh*Grin2d* or scramble shRNA ($n = 4$ per group) in mice pre-treated with aspartate or PBS. Hypusine quantification relative to total eIF5A is shown at the top of each lane. **f**, Percentage of CD90.1$^+$ 4T1 cells treated with sh*Grin2d* or scramble shRNA ($n = 10$ per group) in mice pre-treated with aspartate or PBS. **g**, Percentage of CD90.1$^+$ EMT6.5 cells treated with sh*Grin2d* ($n = 10$) or scramble shRNA ($n = 9$) in mice pre-treated with aspartate. **h**, Percentage of CD90.1$^+$ 4T1 cells in mice treated with memantine-HCl ($n = 15$) or PBS ($n = 21$), normalized by primary tumour mass. Two-way ANOVA with Tukey's multiple-comparison tests (**a**,**c**,**f**); unpaired two-tailed *t*-test with Welch's correction (**g**,**h**). Data are mean ± s.d. unless indicated otherwise.

cells[6,9,10], mouse B16F10 melanoma cells and human HUH7 hepatocellular carcinoma cells in lung-like medium (LLM), which resembles the glucose, amino acid and organic acid concentrations of lung interstitial fluid, and deprived or supplemented this medium with 700 µM aspartate (Supplementary Table 1). In line with the in vivo data, aspartate supplementation increased eIF5A hypusination and tumour spheroid growth (Extended Data Fig. 2a–d). We verified increased overall translation and an enrichment of translation-related gene sets in MCF10A HRAS^{V12} and/or 4T1 spheroids upon aspartate supplementation (Extended Data Fig. 2e,f). *DHPS* (*Dhps* in mouse) silencing abrogated the aspartate-induced tumour spheroid growth (Fig. 2a,b), which was phenocopied by silencing of *EIF5A1* (also known as *EIF5A*; *Eif5a1* (or *Eif5a*) in mouse) and, to some extent, *EIF5A2* (*Eif5a2* in mouse) (Extended Data Fig. 2g–i). This shows that the LLM-based spheroid model recapitulates our in vivo findings.

Aspartate promotes NMDA receptor activity

Next, we assessed the fate of aspartate in tumour spheroids with ^{13}C tracer analysis[11]. When supplementing $^{13}C_4$-aspartate to 4T1 tumour spheroids, we unexpectedly found that aspartate was not metabolized into its downstream products (Extended Data Fig. 2j,k), suggesting that aspartate may be binding to a cell surface protein. Therefore, we analysed intracellular and cell surface aspartate separately (Extended Data Fig. 2l) and found that most of the detected $^{13}C_4$-aspartate was on the cell surface (Fig. 2c). Next, we searched for receptors that can bind aspartate. The *N*-methyl-D-aspartate (NMDA) receptor, an ionotropic receptor of the brain that is activated by glutamate and glycine, can also bind aspartate; we focused on the glutamate ionotropic receptor NMDA type subunit 2D (GRIN2D), which is the most responsive L- and D-aspartate-binding subunit in biochemical assays[12]. Indeed, *Grin2d* silencing significantly decreased the fraction of $^{13}C_4$-aspartate, but not $^{13}C_5$-glutamate, on the cell surface (Fig. 2c and Extended Data Fig. 2m). L- and D-Aspartate, but not glutamate, increased tumour spheroid growth and eIF5A hypusination (Extended Data Fig. 2n–p). This non-responsiveness to glutamate may be explained by the observation that GRIN2D was localized on the surface of cancer cells in 4T1 lung metastases (Extended Data Fig. 2q), whereas *Grin2b*, which encodes the classical glutamate-responding NMDA receptor subunit, was barely expressed relative to *Grin2d* in 4T1 metastases (Extended Data Fig. 2r). Next, we assessed NMDA receptor activity by measuring intracellular calcium response. Only aspartate, but not glutamate, stimulated a GRIN2D-dependent calcium response, which was abrogated by the

NMDA receptor inhibitor MK-801[13] (Fig. 2d, Extended Data Fig. 2s,t and Supplementary Videos 1–3). Thus, we concluded that aspartate binds to GRIN2D and activates the NMDA receptor in cancer cells.

Hypusination depends on NMDA receptor activity

Subsequently, we tested whether NMDA receptor activity regulates eIF5A hypusination. *Grin2d* silencing decreased aspartate- or TSF-induced hypusination in tumour spheroids and/or lung metastases (Fig. 2e and Extended Data Fig. 3a,b) as well as tumour spheroid (4T1 and MCF10A HRAS^{V12}) and/or lung metastasis (4T1 and EMT6.5) growth (Fig. 2f,g and Extended Data Fig. 3c,d). The same result was observed upon treatment with MK-801 (Extended Data Fig. 3e,f) or the clinically approved NMDA receptor inhibitor memantine[13] (Fig. 2h). Thus, we conclude that the activation of the NMDA receptor by aspartate induces eIF5A hypusination and triggers aggressive growth of lung metastases.

NMDA receptor activity increases DOHH

Next, we investigated how NMDA receptor activity increases eIF5A hypusination. The activity of DHPS and DOHH is required for hypusination (Extended Data Fig. 1h). Interestingly, we observed that aspartate increased *Dohh* but not *Dhps* expression in tumour spheroids (Extended Data Fig. 3g), and the same was observed in lung metastases from mice treated with TSFs (Extended Data Fig. 3h). Moreover, the aspartate-induced increase in *Dohh* expression was abrogated by *Grin2d* silencing in tumour spheroids (Extended Data Fig. 3i). Accordingly, we found increased co-expression of DOHH and hypusine in lung metastases of aspartate pre-treated mice compared with control or *Grin2d*-silenced metastases (Fig. 3a). Notably, overexpression of *Dohh* was sufficient to increase eIF5A hypusination and tumour spheroid growth in the absence of aspartate (Extended Data Fig. 3j,k) and metastasis aggressiveness in control mice (Fig. 3b). Thus, this demonstrates that increased *Dohh* expression is sufficient to promote eIF5A hypusination, resulting in more aggressive lung metastases.

Next, we explored how NMDA receptor activity induces *DOHH* expression. We used computational prediction of potential transcription factors that regulate *DOHH* using the Harmonizome database[14]. Out of the predicted transcription factors, only CREB was known to be regulated by NMDA receptor activity[15] (Extended Data Fig. 3l). In line with this, we observed that aspartate induced CREB phosphorylation, which decreased upon *Grin2d* silencing in tumour spheroids and lung metastases (Extended Data Fig. 3m,n). Moreover, inhibition of CREB with compound 3i[16] decreased *Dohh* (but not *Dhps*) expression, eIF5A hypusination and tumour spheroid growth (Extended Data Fig. 3o–q). Thus, we concluded that aspartate-induced NMDA receptor activity results in CREB phosphorylation, driving increased *DOHH* expression.

eIF5A-induced translation increases collagen

Next, we investigated the translational programme that is activated downstream of eIF5A hypusination using polysome profiling. We identified multiple signatures indicative of TGFβ signalling among the highest-ranking gene sets regulated by aspartate and decreased upon *Dhps* and *Grin2d* silencing (Extended Data Fig. 4a,b). This was functionally confirmed by analysing phosphorylation of the canonical TGFβ signalling target SMAD3[17] (Extended Data Fig. 4c). Moreover, inhibition of TGFβ with LY364947 decreased aspartate-induced SMAD3 phosphorylation and tumour spheroid growth (Extended Data Fig. 4d,e). Accordingly, lung metastases from mice pre-treated with aspartate exhibited increased co-expression of hypusine and phosphorylated SMAD3 compared with control and *Grin2d*-silenced metastases (Fig. 4a). Thus, we concluded that eIF5A hypusination increases canonical TGFβ signalling.

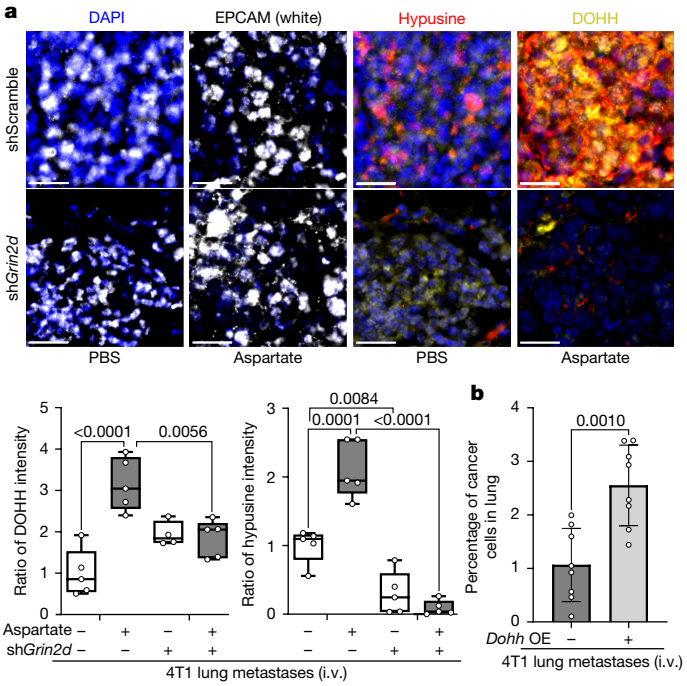

Fig. 3 | Aspartate-induced NMDA receptor activity regulates DOHH expression. a, Detection of hypusine and DOHH in 4T1 metastases treated with sh*Grin2d* or scramble shRNA (shScramble) in mice pre-treated with aspartate or PBS. Top, representative images from $n = 5$ independent mice per group. Scale bars, 25 µm. Bottom, ratio of DOHH (left) and hypusine (right) intensities normalized to 4T1 metastases treated with scramble shRNA and PBS. Two-way ANOVA with Tukey's multiple-comparison tests. Staining was performed as multiplex staining, and only the relevant stains are shown; the same metastatic regions and hypusine staining are used in Fig. 4a,c and Extended Data Fig. 3n. **b**, Percentage of CD90.1$^+$ 4T1 cells overexpressing *Dohh* (*Dohh* OE) or empty vector control ($n = 8$ per group) in mouse lungs. Data are mean ± sd. Unpaired two-tailed *t*-test with Welch's correction. For all box plots in all the figures, box hinges indicate the first and third quartiles of the corresponding data, mid lines represent medians, and whiskers span the range of the data; individual data points are indicated with dots.

Subsequently, we explored how TGFβ signalling enables the aggressiveness of lung metastases. We focused on collagen synthesis, which is known to be regulated by TGFβ signalling[17] and promotes lung metastasis[10]. We found a signature indicative of collagen remodelling in lung metastases from TSF-treated mice (Extended Data Fig. 4f). Moreover, we detected increased *COL1A1* expression and increased abundance of type I collagen in aspartate-treated tumour spheroids (Extended Data Fig. 4g,h), which decreased upon *DHPS* and *GRIN2D* silencing, as well as inhibition of TGFβ signalling (Extended Data Fig. 4i–k). In addition, we observed that supplementation with type I collagen rescued the impaired growth of *Dhps*- and *Grin2d*-silenced spheroids as well as TGFβ inhibitor-treated 4T1 spheroids (Extended Data Fig. 4l,m). Accordingly, aggressive metastases from mice pre-treated with aspartate showed an increased abundance of type I–III collagens as well as COL1A1 and COL6A1 compared with controls (Fig. 4b,c and Extended Data Fig. 4n), which was abrogated by *Dhps* and *Grin2d* silencing (Fig. 4b,c and Extended Data Fig. 4n). Thus, the translational programme induced by eIF5A hypusination converges via TGFβ signalling into metastasis-promoting collagen synthesis by cancer cells.

Evidence of aspartate signalling in patients

Finally, we investigated lung metastases from patients with breast cancer collected via the rapid postmortem tissue donation programme

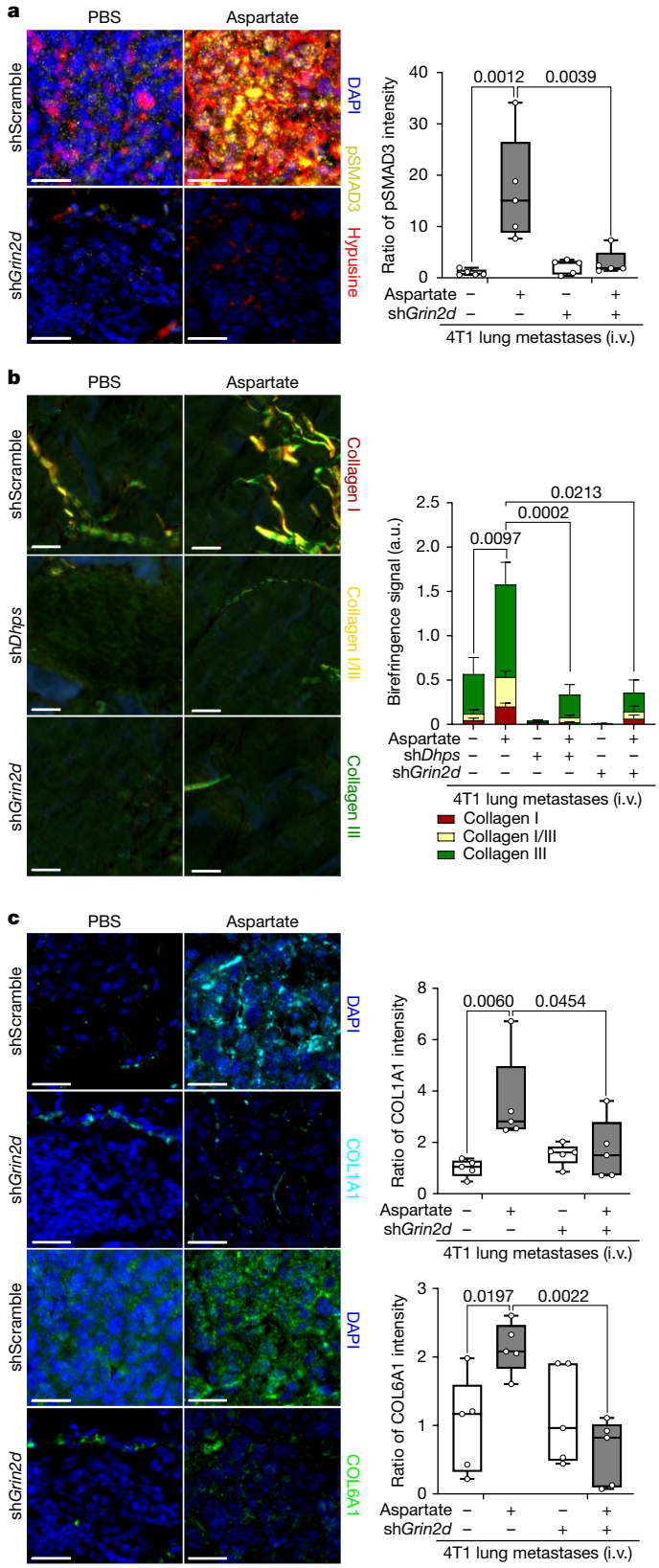

Fig. 4 | Alternative translation induced by eIF5A hypusination results in collagen synthesis. a, Phosphorylated SMAD3 (pSMAD3) and hypusine in 4T1 metastases treated with sh*Grin2d* or scramble shRNA in mice pre-treated with aspartate or PBS. Left, representative images from $n = 5$ independent mice per group. Scale bars, 25 µm. Right, ratio of pSMAD3 intensity normalized to 4T1 metastases treated with scramble shRNA and PBS. Two-way ANOVA with Tukey's multiple-comparison tests. **b**, Left, representative images of linearized collagen detected in 4T1 metastases treated with sh*Grin2d*, sh*Dhps* or scramble shRNA in mice pre-treated with aspartate or PBS. Red mostly indicates thick collagen I fibres and green mostly indicates thin collagen III fibres (Methods). Scale bars, 10 µm. Right, quantification of linearized collagen. There was a significant increase in collagen III fibres with aspartate treatment ($P = 0.0097$), which was abrogated by silencing *Dhps* ($P = 0.0002$) or *Grin2d* ($P = 0.0213$). $n = 4$ PBS or aspartate plus scramble RNA, $n = 4$ PBS plus sh*Dhps*, $n = 5$ aspartate plus sh*Dhps*, $n = 3$ PBS plus sh*Grin2d*, and $n = 4$ aspartate plus sh*Grin2d*. Data are mean ± s.e.m. Two-way ANOVA with Šídák's multiple-comparison tests. a.u., arbitrary units. **c**, COL1A1 and COL6A1 detection in 4T1 metastases treated with sh*Grin2d* or scramble shRNA in mice pre-treated with aspartate or PBS. Left, representative images of $n = 5$ independent mice per group. Scale bars, 25 µm. Right, ratio of COL1A1 (top) and COL6A1 (bottom) intensities normalized to 4T1 metastases treated with scramble shRNA and PBS. Two-way ANOVA with Dunnett's multiple-comparison tests. COL1A1 and COL6A1 staining was performed on consecutive sections. Staining in **a**,**c** was performed as multiplex staining, and only the relevant stains are shown here; the same metastatic regions and hypusine staining are used in Fig. 3a and Extended Data Fig. 3n.

UPTIDER[18] (KU/Universitair Ziekenhuis Leuven (UZ) Leuven) and publicly available gene expression data. In line with the mouse data, we found that patients with breast cancer had increased aspartate concentrations in their lung interstitial fluid ($n = 3$ individuals without cancer, $n = 10$ patients with breast cancer; Fig. 5a). Accordingly, lung metastases ($n = 16$) showed increased expression of *GRIN2D* (but not other NMDA receptor subunits) compared with other metastatic sites (bone, brain and liver; $n = 20$) in a cohort of patients with metastatic breast cancer (Fig. 5b and Extended Data Fig. 5a). Lung metastases also displayed higher eIF5A hypusination compared with adjacent (non-tumour) tissues from patients with breast cancer ($n = 3$, Fig. 5c). Moreover, we also identified an increased translation initiation/elongation signature in lung metastases ($n = 16$) compared with metastases from other organs ($n = 20$) of patients with breast cancer (Fig. 5d). Additionally, we found that lung metastases exhibited increased amounts of GRIN2D, hypusine, DOHH, phosphorylated CREB, phosphorylated SMAD3, COL1A1, COL6A1 and collagen I–III compared with adjacent (non-tumour) tissues in patients with breast cancer ($n = 7$, Fig. 5e,f and Extended Data Figs. 5b–d and 6). Thus, we provide evidence for aspartate signalling in lung metastases from patients with breast cancer.

In this work we identified a function of aspartate as a signalling molecule in cancer cells that promotes metastasis aggressiveness. Specifically, we found that pulmonary aspartate activates the NMDA receptor, which promotes eIF5A hypusination and an alternative translation programme that drives collagen synthesis (Fig. 5g). Aspartate is present at very low levels in blood plasma, and has been considered to be important predominantly for fuelling protein and nucleotide synthesis as well as maintaining redox homeostasis[19]. Several cancers have been shown to express the NMDA receptor[20,21]. However, its role in cancer cells has been linked mainly with pseudosynaptic behaviour and glutamate metabolism[21–23]. In addition, it has been shown that TGFβ can induce eIF5A hypusination in high-grade metastatic breast cancers, increasing the translation of the pro-metastatic non-receptor tyrosine kinase PEAK1[24]. Here, we identify an additional role of aspartate as a signalling molecule that binds and activates the NMDA receptor, which induces eIF5A activity via hypusination, leading to eIF5A-induced translational regulation of collagen synthesis.

Cancer cell plasticity is essential for metastasis formation[25,26], and this plasticity often depends on translational reprogramming[27]. Here we show that nutrient priming of the lung by the secretome of primary breast tumours leads to the induction of an alternative translational programme in disseminated cancer cells, resulting in increased

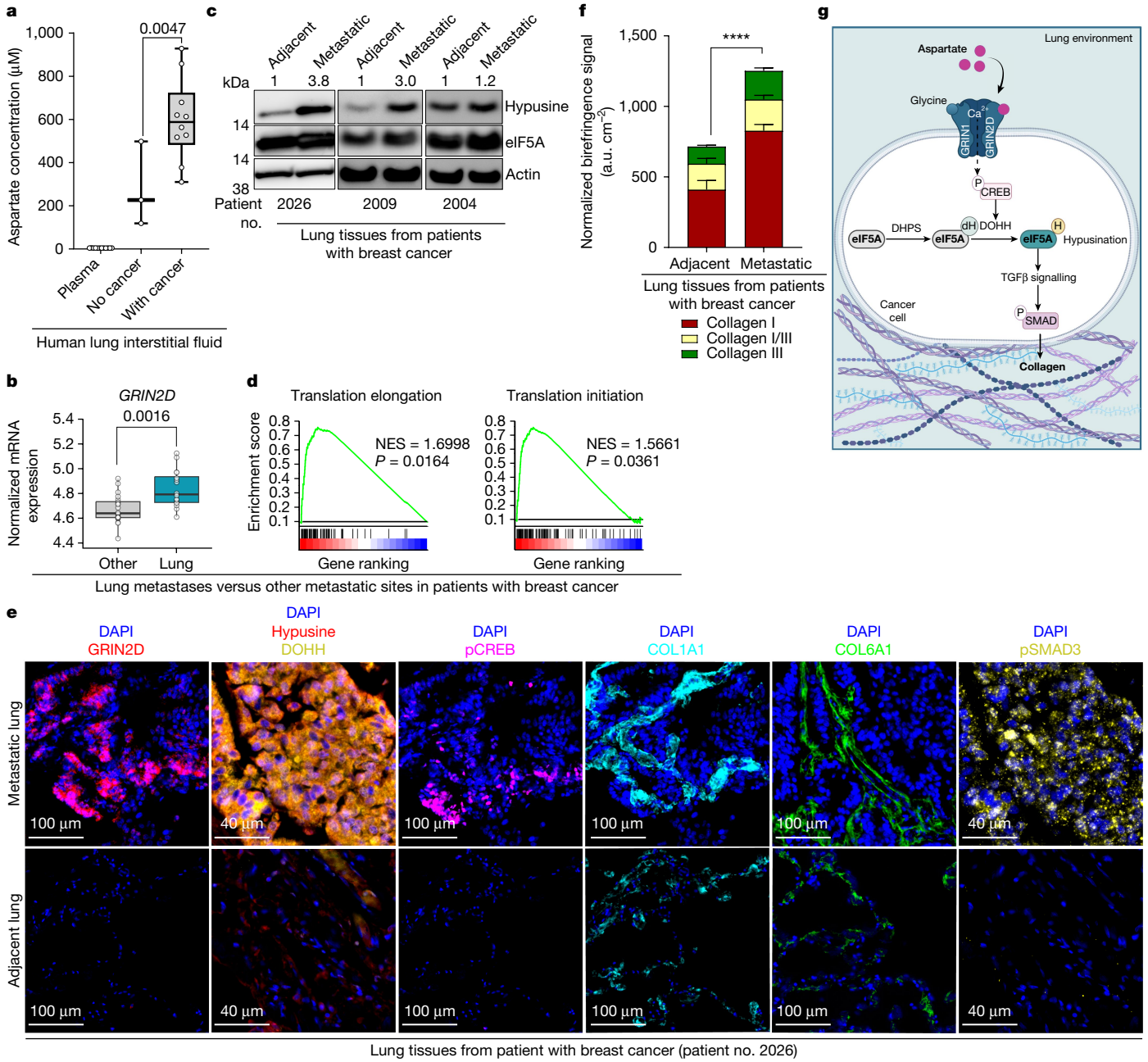

Fig. 5 | Evidence for aspartate signalling in lung metastases of patients with breast cancer. a, Aspartate concentration in plasma or lung interstitial fluid of patients with breast cancer without detected lung metastases ($n = 10$) versus non-cancer samples ($n = 3$). One-way ANOVA ($P < 0.0001$) with Tukey's multiple-comparison tests. Plasma versus lung interstitial fluid of individuals without cancer: $P = 0.0121$; plasma versus lung interstitial fluid of patients with breast cancer: $P < 0.0001$. **b**, *GRIN2D* expression in lung versus bone, brain and liver metastases from biopsies from patients with breast cancer. $n = 16$ lung metastases and $n = 20$ non-lung metastases. *P* value based on differential expression analysis with limma. **c**, Hypusine detection in lung metastases and adjacent non-cancerous tissues from patients with breast cancer from the UPTIDER programme. Hypusine quantification relative to total eIF5A is shown at the top of each lane. **d**, Gene set enrichment analysis enrichment plots for translation elongation (left) and initiation (right) gene sets based on differential expression analysis comparing lung versus non-lung (bone, brain and liver) metastases of patients with breast cancer. *P* values based on adaptive multilevel splitting Monte Carlo approach in fgsea. NES, normalized enrichment score. **e**, Representative images of GRIN2D, hypusine, DOHH, phosphorylated CREB, COL1A1, COL6A1 and phosphorylated SMAD3 detection in metastases and adjacent non-cancerous lung tissues of patients with breast cancer from the UPTIDER programme ($n = 7$ individuals). Representative images for additional patients are shown in Extended Data Fig. 6. **f**, Quantification of linearized collagen detection using picrosirius red in metastases and adjacent non-cancerous lung tissues of patients with breast cancer from the UPTIDER programme ($n = 5$). There was a significant increase of linearized collagen in metastatic tissue compared with adjacent noncancerous tissue (****$P < 0.0001$). Data were normalized to metastasis area (cm^2) and are shown as mean ± s.e.m. Two-way ANOVA with Šídák's multiple-comparison tests. Representative image shown in Extended Data Fig. 5d. **g**, Schematic of the identified mechanism of aspartate signalling in lung metastases. dH, deoxyhypusine; H, hypusine; P, phosphorylation. Created with BioRender.com.

metastasis aggressiveness. These findings may open research into aspartate as an extracranial signalling molecule that regulates alternative translation, and nutrient priming of the pre-metastatic niche as an inducer of metastasis aggressiveness. Moreover, the existence of clinically approved NMDA receptor and DOHH inhibitors may facilitate the translation of these findings to the clinic.

Online content

Any methods, additional references, Nature Portfolio reporting summaries, source data, extended data, supplementary information, acknowledgements, peer review information; details of author contributions and competing interests; and statements of data and code availability are available at https://doi.org/10.1038/s41586-024-08335-7.

1. Gerull, W. D., Puri, V. & Kozower, B. D. The epidemiology and biology of pulmonary metastases. *J. Thorac. Dis.* **13**, 2585–2589 (2021).
2. Mohammed, T.-L. H. et al. ACR appropriateness criteria screening for pulmonary metastases. *J. Thorac. Imag.* **26**, W1–W3 (2011).
3. Crist, S. B. et al. Unchecked oxidative stress in skeletal muscle prevents outgrowth of disseminated tumour cells. *Nat. Cell Biol.* **24**, 538–553 (2022).
4. Peinado, H. et al. Pre-metastatic niches: organ-specific homes for metastases. *Nat. Rev. Cancer* **17**, 302–317 (2017).
5. Doglioni, G., Parik, S. & Fendt, S. M. Interactions in the (pre)metastatic niche support metastasis formation. *Front. Oncol.* **9**, 219 (2019).
6. Altea-Manzano, P. et al. A palmitate-rich metastatic niche enables metastasis growth via p65 acetylation resulting in pro-metastatic NF-κB signaling. *Nat. Cancer* **4**, 344–364 (2023).
7. Pelechano, V. & Alepuz, P. eIF5A facilitates translation termination globally and promotes the elongation of many non polyproline-specific tripeptide sequences. *Nucleic Acids Res.* **45**, 7326–7338 (2017).
8. Park, M. H., Nishimura, K., Zanelli, C. F. & Valentini, S. R. Functional significance of eIF5A and its hypusine modification in eukaryotes. *Amino Acids* **38**, 491–500 (2010).
9. Elia, I. et al. Proline metabolism supports metastasis formation and could be inhibited to selectively target metastasizing cancer cells. *Nat. Commun.* **8**, 15267 (2017).
10. Elia, I. et al. Breast cancer cells rely on environmental pyruvate to shape the metastatic niche. *Nature* **568**, 117–121 (2019).
11. Buescher, J. M. et al. A roadmap for interpreting ^{13}C metabolite labeling patterns from cells. *Curr. Opin. Biotechnol.* **34**, 189–201 (2015).
12. Erreger, K. et al. Subunit-specific agonist activity at NR2A-, NR2B-, NR2C-, and NR2D-containing *N*-methyl-D-aspartate glutamate receptors. *Mol. Pharmacol.* **72**, 907 (2007).
13. Song, X. et al. Mechanism of NMDA receptor channel block by MK-801 and memantine. *Nature* **556**, 515–519 (2018).
14. Rouillard, A. D. et al. The harmonizome: a collection of processed datasets gathered to serve and mine knowledge about genes and proteins. *Database* **2016**, baw100 (2016).
15. West, A. E. et al. Calcium regulation of neuronal gene expression. *Proc. Natl Acad. Sci. USA* **98**, 11024–11031 (2001).
16. Xie, F. et al. Identification of a potent inhibitor of CREB-mediated gene transcription with efficacious in vivo anticancer activity. *J. Med. Chem.* **58**, 5075–5087 (2015).
17. Verrecchia, F. & Mauviel, A. Transforming growth factor-beta signaling through the Smad pathway: role in extracellular matrix gene expression and regulation. *J. Invest. Dermatol.* **118**, 211–215 (2002).
18. Geukens, T. et al. Rapid autopsies to enhance metastatic research: the UPTIDER post-mortem tissue donation program. *NPJ Breast Cancer* **10**, 31 (2024).
19. Vettore, L., Westbrook, R. L. & Tennant, D. A. New aspects of amino acid metabolism in cancer. *Br. J. Cancer* **122**, 150–156 (2020).
20. North, W. G., Gao, G., Memoli, V. A., Pang, R. H. & Lynch, L. Breast cancer expresses functional NMDA receptors. *Breast Cancer Res. Treat.* **122**, 307–314 (2010).
21. Li, L. & Hanahan, D. Hijacking the neuronal NMDAR signaling circuit to promote tumor growth and invasion. *Cell* **153**, 86–100 (2013).
22. Zeng, Q. et al. Synaptic proximity enables NMDAR signalling to promote brain metastasis. *Nature* **573**, 526–531 (2019).
23. Krieg, S., Fernandes, S. I., Kolliopoulos, C., Liu, M. & Fendt, S.-M. Metabolic signaling in cancer metastasis. *Cancer Discov.* **14**, 934–952 (2024).
24. Güth, R. et al. DHPS-dependent hypusination of eIF5A1/2 is necessary for TGFβ/fibronectin-induced breast cancer metastasis and associates with prognostically unfavorable genomic alterations in TP53. *Biochem. Biophys. Res. Commun.* **519**, 838–845 (2019).
25. Karras, P., Black, J. R. M., McGranahan, N. & Marine, J. C. Decoding the interplay between genetic and non-genetic drivers of metastasis. *Nature* **629**, 543–554 (2024).
26. Fendt, S.-M., Frezza, C. & Erez, A. Targeting metabolic plasticity and flexibility dynamics for cancer therapy. *Cancer Discov.* **10**, 1797–1807 (2020).
27. Lee, L. J. et al. Cancer plasticity: the role of mRNA translation. *Trends Cancer* **7**, 134–145 (2021).

[1]Laboratory of Cellular Metabolism and Metabolic Regulation, VIB Center for Cancer Biology, VIB, Leuven, Belgium. [2]Laboratory of Cellular Metabolism and Metabolic Regulation, Department of Oncology, KU Leuven and Leuven Cancer Institute (LKI), Leuven, Belgium. [3]Laboratory of Cancer Signaling, GIGA-Institute, University of Liège, Liège, Belgium. [4]Laboratory of Molecular and Cellular Signaling, Department of Cellular and Molecular Medicine, KU Leuven, Leuven, Belgium. [5]Department of Gastroenterology, Affiliated Hospital of Jiangsu University, Jiangsu University, Zhenjiang, China. [6]Laboratory of Intravital Microscopy and Dynamics of Tumor Progression, VIB Center for Cancer Biology, VIB, Leuven, Belgium. [7]Laboratory of Intravital Microscopy and Dynamics of Tumor Progression, Department of Oncology, KU Leuven, Leuven, Belgium. [8]Intravital Imaging Expertise Center, VIB Center for Cancer Biology, VIB, Leuven, Belgium. [9]Laboratory for Molecular Cancer Biology, VIB Center for Cancer Biology, VIB, Leuven, Belgium. [10]Laboratory for Molecular Cancer Biology, Department of Oncology, KU Leuven, Leuven, Belgium. [11]Leibniz Institut für Analytische Wissenschaften-ISAS-e.V., Dortmund, Germany. [12]Department of Dermatology, University Hospital Essen and German Cancer Consortium, Essen, Germany. [13]Department of Gynaecology and Obstetrics, UZ Leuven, Leuven, Belgium. [14]Laboratory for Translational Breast Cancer Research, Department of Oncology, KU Leuven, Leuven, Belgium. [15]Spatial Metabolomics Expertise Center, VIB Center for Cancer Biology, VIB, Leuven, Belgium. [16]Department of Pathology, UZ Leuven, Leuven, Belgium. [17]Department of Imaging and Pathology, Laboratory of Translational Cell And Tissue Research, KU Leuven, Leuven, Belgium. [18]Medizinische Fakultät, Medizinische Proteom-Center (MPC), Ruhr-Universität Bochum, Bochum, Germany. [19]WELBIO Department, WEL Research Institute, Wavre, Belgium. [20]Present address: Laboratory of Metabolic Regulation and Signaling in Cancer, Andalusian Molecular Biology and Regenerative Medicine Centre (CABIMER)–University of Seville–CSIC–University Pablo de Olavide, Seville, Spain. [21]Present address: Children's Research Institute and the Department of Pediatrics, University of Texas Southwestern Medical Center, Dallas, TX, USA. [22]These authors contributed equally: Juan Fernández-García, Sebastian Igelmann, Patricia Altea-Manzano. ✉e-mail: sarah-maria.fendt@kuleuven.be

Methods

Cell culture

Human MCF10A breast epithelial cells, HEK293T epithelial cells, mouse 4T1 mammary gland cancer cells and human HUH7 hepatocellular carcinoma cells were obtained from ATCC. Mouse EMT6.5 mammary gland cancer cells were provided by R. Anderson. Mouse B16F10 melanoma cells were provided by I. Elia. Mouse 4T07 cells were provided by A. Gomes. MCF10A cells expressing $HRAS^{V12}$ (MCF10A $HRAS^{12}$) were generated as previously described[9]. Human MCF10A $HRAS^{V12}$ cells were maintained in Dulbecco's Modified Eagle's Medium F12 (DMEM/F12, Life Technologies) supplemented with 5% heat-inactivated horse serum (Life Technologies), 1% penicillin (50 U ml^{-1}, Life Technologies), 1% streptomycin (50 µg ml^{-1}, Life Technologies), 0.5 µg ml^{-1} hydrocortisone, 100 ng ml^{-1} cholera toxin, 10 µg ml^{-1} human insulin and 20 ng ml^{-1} recombinant human epidermal growth factor. Human HEK293T and HUH7 cells were cultured in high-glucose (4.5 g l^{-1}) Dulbecco's modified Eagle's medium (Life Technologies) supplemented with 10% heat-inactivated fetal bovine serum (Life Technologies), 1% penicillin (50 U ml^{-1}, Life Technologies) and 1% streptomycin (50 µg ml^{-1}, Life Technologies). Mouse 4T1, 4T07 and EMT6.5 cells were cultured in Roswell Park Memorial Institute (RPMI, Life Technologies) 1640 medium supplemented with 10% heat-inactivated fetal bovine serum (Life Technologies), 1% penicillin (50 U ml^{-1}, Life Technologies) and 1% streptomycin (50 µg ml^{-1}, Life Technologies). Mouse B16F10 cells were cultured in Roswell Park Memorial Institute (RPMI, Life Technologies) 1640 medium supplemented with 1% sodium pyruvate (1 mM, Gibco), 1% HEPES (10 mM), 10% heat-inactivated fetal bovine serum (Life Technologies), 1% penicillin (50 U ml^{-1}, Life Technologies) and 1% streptomycin (50 µg ml^{-1}, Life Technologies). All cells were screened to be mycoplasma free via routine testing with the MycoAlert Mycoplasma Detection Kit (Lonza) and the MycoStrip Mycoplasma Detection Kit (InvivoGen). For 3D spheroid growth assays, cells were plated on top of a soft agar mixture[9,28] of 50% agar and 50% LLM (Supplementary Table 1). The 4T1 and MCF10A $HRAS^{V12}$ cells were cultured for 3 to 5 days in freshly made (less than 3 days old) LLM supplemented with or without 700 µM aspartate and with 5% heat-inactivated horse serum (Life Technologies) 1% penicillin (50 U ml^{-1}, Life Technologies) and 1% streptomycin (50 µg ml^{-1}, Life Technologies). MCF10A $HRAS^{V12}$ cells were further supplemented with 0.5 µg ml^{-1} hydrocortisone, 100 ng ml^{-1} cholera toxin, 10 µg ml^{-1} human insulin and 20 ng ml^{-1} recombinant human epithelial growth factor. 1.5% of reduced growth factor Matrigel (Corning) without phenol red and 1.5% Collagen I, Rat Tail (45 µg ml^{-1}, Gibco) were added into LLM before seeding by using tips precooled to −20 °C. The NMDA receptor inhibitor MK-801 (Tocris, 0924) was used at a final concentration of 50 µM. The CREB inhibitor Compound-3i, 666-15 (Selleck Chem, S8846) was used at a final concentration of 600 nM. The TGFβ inhibitor LY364947 (Selleck Chem, S2805) was used at a final concentration of 5 µM. Tunicamycin (Merck Millipore, T7765) was used at 0.1 µg ml^{-1}. Representative images of 3D spheroids were taken at the end of the experiment (3–5 days) with the Motic Images Plus 2.0 software (Motic) and were quantified using a custom script in ImageJ.

Generation of knockdown and overexpression cell lines

Dhps, *Grin2d*, *eIf5a1* and *eIf5a2*-silenced cell lines were generated using the lentiviral pLKO-shRNA1.5 vector expressing shRNAs targeting *Dhps*, *Grind2d, eIf5a1* or *eIf5a2*. The pLKO plasmids were obtained from the Belgian Coordinated Collections of Microorganisms (BCCM). The pLKO plasmid (SHC016) expressing a non-targeting shRNA sequence was used as control and was obtained from the BCCM. In brief, lentiviral particles were produced in HEK293T cells. Transduction of 4T1, EMT6.5 and MCF10A $HRAS^{V12}$ was performed overnight and the medium was replaced the next day. Polyclonal cells were selected with puromycin (2 µg ml^{-1} for 4T1 cells, 1 µg ml^{-1} for EMT6.5 cells and 0.3 µg ml^{-1} for MCF10A $HRAS^{V12}$). To generate the *Dohh*, *Grin2d* and *Grin2b*-overexpressing cell lines, the pLVX-IRES-Hyg plasmid (Takara Bio, 632182) was digested with BamHI and XhoI (NEB). A codon-optimized coding sequence of *Dohh, Grin2d* or *Grin2b* was purchased as a gBlock (Integrated DNA Technologies, IDT) and inserted into the pLVX-IRES-Hyg backbone using Gibson assembly (NEB). The empty pLVX-IRES-Hyg plasmid was used as control. Lentiviral particles were produced in HEK293T cells and cells were transduced overnight and fresh medium was replaced the next day. Polyclonal cells were selected with hygromycin at 100 µg ml^{-1}. A list of sequences used to generate knockdown and overexpression cell lines is described in Supplementary Table 2. Validation of knockdown and overexpression cell lines by quantitative PCR and western blot analysis is presented in Extended Data Fig. 7.

In vivo mouse experiments

All animal experiments were approved by the Institutional Animal Care and Research Advisory Committee of KU Leuven (ECD P025/2020) in compliance with all relevant ethical regulations. Mice were housed under a regimen of 12 h light:12 h dark in non-specific pathogen-free (conventional) facility with a constant supply of food and water. Temperature was checked daily and maintained at 22 ± 2 °C, humidity was checked daily and maintained between 45–70%. Sample size was determined using power calculations with $B = 0.8$ and $P < 0.05$ based on preliminary data and in compliance with the 3R system: replacement, reduction, refinement. All mice were randomized before injections and samples were analysed in a blinded manner. Female BALB/C (Envigo) mice (aged 6–8 weeks) were injected with 4T1 or EMT6.5 cells in the mammary fat pad (m.f.p., 1×10^6 cells) in 50 µl PBS or intravenously (i.v., 25×10^3 cells or 1×10^5) in 100 µl PBS or intrasplenically (25×10^3 cells; spleen was surgically removed two minutes after injection: mice were anaesthetised with 2% isofluorane in pure oxygen at 2 l min^{-1} and carprofen at 5 mg kg^{-1} was administered subcutaneously before and after surgery) in 50 µl PBS. Mice were euthanized after 21–23 days (m.f.p.), 13-17 days (i.v.) or 14 days (intrasplenic) by intraperitoneal injection of 10 µl g^{-1} containing ketamine (100 mg kg^{-1})-xylazine (10 mg kg^{-1}) for experiments involving organ dissociation or 50 µl of a 60 mg ml^{-1} Dolethal (pentobarbital sodium) solution (Vetoquinol) for experiments involving metastasis picking or immunohistochemistry (IHC) staining. Primary tumour volumes (calculated using the following formula: volume = (π/6) × length × width × height) were measured during every experiment using a manual calliper and weighted at the end of the experiment. During the course of the experiments, mice were monitored for detection of humane end points, determined using a score sheet (tumour size of 1.8 cm^3, loss of ability to ambulate, laboured respiration, surgical infection or weight loss over 10% of the initial body weight). For all experiments the tumour volume did not exceeded 1.8 cm^3.

Generation of TSFs and in vivo (pre-)metastatic niche formation

The induction of pre-metastatic niche formation was performed as previously described[6]. In brief, for collecting TSFs, 4T1 or EMT6.5 derived primary tumours were resected after 17 days from m.f.p. injection, cut into smaller pieces and incubated at 37 °C in 15 ml g^{-1} of tumour in Dulbecco's Modified Eagle's Medium (Life Technologies) supplemented with 1% penicillin (50 U ml^{-1}, Life Technologies) and 1% streptomycin (50 µg ml^{-1}, Life Technologies). For control medium formation, the same medium was incubated in parallel. After 72 h, medium was filtered with a 70-µm cell strainer and centrifuged at 1,000*g* for 10 min. Supernatants from three biologically independent tumours were pooled together to cover for biological variability and 20 mM HEPES was added, subsequently medium was filtered with a 0.2-µm filter and stored at 4 °C for maximum 5 days from collection. Female BALB/C mice (6 weeks old) were then injected i.v. with 200 µl of TSFs or control medium 3 times per week for 3 weeks and subsequently either euthanized (pre-metastatic niche: for lung interstitial fluid

extraction or single-cell RNA sequencing), or injected i.v. with 25×10^3 CD90.1-expressing 4T1 or EMT6.5 cancer cells and then euthanized after 16 (4T1) or 14 (EMT6.5) days after cancer cell injection. Subsequently, lungs were analysed for single-cell RNA sequencing, flow cytometry or protein analysis from snap-frozen metastatic tissues.

In vivo aspartate priming of the lung microenvironment

Female BALB/C mice (6 weeks old) were injected with daily intraperitoneal injections of 20 mM aspartate dissolved in 100 µl PBS (pH 7.4), or PBS (pH 7.4) for 10 days. Afterwards, mice were either euthanized with 50 µl of a 60 mg ml^{-1} Dolethal (pentobarbital sodium) for lung interstitial fluid collection at 0, 4, 7, 10 or 14 days after the last intraperitoneal injection or mice were injected with cancer cells for metastatic burden evaluation. Specifically, 4T1 or EMT6.5 cells expressing CD90.1 were injected i.v. (1×10^5 cells) in 100 µl of PBS and after 14 (4T1) or 13 (EMT6.5) days, lungs were dissociated for flow cytometry analysis or metastatic tissues were snap-frozen for protein analysis.

In vivo memantine treatment

Female BALB/C mice (6 weeks old) were injected (m.f.p.) with 4T1 cells expressing CD90.1, after 5 days (when the tumour nodule was palpable) mice were treated with daily intraperitoneal injections (100 µl) of memantine-HCl (5 mg kg^{-1}, 1 mg ml^{-1}) or vehicle (PBS) for 19 days. Afterwards, mice were euthanized for metastatic burden evaluation by flow cytometry analysis.

RNA isolation, qPCR and droplet digital PCR gene expression analysis

Total RNA from cell lines was isolated using the TRIzol Reagent (Thermo Fisher Scientific) and the isolated RNA was quantified using the NanoDrop One Microvolume UV-Vis spectrophotometer (Thermo Fisher Scientific). RNA was reverse transcribed using the qScript cDNA Synthesis kit (Quantabio) and was measured by quantitative PCR (qPCR) using SYBR Green PCR Master Mix, Low ROX (Quantabio) on the 7500 Fast Real Time PCR System (Applied Biosystems, Life Technologies). Relative mRNA expression levels were determined by normalization relative to an endogenous housekeeping gene (cyclophillin B (*Ppib*) or *Rpl19*). Droplet digital PCR was performed to determine the number of copies for *Grin2b* and *Grin2d* in 4T1 lung metastases (m.f.p., 25 days) using the QX200 Droplet Digital PCR system. Specifically, lung metastases were picked and ground, and total RNA from frozen tissues was isolated using TRIzol Reagent (Thermo Scientific). cDNA synthesis was performed using the qScript cDNA synthesis kit (Quantabio). Droplet digital PCR was performed following Bio-Rad guidelines (Bio-Rad). Specifically, a solution containing 21 µl of 2× ddPCR Supermix for probes (without dUTPs), 20× FAM Taqman probe (for *Grin2b* expression), 20× Hex Taqman probe (for *Grin2d* expression), 7 µl of diluted cDNA (for a final concentration of 1,750 ng) and 1.4 µl of nuclease-free water. Droplets were created using a QX200 Droplet Generator and transferred to a 96-well PCR plate heat-sealed using foil sheets (Pierceable Foil Heat Seal, Bio-Rad, 1814040) and the PX1 PCR plate sealer. The Bio-Rad T100 thermal cycler system was used to amplify the droplets, starting with 3 min enzyme activation at 95 °C, followed by 40 cycles of 95 °C, 30 s and 58 °C, 30 s, 72 °C for 1 min, followed by 72 °C for 5 min. Fluorescence of each reaction was measured using the QX200 Droplet Reader (Bio-Rad) and the results were analysed using the QuantaSoft software v.1.7.4.0917 (Bio-Rad) subsequent to threshold setting on positive controls. The resulting number of positive and negative droplets were used to calculate the concentration of cDNA copies per microlitre of the target genes in the final reaction. A list of primers is provided in Supplementary Table 3.

Protein extraction and western blot analysis

Cultured 3D spheroids were collected in dPBS and lysed in RIPA buffer (Thermo Fisher Scientific, 89901) supplemented with protease (Merck Sigma, 5892970001) and phosphatase (Merck Sigma, 4906845001) inhibitors. Frozen tissues were ground with a tissue lyser and then incubated with RIPA buffer. Protein lysates were quantified with the Pierce BCA Protein Assay Kit (Thermo Fisher Scientific, 23225) and 10–20 µg of proteins were loaded on a precast gel NuPAGE Novex 4–12% Bis-Tris (Thermo Fisher Scientific, NP0336BOX). Proteins were subsequently transferred to a nitrocellulose membrane using the iBlot2 dry transferring system (Thermo Fisher Scientific, IB301031). Transferred membranes were blocked for 1 h at room temperature in a blocking solution of 5% milk or 5% bovine serum albumin in tris-buffered saline with 5% Tween-20 (TBS-T). Subsequently, membranes were incubated overnight at 4 °C with primary antibodies against hypusine (EMD Millipore, ABS1064), eIF5A (BD Biosciences, 611976), phosphorylated CREB (Ser133) (Cell Signaling Technologies, 9198S), CREB (Cell Signaling Technologies, 9104S), phosphorylated SMAD3 (S423 + S425) (Abcam, EP823Y), SMAD3 (Cell Signaling Technologies, 9513S), GRIN2D (Novus Biological, NBP2-94573), GRIN2B (Abcam, Ab93610), DHPS (Santa Cruz Biotechnology, sc-365077), puromycin (Merck Sigma, MABE343), phosphorylated eIF2α (Cell Signaling Technologies, 9721S), ATF4 (Cell Signaling Technologies, 11815S), β-actin (Merck Sigma, A5441), β-Tubulin (Cell Signaling Technologies, 2146S). The primary antibodies were used at 1:1,000 dilution in 5% bovine serum albumin in TBS-T, except for anti-hypusine (1:2,000), anti-ATF4, anti-GRIN2D and anti-DHPS (1:500) and anti-β-actin (1:10,000) antibodies. The day after, membranes were incubated with HRP-linked anti-rabbit (Cell Signaling Technologies, 7074S) or anti-mouse (Cell Signaling Technologies, 7076S) secondary antibodies used at 1:5,000 dilution in 5% milk in TBS-T. Bound antibodies were imaged using an ImageQuant LAS 4000 (GE Healthcare). For gel source data, see Supplementary Fig. 1.

SUnSET assay

Puromycin incorporation into newly synthesized protein was used to evaluate overall protein synthesis as previously described[29]. 4T1 and MCF10A $HRAS^{V12}$ 3D spheroids were cultured for 5 days in LLM with or without aspartate supplementation, afterwards spheroids were starved for 1 h in Hank's Balanced Salt Solution (Gibco 14025-050) and then reactivated in LLM with or without aspartate and incubated with the protein synthesis inhibitor cycloheximide (100 nM, Merck Sigma, C7698) or 0.001% DMSO for 1.5 h; puromycin was added during the last 20 min of incubation at 10 µg ml^{-1}. Next, colonies were collected for protein extraction, loaded on a precast gel and transferred as described above. Before blocking, membranes were blotted with Ponceau red and puromycin incorporation was evaluated via western blotting as described above.

Polysome profiling and sequencing analysis

In order to determine genes whose protein translation is upregulated as a result of aspartate-driven NMDA-receptor signalling and downstream eIF5A hypusination, control (sh*Scr*), GRIN2D-knockdown (sh*Grin2d*) and DHPS-knockdown (sh*Dhps*) 4T1 spheroids were cultured for 5 days in LLM supplemented with 700 µM aspartate (Asp) and, in the case of control spheroids, also under no aspartate supplementation (no Asp + sh*Scr*). Polysome isolation was performed as previously described[30,31]. In brief, spheroids were collected and washed in ice-cold cycloheximide-supplemented PBS, lysed in hypotonic buffer (2.5 mM $MgCl_2$, 5 mM TRIS pH 7.5, 1.5 mM KCl supplemented with RNAse and protease inhibitors) and permeabilized by sequential addition of 0.5% Triton X-100 and 0.5% SDS. Lysates were then centrifuged for 7 min at 16,000*g*. For each condition, supernatant containing the cytosolic lysate was then loaded on top of a non-linear sucrose gradient (5% – 34% – 55%) and further ultracentrifuged at 200,000*g* for 2 h at 4 °C. Total RNA input (~ 10% of the cytosolic lysate) was immediately lysed in Trizol solution (TriPure Isolation Reagent, ref. 11667165001, Sigma), snap-frozen in liquid nitrogen, and kept for RNA extraction (see 'Total RNA sequencing'). Polysome fractions were collected using

a piston gradient fractionator (BioComp). Matched polysomal (efficiently translated mRNA; associated with more than 3 ribosomes) and sub-polysomal (associated with fewer than three ribosomes) gradient fractions from four independent spheroid pellets per condition were then lysed in Trizol, snap-frozen in liquid nitrogen and kept at −80 °C for RNA extraction. mRNA library preparation was performed using the Illumina Stranded mRNA Prep kit (20040534, Illumina). After quantification with qPCR, libraries were sequenced on a NovaSeq 6000 System (Illumina) using the NovaSeq 6000 S4 Reagent kit v1.5 (20028312, Illumina), generating 2× 150-bp paired-end reads. The resulting reads were trimmed for adapters and low-quality base calls using Trim Galore (v0.6.6; https://github.com/FelixKrueger/TrimGalore), after which quality control was performed with FastQC (v0.11.9; https://www.bioinformatics.babraham.ac.uk/projects/fastqc). High-quality reads were then mapped to the mm39 reference mouse genome (GRCm39) using STAR (v2.6.1; https://github.com/alexdobin/STAR) and quantified using Salmon (v1.4.0; https://combine-lab.github.io/salmon). Gene counts for all four matched polysomal/sub-polysomal sample pairs collected under all four conditions of interest (Asp sh*Scr*, Asp sh*Grin2d*, ASP sh*Dhps*, no Asp + sh*Scr*) were processed simultaneously within the DESeq2 (v1.34.0; https://bioconductor.org/packages/release/bioc/html/DESeq2.html) framework[32]. In brief, Salmon-derived counts were first rounded to the closest integers, after which genes with no expression in at least three out of four replicates for at least one of the eight condition−fraction combinations were excluded from the analysis. Integer counts for the remaining 17,757 genes were then modelled within DESeq2, using a design accounting for the paired nature of the polysomal/sub-polysomal fractions for each replicate and condition, of the form

$$\text{Counts} \sim \text{Condition} + \text{Condition} : \text{Replicate} + \text{Condition} : \text{Fraction}$$

where : denotes an interaction, 'Condition' denotes either of Asp + sh*Scr*, Asp + sh*Grin2d*, Asp sh*Dhps*, or no Asp + sh*Scr*, 'Fraction' denotes either of the sub-polysomal (reference level) or polysomal fractions, and Replicate = 1⋯4 . On the basis of this design, the coefficients for the interaction terms Condition : Fraction directly represent the average log fold changes ($\log_2$FC) in mRNA levels between the polysomal/sub-polysomal fractions for each of the four conditions of interest, accounting for replicate pairing. The differences between these log fold changes for the Asp + sh*Scr* condition and those for all other three conditions thus provide a measure of whether protein translation for a specific gene is altered in the presence of aspartate (Asp + sh*Scr* versus no Asp + sh*Scr*) or due to either NMDA receptor activity (Asp sh*Scr* versus Asp sh*Grin2d*) or hypusine production (Asp sh*Scr* versus Asp + sh*Dhps*). These log fold-change differences were determined directly within DESeq2, further being subject to shrinkage using the ashr adaptive shrinkage estimator[33] (https://github.com/stephens999/ashr). The resulting shrunken log fold-change differences ($\Delta\log_2$FC) and their associated *P* values were then combined to derive a translation ranking metric TRM = $-\Delta\log_2\text{FC} \times \log_{10}(P\text{ value})$, whereby highly positive or negative values of TRM indicate genes for which protein translation is highly up or downregulated, respectively.

Pre-ranked gene-set enrichment analysis (GSEA[34]; https://www.gsea-msigdb.org/gsea) was then performed, using the R package fgsea[35] (v1.20.0; https://github.com/ctlab/fgsea; multilevel implementation with 10,000 initial permutations and no lower bound for *P* value estimation), for each of the 3 comparisons of interest, based on the ranking metric TRM, and considering a collection of 3,065 mouse gene sets. The latter comprised all HALLMARK and CURATED (C2) gene sets in the Broad Institute Molecular Signatures Database (MSigDB[36,37]; https://www.gsea-msigdb.org/gsea/msigdb) except for those in category C2:CGP, all of them obtained via the R package msigdbr (v7.4.1; https://igordot.github.io/msigdbr), plus all KEGG[38] (https://www.genome.jp/kegg) metabolism gene sets, obtained by querying KEGG's REST API (https://www.kegg.jp/kegg/rest). Only gene sets containing between 3 and 1,500 genes were considered in this analysis. Gene sets with positive normalized enrichment scores (NES) in all 3 comparisons were identified and ranked based on their average NES among all comparisons, with the top 15 of these being shown in the manuscript. To build the word cloud with the top enriched terms based on increased translation in Asp + sh*Scr* versus all other three conditions, combined, average shrunken log fold-change differences ($\Delta\log_2$FC) between the Asp + sh*Scr* condition and all other three conditions were first determined for each gene, again directly within DESeq2. The latter were then used, together with the associated *P* values, to derive a global translation ranking metric, analogously as described above. This global translation ranking metric was then used to perform GSEA, identically as described above, after which upregulated gene sets were ranked on the basis of their NES. Gene set names were then split into individual words, or terms, and each of these terms were assigned a ranking percentile (RP) based on the ranking of their associated gene set, rounded up to multiples of 0.1%. A score for each individual term in each gene set was then computed as 100/RP (thus covering the range 1–1,000), after which an overall score for each term was determined by averaging its scores among all gene sets in which the term appeared. The latter overall scores were then used as weights to create the word cloud, based on the 100 terms with the highest overall scores. Common and/or uninformative terms, such as prepositions (for example, WITH, VIA, THROUGH…), conjunctions (for example, AND, OR…), or generic terms (for example, GENE, PATHWAY, REGULATION, TARGET…) were removed from the ranked list of terms prior to generating the word cloud.

Total RNA sequencing

Total RNA fractions from Asp + sh*Scr*, Asp + sh*Grin2d*, Asp + sh*Dhps*, and no Asp + sh*Scr* 4T1 spheroids, preserved from the input of the polysome profiling experiments, were subject to mRNA library preparation, sequencing, trimming, and mapping identically as described in 'Polysome profiling and sequencing analysis'. Gene counts were again processed within the DESeq2 framework, with Salmon-derived counts first rounded to the closest integers, and genes with no expression in at least two out of four replicates for at least one of the four conditions being excluded from the analysis. Integer counts for the remaining 19,525 genes were then modelled within DESeq2 to determine log fold changes between the Asp + sh*Scr* and no Asp + sh*Scr* conditions. The resulting (Asp + sh*Scr* versus no Asp + sh*Scr*) log fold changes ($\log_2$FC) and their associated *P* values for each gene were then combined to derive a ranking metric RM = $-\log_2\text{FC} \times \log_{10}(P\text{ value})$, whereby highly positive or negative values of RM indicate respectively genes with highly up or downregulated expression in the presence versus absence of aspartate. Pre-ranked GSEA was then performed based on this ranking metric RM, and otherwise identically as described in 'Polysome profiling and sequencing analysis'. Gene sets were ranked based on their normalized enrichment score (NES), with the top 15 gene sets with highest positive NES being shown in the manuscript.

Collagen staining

4T1 and MCF10A HRAS^{V12} spheroids grown for 5 (4T1) or 4 days (MCF10A HRAS^{V12}) in LLM were transferred to 35-mm glass bottom dishes coated with fibronectin and allowed to loosely attach. Spheroids were subsequently fixed with 4% paraformaldehyde in PBS for 30 min, permeabilized with 0.5% Triton X-100 in PBS for 20 min and blocked for 30 min with 1% bovine serum albumin in PBS. Spheroids were then incubated overnight at 4 °C with primary antibody against collagen I (Abcam, Ab34710; 1:500 dilution), washed with PBS and incubated for 1 h with the Alexa Fluor 555-conjugated secondary antibody (Life Technologies, A31272). Next, spheroids were washed with PBS and nuclei were stained with 6 μM

of 4′,6-diamidino-2-phenylindole (DAPI; Sigma Aldrich, D9542) for 15 min. Fluorescence Mounting Medium (Dako, S3023) was used to mount coverslips. Samples were imaged on a SP8X inverted confocal microscope (Leica Microsystem) equipped with a 405 nm and a white light laser. *Z*-stacks were performed using the LAS AF acquisition software (Leica Microsystem). Type I collagen fluorescence intensity quantification was performed with Imaris Image Analysis Software 9 (Bitplane) and normalized over total nuclei number identified with DAPI.

Single-cell cytosolic Ca^{2+} live imaging and quantification

To evaluate cytosolic Ca^{2+} levels, 4T1 cells overexpressing *Grin2d* or *Grin2b* were plated in 4-chamber 35-mm glass bottom dishes (Cellvis, D35C4-20-0-N) for 3 days. Notably, overexpression cells were used to account for comparability between isoform expression levels and to perform Ca^{2+} imaging requiring adherent conditions which results in low basal levels of *Grin2d* expression compared to aspartate stimulated spheroid growth (Extended Data Fig. 7o). Cells were loaded for 45 min with 2 µM of the Ca^{2+} indicator Cal-520 AM (Aat Bioquest) diluted in cell culture medium with the addition of 0.02% of Pluronic F-127 (20% solution in DMSO, Thermo Fischer Scientific) in a humidified incubator at 37 °C and 5% CO_2. The cells were washed once with cell culture medium, and the incubation was continued for 30 min to complete dye de-esterification. Immediately before the Ca^{2+} imaging experiments, the cell culture medium was replaced with a pre-warmed (37 °C) modified Krebs solution (135 mM NaCl, 6.2 mM KCl, 1.2 mM $MgCl_2$, 12 mM HEPES, pH 7.3, 11.5 mM glucose and 1.5 mM $CaCl_2$). Glycine (required for NMDA receptor activation and always added as first treatment), glutamate and aspartate were resuspended into the modified Krebs solution and gently added (sequentially) to the chamber after 30 s of basal acquisition to reach a final concentration of 921 µM for glycine, 774 µM for glutamate and 700 µM for aspartate. Before the end of each recording, cells were exposed to 5 µM ionomycin, a Ca^{2+} ionophore agent, to ensure adequate Cal520 loading and cell responses, and to determine the maximal Ca^{2+} responses. Imaging was performed using a Nikon eclipse Ti2 inverted fluorescence microscope (Nikon) equipped with excitation filter FF01-378/474/554/635 and dichroic mirror FF01-432/515/595/730 and emission filter 515/30, all from Semrock. Excitation was performed at 470 nm using a CoolLed pR-4000 (CoolLed). Emission was measured at 515 nm using an emission filter 515/30. Acquisition of the emitted fluorescent signal was performed using a pco.edge 4.2bi sCMOS camera (pCO) as a function of time (a frame per second). FIJI software was utilized to perform image analysis and to obtain dynamic traces of background-corrected fluorescence intensity versus time $F_C(t)$ for each individual cell C measured in each sample ($C = 1 \ldots N$, where N is the total number of cells identified in that sample). The background-corrected fluorescence intensity traces $F_C(t)$ for the different cells in each sample were first normalized relative to baseline levels as $\Delta(F/F_0)_C(t) = F_C(t)/F_{C_0} - 1$. Here, F_{C_0} is the baseline level for each cell C, determined as the median of $F_C(t)$ across 20 consecutive time points, common to all cells in a given sample, and defined within the time range (1) prior to the addition of the treatments of interest (in our case, glutamate and aspartate); and (2) displaying a high signal stability across all cells in the sample. Normalized calcium response amplitudes for the different added treatments T (where T is glycine, glutamate, aspartate, or ionomycin) were then determined for each cell C as $\Delta(F/F_0)_{C,T} = \max_{t \in T} \{\Delta(F/F_0)_C(t)\}$, where the maximum for each treatment T ($\max_{t \in T}$) is determined within the range of times defined by the addition of the corresponding treatment and that of the immediately subsequent one. Finally, both the normalized calcium response traces $\Delta(F/F_0)_C(t)$ and amplitudes $\Delta(F/F_0)_{C,T}$ for the different treatments T were normalized, for each cell C, relative to the normalized calcium response amplitude upon ionomycin treatment for that cell, $\Delta(F/F_0)_{C,\text{ionomycin}}$, prior to determining sample-averaged normalized traces and/or performing statistical analysis between different treatments/conditions. Sample-averaged traces (and their associated standard errors of the mean) were determined by averaging the ionomycin-normalized traces across all cells in each sample at every given time point. Because ionomycin normalization was performed on a per-cell basis, this necessarily results in the averaged traces not reaching a value of 1 at the end of the experiment (as this would require all cells in a sample to display their peak response to ionomycin at the exact same time point). Cells lacking a response to ionomycin were excluded from the analysis from the start, and are therefore not shown in the presented trace/quantification plots. We also excluded from the latter cells for which the fluorescence intensity response after addition of a given treatment did not drop back down to baseline levels before the addition of the immediately subsequent treatment. Of note, only about 1% of the total cells measured in our experiments were excluded due to either of these two criteria. Cells displaying a maximal treatment (aspartate/glutamate) response either higher than their respective ionomycin response or lower than baseline levels (and therefore having ionomycin-normalized maximal amplitudes above 1 or below 0 for that specific treatment) were on the other hand not excluded from the analysis, but rather interpreted as bona fide high/low treatment responders, respectively. Data from sequential additions of either aspartate or glutamate were further collected to ensure that sequential addition of two treatments would not result in NMDA receptor overactivation upon the first treatment and an ensuing ablation of the calcium response for the second, and are shown in Extended Data Fig. 7p and Supplementary Videos 4 and 5.

^{13}C-labelling from whole-cell extracts and intracellular or cell receptor extracts

Spheroids were cultured in LLM supplemented with 700 µM of $^{13}C_4$-aspartate or $^{13}C_5$-glutamate (Cambridge Isotope Laboratories). For whole-cell metabolite extracts, spheroids were collected after 5 days and metabolites quenching and extraction were performed as previously described[28]. For intracellular cell fraction and cell receptor fraction metabolite extracts, spheroids were collected after 5 days, washed twice with quenching buffer and dissociated into single cells upon incubation with 200 µl of 0.25% trypsin EDTA (Thermo Fisher Scientific) at 37 °C for 15 min. Cell suspensions were subsequently centrifuged at 300*g* for 5 min to separate the supernatants (containing the cell receptor fractions) from the cell pellets (containing the intracellular fractions). The cell pellets were supplemented with 200 µl trypsin 0.25% and subsequently 800 µl of 100% mass spectrometry-grade methanol containing the internal standards norvaline and glutarate (for a final concentration of 2.5 µg ml^{-1} at 1:1) were added to the cell pellet and the receptor fraction for metabolites extraction. Samples were centrifuged for 10 min at maximum speed at 4 °C and the supernatants containing the polar metabolites fraction were separated from the protein-containing pellets. The polar fractions were subsequently concentrated using a vacuum concentrator and the dried metabolite extracts were stored at −80 °C until mass spectrometry analysis. The protein pellet from the intracellular fraction was quantified by BCA and used for metabolite normalization of both the intracellular and receptor fractions.

To evaluate receptor fraction dissociation, cell pellets following 0.25% trypsin EDTA or StemPro Accutase (Thermo Fisher Scientific) digestion (performed 37 °C for 15 min), were incubated at 4 °C for 10 min with anti-mouse CD16/CD32 (Fc block, BD Biosciences, 553142). Samples were then incubated with anti-CD44 APC antibody (BioLegend, 103011, 1:500 dilution) and, to exclude dead cells, samples were stained with the Viability dye eFluor 450 (Thermo Fischer Scientific, 65-0863-14, 1:500 dilution) for 20 min at 4 °C. Samples were then analysed using a BD FACSCanto II with FACSDiva software (BDBiosciences). The percentage of CD44-positive cells was used to assess the fraction of cell receptor present in the spheroids after dissociation using FlowJo software (as shown in Extended Data Fig. 2l).

Lung, liver and bone interstitial fluid collection

Lung interstitial fluid collection was adapted and performed as previously described[6,39,40]. For human samples, healthy lung tissue was collected from patients undergoing lung surgery for emphysematous lung volume reduction. For mice samples, 6- to 8-week-old BALB/C female mice were euthanized with 50 µl of a 60 mg ml^{-1} Dolethal (pentobarbital sodium) solution (Vetoquinol) and whole lungs or 200 mg liver were collected by surgical resection, washed with blood bank saline and dried from liquid excess. Bone interstitial fluid was collected by displacing femur and tibia and removing the patella. Tissues were then placed in a home-made filtered centrifugation tube supplemented with a 20 µm nylon mesh filter (Repligen). Between 1 µl and 10 µl of lung interstitial fluid was collected following centrifugation at 400*g* at 4 °C for 10 min and immediately stored on dry ice. The obtained interstitial fluid volume was used to determine the concentration of the polar metabolites measured by mass spectrometry.

Brain cerebrospinal fluid collection

Mouse cerebrospinal fluid was collected with a micropipette as previously described[41]. In brief, a small subcutaneous incision was performed in the back of the head and cisterna magna was localized by visual inspection. Subsequently, the cisterna magna was punctured with a micropipette, avoiding brain parenchyma or blood vessels. Thanks to the capillary action, 4–7 µl of cerebrospinal fluid flown into the micropipette and was stored on dry ice for mass spectrometry analysis.

Lung and liver dissociation and flow cytometry analysis

4T1 and EMT6.5 cancer cells expressing the lentiviral vector pLKO.3 Thy1.1 (Addgene plasmid 1479) as a reporter protein were used for flow cytometry analysis. Cells expressing the surface protein Thy1.1 (CD90.1-positive cells) were sorted using FACSAria Fusion (BD Biosciences). For evaluating lung or liver metastatic burden, cells were injected in the m.f.p., i.v. or intrasplenically into 6- to 8-week-old female BALB/C mice and after 21–24 days (m.f.p.), 13–17 days (i.v.) or 14 days (intrasplenic) mice were anaesthetised with an intraperitoneal injection of 10 µl g^{-1} containing ketamine (100 mg kg^{-1})-xylazine (10 mg kg^{-1}). Lungs were perfused through the right ventricle, extracted and washed in blood bank saline. Livers were perfused through the left ventricle for full body perfusion, extracted and washed in blood bank saline. Tissues were then dried and minced with blades and subsequently incubated at 37 °C for 45 min with a solution of 0.3 mg ml^{-1} liberase (Roche) and DNase1 (1 µg ml^{-1}) in 2 ml of RPMI supplemented with 5% fetal bovine serum. The dissociated lungs were quenched with 3% fetal bovine serum in PBS supplemented with 2 mM EDTA, filtered through a 70-µm cell strainer and centrifuged for 5 min at 300*g*. The cell pellet was then washed, centrifuged for 5 min at 300*g*, incubated with Red Blood Cell Lysis buffer (Merck) and strained with a 40 µm cell strainer. The single-cell suspension was counted and 20 × 10^6 cells per ml were incubated at 4 °C for 10 min with anti-mouse CD16/CD32 (Fc block, BD Biosciences, 553142). The samples were then stained at 4 °C for 20 min with fluorophore-conjugated antibodies against CD45 PerCP-Cy5.5 (BD Bioscience, 550994, 1:250 dilution), PDPN APC (BioLegend, 127409, 1:250 dilution) and CD90.1 Alexa Fluor 488 (BioLegend, 202505, 1:400 dilution). To exclude dead cells, samples were also stained with the Viability dye eFluor 450 (Thermo Fischer Scientific, 65-0863-14, 1:500 dilution). The samples were analysed using a BD FACSCanto II with FACSDiva software (BD Biosciences). The percentage of metastasizing cells was measured by assessing the fraction of CD90.1-positive cells in the lung or liver using FlowJo software.

Single-cell RNA sequencing

Female BALB/C mice were injected with TSFs (n = 3) or control medium (n = 3) for 3 weeks, as described above, and subsequently either euthanized (pre-metastatic niche), or injected i.v. with 25 × 10^3 CD90.1-expressing 4T1 cancer cells and then euthanized 11 days (metastatic seeding) or 16 days (metastatic colonization) after cancer-cell injection. Upon mouse euthanasia, lungs were collected and dissociated as described above. Cells were then pooled together from the 3 independent lung dissociations performed per group, resuspended in cell-culture medium at a density of 1 × 10^6 cells ml^{-1}, and kept on ice for immediate processing. Approximately 15 µl of each suspension were processed for single-cell library preparation, as previously described[6], whereas the remainder of the single-cell suspension was processed in parallel for flow cytometry analysis, as described above. Barcoded single-cell cDNA libraries were generated using the Chromium Single Cell 5′ V1.1 Library Kit (10x Genomics), following the manufacturer's guidelines, and aiming for a total of 10,000 cells per library. Single-cell libraries were sequenced on a NovaSeq 6000 System (Illumina), and the sequenced reads were then mapped to a customized version of the mm10 mouse genome (mm10 build GRCm38.p6, including an extra chromosome with the CD90.1 sequence used in the transduced lentiviral vector), using the Cell Ranger v5.0.1 software (10x Genomics). The resulting single-cell gene expression data were analysed within the R/Bioconductor framework (www.r-project.org and www.bioconductor.org). Raw unique molecular identifier (UMI) count matrices for all samples were first imported using Seurat (v4.1.0)[42] (www.satijalab.org/seurat), and immediately subject to ambient RNA correction using a customized version of the SoupX (v1.6.2) R pipeline (https://github.com/constantAmateur/SoupX)[43]. Specifically, two modifications were applied to the standard SoupX pipeline. First, the automatically determined (global) ambient contamination fractions for each of the samples were multiplicatively increased by a factor of 2, to account for the fact that, as reported in the literature, the automatic determination method tends to underestimate ambient contamination levels for single-cell RNA-sequencing data[44]. Second, rather than assuming a fixed contamination fraction for all cells, the latter was adapted for each cell based on its specific library size (total UMI counts), to achieve a uniform distribution of subtracted counts across all cells in each sample, in keeping with the nature of the ambient RNA contamination problem[44]. Ambient-corrected count matrices for the different samples were then merged and converted for further processing with Monocle3-alpha (v2.99.3)[45] (www.github.com/cole-trapnell-lab/monocle-release/tree/monocle3_alpha). Low-quality cells were filtered out based on standard quality-control metrics, with thresholds chosen based on evaluating quality-control histograms for the merged dataset. In particular, cells were filtered based on their mitochondrial RNA content (allowing for a maximum of 10%), library size (removing cells with total UMI counts below 800), and number of detected genes (removing cells expressing less than 200 genes). Genes not expressed in any of the cells remaining after quality-control filtering were ignored in all subsequent analyses. Size-factor and variance-stabilizing normalization (based on fitting to a negative binomial distribution) were then applied to the filtered dataset, and highly variable genes (HVGs) were identified based on their departure from the average normalized dispersion versus expression trend observed among all genes. After excluding mitochondrial, ribosomal protein, and cell cycle-associated genes, the top 1,000 HVGs with size-factor normalized expression levels above 0.01 were selected. Principal component analysis (PCA) was then performed on the size factor-normalized and variance-stabilized count matrix restricted to these genes only, followed by 2D uniform manifold approximation and projection[46] (UMAP) dimensional reduction based on the resulting top 50 principal components (with correlation distance metric, number of neighbors = 15, and minimum distance = 0.1, and without further PCA scaling). After that, cells were clustered in the UMAP plane by applying the Louvain[47] graph-based algorithm at high resolution (resolution = 0.001, with k_{NN} = 7), in order to attain a fine-grained cluster structure (183 clusters). The resulting fine-grained clusters were then manually annotated to specific cell types, based on evaluating the expression profiles of several cell type-specific markers across the different

fine-grained clusters. These cell-type annotations were further refined based on applying a second (analogous) step of dimensional reduction and (sub-)clustering analysis, separately to each of the preliminarily annotated cell-types. This in turn allowed us to more easily identify and filter out ambiguously annotated sub-clusters, most notably clusters originating from heterogeneous cell multiplets, characterized by simultaneously presenting markers associated to two or more cell types. Our multiplet identification was confirmed based on the distribution of doublet scores estimated across the different cells in each separate sample using the R package scDblFinder (v1.8.0)[48] (https://bioconductor.org/packages/release/bioc/html/scDblFinder.html). Specifically for the case of cancer cells, the latter could be unambiguously identified upon the first clustering step based on CD90.1 expression, and no re-annotation or doublet removal were needed upon sub-clustering. Differential expression analysis, based on comparing cancer cells under TSFs or control medium pre-treatment at 16 days of metastatic colonization only, was performed within the Seurat framework, using the function FindMarkers with default parameters other than preserving all genes in the output regardless of their determined fold-changes and/or their fraction of expressing cells across samples. The resulting (TSFs versus control) log fold changes ($\log_2$FC) and their associated *P* values for each gene were then combined with the maximum fraction of cancer cells expressing that gene among the two conditions being compared (X_{max}, where $X_{max} = 1$ for genes expressed in 100% of cancer cells in either of the two conditions) to derive an adjusted ranking metric $RM_{adj} = -\log_2FC \times \log_{10}(P\text{ value}) \times X_{max}$, whereby highly positive or negative values of RM_{adj} indicate respectively genes with highly up or downregulated expression under TSF pre-treatment. Pre-ranked GSEA was then performed based on this adjusted ranking metric RM_{adj}, and otherwise identically as described in 'Polysome profiling and sequencing analysis'. Gene sets were ranked on the basis of their NES, with the top 15 gene sets with highest positive NES being shown in the manuscript. The NES plot corresponding to genes signature indicative of ECM remodelling was generated by extracting from the full gene-set collection all gene sets including either of the terms COLLAGEN, MATRISOME, ECM or EXTRACELLULAR_MATRIX. The scRNA-seq raw data for the pre-metastatic niche were previously also used in ref. 6.

Participant selection

For the collection of lung interstitial fluid from healthy subjects, all participants included in this study participated based on an informed consent. The study was approved by the local ethics committee (Medical Ethics Committee KU/UZ Leuven, protocol S57123). Sample collection was performed as described[6,40]. In brief, human lung healthy tissues was collected from patients undergoing lung surgery for emphysematous lung volume reduction (Supplementary Table 4) and lung interstitial fluid was collected as described above.

UPTIDER samples

Snap-frozen, paraffin embedded and fresh tissue samples from lung metastases and healthy tissues were obtained through the ethically approved UPTIDER programme (KU/UZ Leuven Program for Postmortem Tissue Donation to Enhance Research, NCT04531696, S64410). Patients with metastatic breast cancer who decided to participate based on an informed consent in UPTIDER were included in our study. Lung interstitial fluid was collected from fresh tissue samples, proteins from metastatic and non-metastatic lungs were extracted from snap-frozen tissues and IHC was performed from paraffin embedded tissues, as described above. Clinicopathological information for every patient in the UPTIDER dataset is shown in Supplementary Table 5.

H&E, picrosirius red staining and birefringence analysis

Haematoxylin and eosin (H&E) staining of lung was performed to identify metastatic lesions, while Picrosirius red staining was used to image fibrillar collagen in lung metastatic lesions. Female BALB/C mice were euthanized with 50 µl of a 60 mg ml^{-1} Dolethal (pentobarbital sodium) solution (Vetoquinol) and lungs were infused through the trachea with 10% neutral-buffered formalin. Tissues were then incubated overnight in 10% neutral-buffered formalin and transferred into 70% ethanol. Tissues were further processed and embedded into paraffin using Histokinette STP 120-2 (Fisher Scientific). Afterwards, lung samples were deparaffinized, rehydrated and sliced sections of 7 µm were stained with H&E or with 0.1% picrosirius red (Polysciences)[9]. H&E staining was performed with Leica Autostainer XL (ST5010) with manufacture's recommended H&E protocol. H&E images were scanned on a Zeiss Axio Scan.ZI (20×) with a ZEN software (v3.4) and the analysis was performed using the ZEN Blue software (Zeiss). Lung metastatic burden was quantified by analysing the total metastasis area. For picrosirius red staining, images were acquired with AxioScan 7 equipped with polarized light source (20×) with a ZEN software (v.3.4). For human samples, picrosirius red tissue were counterstained with Weigert's haematoxylin to identify metastatic regions, as described[49]. For fibrillar collagen analysis, individual metastases were identified and isolated in the birefringence images; area that included blood vessels or lungs rim were excluded from our analysis due to their endogenous collagen enrichment. Quantitative measurements of fibrillar collagen I signal (red), collagen III (green) and collagen I/III (yellow) were carried out in ImageJ software using an in-house script as previously published[50]. For each image, Hue-Saturation-Balance (HSB) thresholding was applied, where $2 \geq H \leq 27 \mid 0 \geq S \leq 255 \mid 140 \geq B \leq 255$ was used for red-orange (high birefringent) fibres, $28 \geq H \leq 47 \mid 0 \geq S \leq 255 \mid 140 \geq B \leq 255$ for yellow (medium birefringent) fibres, and $48 \geq H \leq 140 \mid 0 \geq S \leq 255 \mid 140 \geq B \leq 255$ for green (low birefringent) fibres. The relative area (as a percentage of total tissue area) was then calculated.

Multiplex immunohistochemistry staining of human and mice lungs

For multiplex immunohistochemistry the OPAL 6 plex kit (Akoya) was used. Each primary antibody dilution was optimized in a single staining and subsequently, optimal position of antibody was determined in a multiplex staining. In detail, 7-µm-thick slices of tissue previously embedded as described in H&E section were cut and mounted on BOND Plus Slides (Leica). Slides were dried for 16 h at 37 °C and then stored at room temperature until the experiment. All the staining steps were performed with the BOND RX Fully Automated Research Stainer 21.2821 (Leica). On day of experiment tissue was deparaffinized with DEWAX solution (Leica) followed by antigen retrieval with AR6 (Leica). Tissues were then blocked with blocking buffer (10% goat serum, Invitrogen, 0.5% BSA in TBS Buffer) for 30 min. Primary antibodies were diluted in TNB (Tris-NaCl Blocking buffer): 100 mM of Tris-HCl pH 7.5, 150 mM NaCl, 0.5% w/v of blocking reagent (Akoya, FP1020). Subsequently, slides were incubated for 1 h at room temperature with the corresponding antibody, rinsed twice with BOND wash buffer (Leica) followed by three washes of 5 min each with BOND wash buffer. Corresponding secondary HRP (Dako rabbit or Opal kit for mouse HRP) were incubated for 10 min followed by 2 rinses and 2 washes of 5 min with BOND wash solution. After the washes, the OPAL dye was incubated for 15 min. The slides were then washed again and followed by either DAPI (Spectral DAPI Akoya) or in case of multiplex staining the next round of staining starting with antigen retrieval for 10 min at 100 °C, blocking, primary antibody, washes, HRP antibody, washes, OPAL dye, washes and DAPI. Afterwards, the staining slides were removed from the autostainer and mounted with antifade diamond mounting medium (Invitrogen) and imaged using AKOYA Phenoimager. Spectral unmixing was performed online with standard library provided by AKOYA Version 2.0 onwards and unmixed images were analysed using Qupath version 0.5 onwards. The following primary antibodies were used: hypusine (EMD Millipore, ABS1064, 1:50 dilution for mouse tissues, 1:75 dilution for human tissues), phosphorylated SMAD3 (S423 + S425) (Abcam, EP823Y, 1:100 dilution), phosphorylated CREB (Ser133) (Cell Signaling

Technologies, 9198S, 1:200), DOHH (Sigma-Aldrich, HPA041953, 1:300 dilution), GRIN2D (Novus Biological, NBP2-94573, 1:300 dilution), PanCK (Dako, M3515, 1:200 dilution), EPCAM (Abcam, Ab71916, 1:1,000 dilution), collagen I (Cell Signaling Technologies, E8F4L XP 1:300), collagen VI (Abcam, Ab182744, 1:1,000 dilution) and for membrane stain detection ATP1A1 (Proteintech, 14418-1-ap 1:200 dilution) and Wheat Germ Agglutinin, HRP Conjugate (Biotium, 29073, 1 μg ml^{-1}). For image analysis, metastases were detected using EPCAM for mouse tissue and PanCK for human tissue, followed by the analysis of staining for hypusine, DOHH, phosphorylated SMAD3, COL6A1, GRIN2D, phosphorylated CREB and COL1A1.

For mouse tissue, quantification for hypusine, DOHH, phosphorylated SMAD3, GRIN2D and phosphorylated CREB was performed by determining the mean fluorescence intensity per unit area across five independent regions (all EPCAM-positive), or as percentage of positive cells (only for DOHH and hypusine) per region in five different metastases. For COL6A1 and COL1A1, which can be secreted and accumulated in surrounding EPCAM-positive areas, quantification was performed by determining the mean fluorescence intensity per unit area across five independent regions (including EPCAM-positive area and closely surrounding area). If blood vessel and tissue borders were present in the selected area, COL1A1 and COL6A1 signals resulting from those endogenously high-collagen regions were excluded from the analysis. The following multiplex combinations were performed: (1) GRIN2D, membrane marker, phosphorylated CREB, EPCAM and COL1A1; and (2) DOHH, hypusine, phosphorylated SMAD3, COL6A1 and EPCAM.

For human tissue, quantification for hypusine, DOHH, phosphorylated SMAD3, GRIN2D and phosphorylated CREB was performed by determining the fluorescence intensity per cell (hypusine, DOHH and GRIN2D) or per nucleus (phosphorylated SMAD3 and phosphorylated CREB) across five independent regions for each metastatic (PanCK positive) or adjacent tissue. Statistical analysis was performed based on fluorescence intensity values per single cell. For COL6A1 and COL1A1, which can be secreted and accumulated in surrounding PanCK positive areas, quantification was performed by determining the mean fluorescence intensity per unit area across five independent regions for each metastatic (PanCK positive) or adjacent tissue. Statistical analysis was performed based on fluorescence intensity values per unit area. If blood vessel and tissue borders were present in the selected area, COL1A1 and COL6A1 signals resulting from those endogenously high-collagen regions were excluded from the analysis. For representative images visualization, fluorescent tissue background was subtracted using the intensity values of the autofluorescent channel obtained during tissue scanning in the AKOYA Phenoimager. Representative images from participants quantified in Extended Data Fig. 5c and corresponding H&E staining of the whole lung sections are shown in Fig. 5e and Extended Data Fig. 6.

Mass spectrometry

Polar metabolites were analysed by gas chromatography or liquid chromatography mass spectrometry. For polar metabolites measurements analysed by gas chromatography, dried metabolites samples were derivatized as previously described[9]. Isotopologue distributions and metabolite concentrations were measured using a 7890A gas chromatography system (Agilent Technologies) combined with a 5975C Inert MS System (Agilent Technologies) or a 8860 gas chromatography system combined with a 5977C Inert MS System (Agilent Technologies). The inlet temperature was set at 270 °C and 1 μl of sample was injected into a DB35MS column with a split ratio of 1:1, 3:1 or 9:1. The carrier gas flow of helium was fixed at 1 ml min^{-1}. After the injection, the gas chromatography oven was kept at 100 °C for 1 min, increased up to 105 °C with a gradient of 2.5 °C min^{-1} for 2 min, then ramped to 240 °C with a gradient of 3.5 °C min^{-1}, and after that ramped up to 320 °C with a gradient of 22 °C min^{-1}, which was followed by 4 min at 320 °C for 2 min. Mass spectrometry was performed at 70 eV and a mass range of 150–650 atomic mass units was measured. Data was collected using MSD Chemstation Data Analysis software. Metabolites abundances and isotopologue distributions were extracted from raw chromatograms, corrected for naturally occurring isotopes and normalized to the internal standard and protein content (for cell extracts) or volume (for fluid extracts) with a MATLAB script. A standard curve for each metabolite was used to calculate polar metabolite concentrations. The various standard curve dilutions were extracted and run in parallel with the sample. For polar metabolite measurements analysed by liquid chromatography–mass spectrometry, a 1290 Infinity II with a thermal autosampler set at 4 °C, coupled to a Q-TOF 6546 mass spectrometer (Agilent Technologies) or a Dionex UltiMate 3000 LC System (Thermo Scientific) coupled to a Q Exactive Focus Orbitrap mass spectrometer (Thermo Scientific) were used. Dried metabolites sample were resuspended in 80% methanol:water and a volume of 1–10 μl of sample was injected into an Agilent InfinityLab Poroshell 120 HILIC-Z column, 2.1 mm × 150 mm, 2.7 μm, PEEK-lined or injected into an IHILIC Fusion (P). For positive mode analysis, the separation of metabolites was achieved at 25 °C with a flow rate of 0.25 ml min^{-1}. A gradient was applied for 23 min (solvent A: 10 mM ammonium formate in water with 0.1% formic acid; solvent B: 10 mM ammonium formate in water/acetonitrile 10:90 (v:v) with 0.1% formic acid) to separate the targeted metabolites (0 min: 98% B, 3 min: 98% B, 11 min: 70% B, 12 min: 60% B, 16 min: 5% B, 18 min: 5% B, 19 min: 98% B; 23 min: 98% B). The mass spectrometer was operated in positive full scan mode (*m*/*z* range: 50–1,200) using a sheath gas temperature of 225 °C (10 l min^{-1}) and a gas temperature at 225 °C (6 l min^{-1}). The nebulizer was set at 40 psi, the fragmentor at 125 V and the capillary at 3,000 V. For negative mode analysis, the separation of metabolites was achieved at 50 °C with a flow rate of 0.25 ml min^{-1}. A gradient was applied for 32 min (solvent A: 10 mM ammonium acetate in water with 2.5 μM InfinityLab Deactivator Additive, pH 9 – solvent B: 10 mM ammonium acetate in water/acetonitrile 15:85 (v:v) with 2.5 μM InfinityLab Deactivator Additive, pH 9 or 15 mM ammonium acetate in water/acetonitrile 15:85 (v:v) with 2.5 μM InfinityLab Deactivator Additive, pH 9) to separate the targeted metabolites (0 min: 96% B, 2 min: 96% B, 5.5 min: 88% B, 8.5 min: 88% B, 9 min: 86% B, 14 min: 86% B, 19 min: 82% B; 25 min: 65% B, 27 min: 65% B, 28 min: 96% B; 32 min: 96% B). The mass spectrometer operated in negative full scan mode (*m*/*z* range: 50–1,200) using a sheath gas temperature of 350 °C (12 l min^{-1}) and a gas temperature at 225 °C (13 l min^{-1}). The nebulizer was set at 35 psi, the fragmentor at 125 V and the capillary at 3,500 V. For the detection of metabolites using the Q Exactive Focus, a gradient was applied for 35 min with a flow rate of 0.2 ml min^{-1} (solvent A: acetonitrile; solvent B: 10 mM NH_4-formate in water, pH 9.4) to separate the targeted metabolites (0 min: 10% B, 2 min: 10% B, 20 min: 80% B, 23 min: 80% B, 25 min: 40% B, 27 min: 10% B, 35 min: 10% B). The MS was operated in negative full scan mode (*m*/*z* range: 50–1,200). Data were collected using the MassHunter Workstation LC/MS Data Acquisition v.10.1 Build 10.1.48 (Agilent Technologies) or XCalibur v.4.1.31.9 (Thermo Scientific) and were analysed using the Agilent MassHunter Workstation Profinder v.10.0.2. build 10.0.2.162. Data were normalized to internal standard and protein content (for cell extracts).

In silico human gene expression data analysis

To compare gene expression profiles in patient-derived breast cancer metastases at different organ sites, we downloaded the microarray-based dataset GSE14018[51] from the Gene Expression Omnibus (GEO) using the R package GEOquery (v2.62.2). Data for probes with undefined gene symbols or with ambiguous gene assignments (that is, annotated to multiple different genes) were filtered out before further analysis. Among the remaining probes, those presenting duplicated gene symbols were further collapsed into single probes, by preserving only those probes with the highest overall expression levels for each

duplicated gene symbol. A total of 12,502 probes were considered in the final analysis after these filters. Differential expression analysis was performed based on the provided RMA-normalized expression levels for these probes, using the R package limma[52] (v3.50.1) (https://bioinf.wehi.edu.au/limma), and comparing expression levels in 16 lung samples versus 20 samples from all other metastatic sites available in the dataset (5 liver, 8 bone, and 7 brain samples, all considered together). The resulting (lung versus other) log fold changes (log_2FC) and their associated *P* values were then combined to derive a ranking metric $RM = -log_2FC \times log_{10}(P\,value)$, whereby highly positive or negative values of RM indicate respectively genes with highly up or downregulated expression in lung versus all other metastatic sites. Pre-ranked GSEA was then performed analogously as described in 'Polysome profiling and sequencing analysis', only based on this ranking metric RM and considering human gene sets.

Statistical analysis

Statistical data analysis was performed using GraphPad Prism v.9 and v.10 (GraphPad Software) or within the R/Bioconductor framework on $n \geq 3$ biologically independent replicates. Data are presented as mean ± s.d, mean ± s.e.m. or median ± 95% confidence interval, as indicated in the figure legends. Details on statistical tests and post hoc tests are indicated in the legends, and non-significant comparisons are not shown. *P* values $< 10^{-4}$ are indicated as $P < 0.0001$. Mathematical outliers were determined using the Grubbs' or ROUT method of regression (GraphPad) with alpha = 0.05 or coefficient $Q = 1\%$. Independent experiments were pooled and analysed together whenever possible as described in the figure legends. For in vivo experiments, mice were randomized before control or TSF injection and PBS or aspartate injection or injection with the different cell lines. Mice were assigned to unique number before data collection for blinded analysis. For in vitro studies, samples were randomized when possible before data acquisition.

Materials availability

This study did not generate new unique reagents, except of genetically manipulated cell lines based on commercially available constructs. Reagents generated in this study will be made available on request through the lead author or the collaboration partner that generated the resource, but we may require a payment and/or a completed Materials Transfer Agreement if there is potential for commercial application.

Reporting summary

Further information on research design is available in the Nature Portfolio Reporting Summary linked to this article.

Data availability

Mouse single-cell RNA-sequencing data and polysome and total RNA sequencing data generated as part of this study have been deposited in the Gene Expression Omnibus (GEO) under accession GSE236087. The publicly available microarray-based patient-metastasis dataset GSE1401882 can be downloaded from the GEO under accession GSE14018. All other data supporting the findings of this study are available within the Article and the supplementary information, and from the corresponding author on reasonable request. Source data are provided with this paper.

Code availability

No original software and/or algorithms were developed in the present study; however, code used for data analysis can be provided upon request. Any additional information required to reanalyse the data reported in this paper is available from the corresponding author upon request.

28. van Gorsel, M., Elia, I. & Fendt, S. M. ^{13}C tracer analysis and metabolomics in 3D cultured cancer cells. *Methods Mol. Biol.* **1862**, 53–66 (2019).
29. Schmidt, E. K., Clavarino, G., Ceppi, M. & Pierre, P. SUnSET, a nonradioactive method to monitor protein synthesis. *Nat. Methods* **6**, 275–277 (2009).
30. Delaunay, S. et al. Elp3 links tRNA modification to IRES-dependent translation of LEF1 to sustain metastasis in breast cancer. *J. Exp. Med.* **213**, 2503–2523 (2016).
31. Liang, S. et al. Polysome-profiling in small tissue samples. *Nucleic Acids Res.* **46**, e3 (2018).
32. Love, M. I., Huber, W. & Anders, S. Moderated estimation of fold change and dispersion for RNA-seq data with DESeq2. *Genome Biol.* **15**, 550 (2014).
33. Stephens, M. False discovery rates: a new deal. *Biostatistics* **18**, 275–294 (2017).
34. Subramanian, A. et al. Gene set enrichment analysis: a knowledge-based approach for interpreting genome-wide expression profiles. *Proc. Natl Acad. Sci. USA* **102**, 15545–15550 (2005).
35. Korotkevich, G. et al. Fast gene set enrichment analysis. Preprint at *bioRxiv* https://doi.org/10.1101/060012 (2021).
36. Liberzon, A. et al. Molecular signatures database (MSigDB) 3.0. *Bioinformatics* **27**, 1739–1740 (2011).
37. Liberzon, A. et al. The Molecular Signatures Database (MSigDB) hallmark gene set collection. *Cell Syst.* **1**, 417–425 (2015).
38. Kanehisa, M. & Goto, S. KEGG: Kyoto Encyclopedia of Genes and Genomes. *Nucleic Acids Res.* **28**, 27–30 (2000).
39. Christen, S. et al. Breast cancer-derived lung metastases show increased pyruvate carboxylase-dependent anaplerosis. *Cell Rep.* **17**, 837–848 (2016).
40. Rinaldi, G. et al. In vivo evidence for serine biosynthesis-defined sensitivity of lung metastasis, but not of primary breast tumors, to mTORC1 inhibition. *Mol. Cell* **81**, 386–397 e387 (2021).
41. Parik, S. et al. GBM tumors are heterogeneous in their fatty acid metabolism and modulating fatty acid metabolism sensitizes cancer cells derived from recurring GBM tumors to temozolomide. *Front. Oncol.* **12**, 988872 (2022).
42. Hao, Y. et al. Integrated analysis of multimodal single-cell data. *Cell* **184**, 3573–3587 e3529 (2021).
43. Young, M. D. & Behjati, S. SoupX removes ambient RNA contamination from droplet-based single-cell RNA sequencing data. *Gigascience* **9**, giaa151 (2020).
44. Janssen, P. et al. The effect of background noise and its removal on the analysis of single-cell expression data. *Genome Biol.* **24**, 140 (2023).
45. Cao, J. et al. The single-cell transcriptional landscape of mammalian organogenesis. *Nature* **566**, 496–502 (2019).
46. McInnes, M., Healy, J. & Melville, J. UMAP: uniform manifold approximation and projection for dimension reduction. Preprint at *arXiv* https://doi.org/10.48550/arXiv.1802.03426 (2018).
47. Blondel V. D., Guillaume J.-L., Lambiotte R. & Lefebvre E. Fast unfolding of communities in large networks. *J. Stat. Mech.* https://doi.org/10.1088/1742-5468/2008/10/P10008 (2008).
48. Germain, P.-L., Lun, A., Garcia Meixide, C., Macnair, W. & Robinson, M. D. Doublet identification in single-cell sequencing data using scDblFinder. *F1000Research* **10**, 979 (2022).
49. Denis, J. F. et al. Activation of Smad2 but not Smad3 is required to mediate TGF-β signaling during axolotl limb regeneration. *Development* **143**, 3481–3490 (2016).
50. Vennin, C. et al. Transient tissue priming via ROCK inhibition uncouples pancreatic cancer progression, sensitivity to chemotherapy, and metastasis. *Sci. Transl. Med.* **9**, eaai8504 (2017).
51. Fridlender, Z. G. et al. Polarization of tumor-associated neutrophil phenotype by TGF-beta: "N1" versus "N2" TAN. *Cancer Cell* **16**, 183–194 (2009).
52. Ritchie, M. E. et al. limma powers differential expression analyses for RNA-sequencing and microarray studies. *Nucleic Acids Res.* **43**, e47 (2015).

Acknowledgements The authors thank J. Lamote and S. Vinckier for providing advice and expertise for flow cytometry and for microscopy experiments; N. Hersmus and N. Peredo for digital PCR support and for imaging video annotations; all physicians from the Multidisciplinary Breast Center Leuven for their clinical contribution to the UPTIDER cohorts; and the whole UPTIDER team and all the patients who agreed to donate tissues postmortem. We acknowledge the members of the Laboratory of Cellular Metabolism and Metabolic Regulation (VIB-KU Leuven) for performing blinded analysis of several H&E and picrosirius red staining experiments shown. We apologize to all colleagues whose work we could not cite owing to space restrictions. The figures present in Extended Data Fig. 1c (agreement number: YZ27DAESEJ), Extended Data Fig. 1h (agreement number: LJ27DAFBLZ) and Fig. 5g (agreement number: OF27DLNP8H) were created in BioRender.com. The work conducted in the Leibniz-Institut für Analytische Wissenschaften – ISAS – e.V. was supported by the "Ministerium für Kultur und Wissenschaft des Landes Nordrhein-Westfalen" and "Der Regierende Bürgermeister von Berlin, Senatskanzlei Wissenschaft und Forschung", and was further supported by the Bundesministerium für Bildung und Forschung, BMBF. G.D. and J.F.-G. received funding from Research Foundation Flanders (FWO) PhD (11E9520N) and senior postdoctoral fellowships (12V9620N). G.D. has previously received funding from Kom op tegen Kanker and J.F.-G. previously received an FWO junior fellowship. S.I. received funding from EMBO postdoctoral fellow (ALTF 13-2022) and from Research Foundation Flanders (FWO) junior postdoctoral fellowship (1266225N). P.A.-M. was supported by a Marie Sklodowska-Curie Actions individual fellowship (MSCA-IF-2018-839896) and has received funding from European Union (ERC-StG-101116912) and Beug Foundation. X.-Z.L. received sequential funding from EMBO postdoctoral fellowship (ALTF 401-2022), the Gilead Sciences Research Scholars Program in Solid Tumors and Research Foundation Flanders (FWO) junior postdoctoral fellowship (1231025N). Y.L. received a Chinese Scholarship Council fellowship. M.R. has been an FWO and Stichting tegen Kanker fellow. G.F. is recipient of a post-doctoral fellowship sponsored by the KOOR from the University Hospitals Leuven. The UPTIDER programme is supported by a grant from the University Hospitals from Leuven (KOOR 2021), as well as a C1 grant (14/21/114) from KU Leuven. P.C. acknowledge the Belgian Foundation for Cancer Research (2020-068). G.B. acknowledges funding from Research Council KU Leuven (C14/19/099 and AKUL/19/34) and from the Research Foundation Flanders (G094522N) and coordinates an FWO research network (WOG) on 'Ca^{2+}

signalling in health, disease and therapy' (CaSign; W001422N). J.-C.M. received funding from Stichting Tegen Kanker (#2022-178) and FWO (G045824N and G0C5320N). H.F.A. together with S.-M.F. has received funding from the King Baudouin Foundation and H.F.A. was a Stichting tegen Kanker fellow. S.-M.F. acknowledges funding from FWO Project G011724N, Beug Foundation, Fonds Baillet Latour, Francqui Stichting, Foundation ARC, KU Leuven, Stichting tegen Kanker and Interuniversity BOF (iBOF) programme.

Author contributions Concept and design: G.D. and S.-M.F. Development of methodology: G.D., S.I., P.A.-M., A.B., R.L.R., M.N., T.T. and P.K. Acquisition of data (including providing animals, acquiring and managing patient samples and providing facilities): G.D., S.I., P.A.-M., A.B., Y.L., M.N., N.A., P.K., Y.-H.H., F.A.S., L.M.N.M., G.A., A. Scopelliti, M.R., I.V., A.M.F.C., P.N., M.M., K.V.B., M.P., G.F., A. Sickmann, J.-C.M., C.L.G.J.S., C.D. and P.C.. Analysis and interpretation of data (including statistical analysis, biostatistics and computational analysis): G.D., J.F.-G., S.I., P.A.-M., R.L.R., M.N., M.L., M.P., A.M.F.C., A.T., G.B. and S.-M.F. Writing, review and/or revision of the manuscript: G.D., T.T. and S.-M.F. Administrative, technical or material support (reporting or organizing data and constructing databases): G.D., J.F.-G., S.E.K., X.-Z.L., T.T., I.V. and D.B. Funding acquisition: G.D., H.F.A. and S.-M.F. Study supervision: S.-M.F.

Competing interests S.-M.F. has received funding from BlackBelt Therapeutics, Auron Therapeutics, Gilead and Alesta Therapeutics, is on the advisory board of Alesta Therapeutics and has consulted for Fund+ and Droia Ventures. The other authors declare no competing interests.

Additional information

Supplementary information The online version contains supplementary material available at https://doi.org/10.1038/s41586-024-08335-7.

Correspondence and requests for materials should be addressed to Sarah-Maria Fendt.

Peer review information *Nature* thanks the anonymous reviewer(s) for their contribution to the peer review of this work.

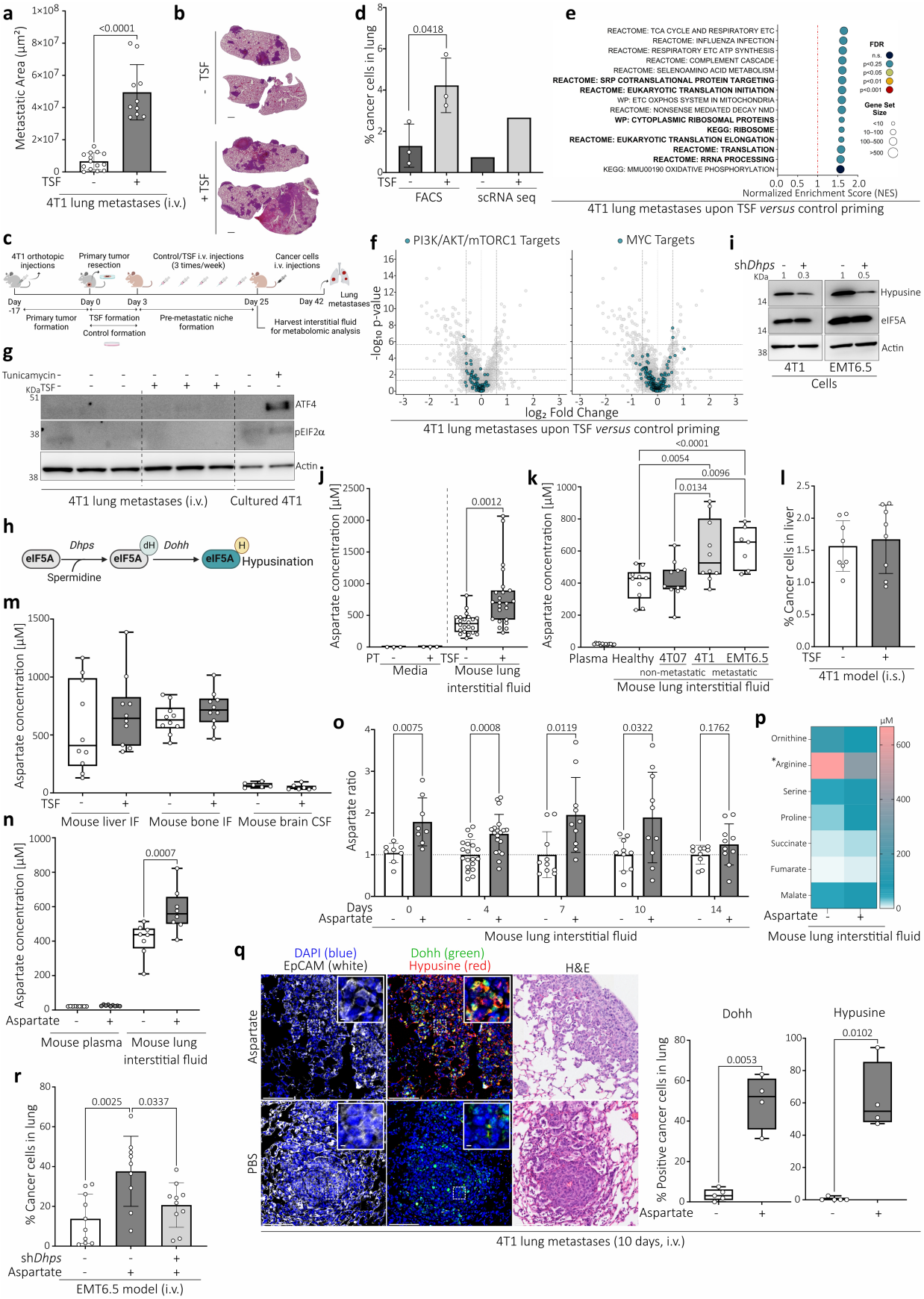

Extended Data Fig. 1 | See next page for caption.

Extended Data Fig. 1 | Aggressive lung metastases display increased translation independent of classical regulators or stress stimuli. a. Total lung metastatic area 17 days after i.v. injections with 4T1 cells in mice pre-treated with tumor secreted factors (TSFs, $n = 10$) or control medium ($n = 14$). Data are presented as mean ± sd. Unpaired two-tailed *t*-test with Welch correction. Representative images are depicted in **b. b**. Representative H&E stainings from **a**., two individual lung lobes from one mouse each were selected with automatic tissue detection algorithm in Zen Software and pasted in a white background, scale bars = 1 mm. **c**. Schematic representation of the pre-metastatic niche formation and lung metastasis model. TSFs, Tumor secreted factors; i.v., intravenous injection. Created with BioRender.com. **d**. Percentage of cancer cells present in the lung 16 days after i.v. injection with CD90.1$^+$ 4T1 cells in mice pre-treated with TSFs or control medium, measured by flow cytometry (FACS, $n = 3$ mice) and scRNA-seq (pool of $n = 3$ mice). FACS data are presented as mean ± s.d. Unpaired two-tailed *t*-test with Welch correction. **e**. GSEA normalized enrichment scores (NES) for the top 15 upregulated gene sets found on cancer cells based on scRNA-seq comparing 4T1 lung metastases from mice pre-treated with control medium or TSFs. Dot colors and areas indicate FDR-adjusted *P*-values and gene-set sizes, respectively. Gene sets related to translation are highlighted in bold. *P*-values based on *fgsea*'s adaptive multilevel splitting Monte Carlo approach, subject to FDR adjustment using the Benjamini-Hochberg (BH) approach. **f**. Volcano plots based on single-cell differential expression analysis comparing cancer cells in 4T1 lung metastases from mice pre-treated with control medium or TSFs. All genes in the Hallmark PI3K-AKT-MTOR signaling gene set (left) and either of the Hallmark MYC targets (V1/V2) gene sets (right) are highlighted in blue. Log_2 Fold Changes (FC) and negative log_{10}-transformed *P*-values are indicated in the x and y axes respectively. The horizontal dashed lines represent (from bottom to top) raw, BH-adjusted and Bonferroni adjusted *P*-values of 0.05, while the vertical ones represent absolute fold-changes of 1.5. *P*-values based on Seurat's Wilcoxon rank-sum test implementation. **g**. ATF4 and phosphorylated eIF2α levels in 4T1 lung metastases in mice pre-treated with TSFs ($n = 3$) or control medium ($n = 3$), and in cultured 4T1 cells treated with or without tunicamycin induced ER-stress. **h**. Schematic representation of eIF5A hypusination pathway. Enzymes are indicated in italics. Solid lines represent single reactions. dH = deoxyhypusine; H = hypusine. Created with BioRender.com. **i**. Hypusine levels in 4T1 (left) or EMT6.5 (right) cells silenced for *Dhps* or scramble shRNA. Quantification of hypusine signal normalized over total eIF5A signal is indicated on top of each lane. **j**. Box and whisker plots of aspartate concentrations in control- or primary tumor (PT)-conditioned medium and lung interstitial fluid of mice pre-treated with TSFs ($n = 23$) or control medium ($n = 22$). Box hinges indicate the 1st/3rd quartiles of the corresponding data, while box mid-lines represent medians, and whiskers span the range of the data. Individual data points are indicated by the white dots. One-way ANOVA ($P < 0.0001$) with Tukey's multiple-comparison tests. **k**. Box and whisker plots of aspartate concentrations in the blood plasma and lung interstitial fluid of healthy mice or mice injected (m.f.p.) with 4T07, 4T1 or EMT6.5 breast cancer cells, 17 days after injection (plasma, $n = 13$; healthy, $n = 10$; 4T07, $n = 11$; 4T1, $n = 10$; EMT6.5, $n = 7$). Box hinges indicate the 1st/3rd quartiles of the corresponding data, while box mid-lines represent medians, and whiskers span the range of the data. Individual data points are indicated by the white dots. One-way ANOVA ($P < 0.0001$) with Tukey's multiple-comparison tests; $P < 0.0001$ between plasma and all lung interstitial fluid conditions. **l**. Percentage of cancer cells present in the liver 14 days after intrasplenic (i.s.) injections with CD90.1$^+$ 4T1 cells in mice pre-treated with TSFs ($n = 8$) or control medium ($n = 8$). Data are presented as mean ± sd. Unpaired two-tailed *t*-test with Welch correction. I.s. injection of 4T1 cancer cells did not yield a change in liver metastases in TSF-treated mice compared to control mice. **m**. Box and whisker plots of aspartate concentrations in the liver and bone interstitial fluid and brain cerebrospinal fluid of mice pre-treated with TSFs or control medium (liver, $n = 10$ control, $n = 10$ TSFs; bone, $n = 10$ control, $n = 10$ TSFs; brain, $n = 6$ control, $n = 7$ TSFs). Box hinges indicate the 1st/3rd quartiles of the corresponding data, while box mid-lines represent medians, and whiskers span the range of the data. Individual data points are indicated by the white dots. Two-way ANOVA with Šídák's multiple-comparison tests. No statistically significant changes are observed upon TSF treatment for any of the organs. **n**. Box and whisker plots of aspartate concentrations in the blood plasma and lung interstitial fluid of mice pre-treated with daily injections of aspartate (20 mM, i.p., 10 days, $n = 8$) or PBS ($n = 8$). Box hinges indicate the 1st/3rd quartiles of the corresponding data, while box mid-lines represent medians, and whiskers span the range of the data. Individual data points are indicated by the white dots. Two-way ANOVA with Tukey's multiple-comparison tests; $P < 0.0001$ between all plasma and all lung interstitial fluid conditions, no statistically significant changes are observed upon aspartate treatment in blood plasma. **o**. Ratio of aspartate concentrations in the lung interstitial fluid of mice pre-treated with daily injections of aspartate (20 mM, i.p., 10 days) *vs* PBS. Days indicate the time of interstitial fluid collection after the last injection of aspartate or PBS. Data are presented as mean ± sd. Unpaired two-tailed *t*-test with Welch correction at each time point. **p**. Average metabolite concentrations in the lung interstitial fluid of mice pre-treated with daily injections of aspartate (20 mM, i.p., 10 days, $n \geq 8$) or PBS ($n \geq 8$). * indicates $P = 0.00174$. All other metabolites show no statistically significant changes. Unpaired two-tailed *t*-test with Welch correction between PBS-treated and aspartate-treated mice. **q**. Hypusine and Dohh detected in lung metastases 10 days after i.v. injections with 4T1 cancer cells, in mice pre-treated with daily injections of aspartate (20 mM, i.p., 10 days) or PBS, assessed by multiplex immunohistochemistry. Left: representative images from $n = 5$ 4T1 PBS, $n = 4$ 4T1 aspartate independent mice are shown. White = EpCAM; red = Hypusine; green = Dohh; blue = DAPI nuclear staining. Scale bars = 100 µm. Scale bars zoom-in = 5 µm. The corresponding H&E staining is represented on the right of the panel. Right: quantification of lung metastasis cells positive for Dohh or Hypusine. Box hinges indicate the 1st/3rd quartiles of the corresponding data, while box mid-lines represent medians, and whiskers span the range of the data. Individual data points are indicated by the white dots. Unpaired two-tailed *t*-test with Welch correction. **r**. Percentage of cancer cells present in the lung 14 days after i.v. injections with CD90.1$^+$ EMT6.5 cells silenced for *Dhps* or scramble shRNA in mice pre-treated with daily injections of aspartate (20 mM, i.p., 10 days) or PBS. $N = 10$ sh*Scr* PBS, $n = 9$ sh*Scr* aspartate, $n = 10$ sh*Dhps* aspartate. Data are presented as mean ± sd. One-way ANOVA ($P = 0.0029$) with Tukey's multiple-comparison tests.

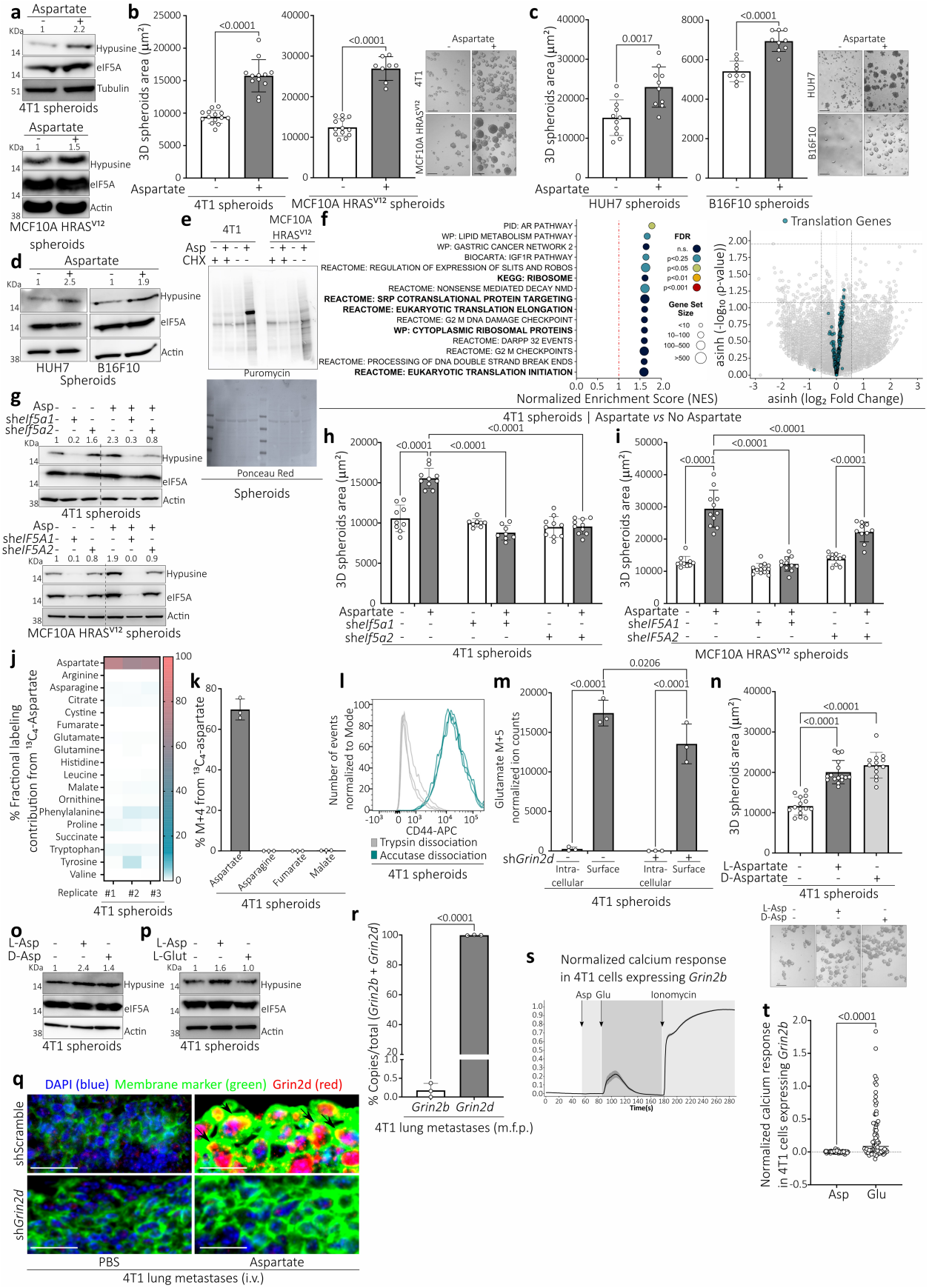

Extended Data Fig. 2 | See next page for caption.

Extended Data Fig. 2 | Pulmonary aspartate increases lung metastasis aggressiveness via NMDA receptor activity. a. Hypusine levels in 4T1 (top) and MCF10A HRAS^{V12} (bottom) spheroids grown in lung-like medium (LLM) supplemented with or without aspartate. A representative image of $n = 3$ independent experiments is shown. Quantification of hypusine signal normalized over total eIF5A signal is indicated on top of each lane. **b**. Total spheroid areas for 4T1 (left) and MCF10A HRAS^{V12} (right) cells grown in LLM supplemented with or without aspartate ($n = 14$ 4T1 no aspartate, $n = 13$ MCF10A HRAS^{V12} no aspartate, $n = 12$ 4T1 aspartate, $n = 8$ MCF10A HRAS^{V12} aspartate). Data are presented as mean ± s.d. (*n* indicates independent samples). Unpaired two-tailed *t*-test with Welch correction. Representative images are shown on the right. Scale bar = 250 µm. **c**. Total spheroid areas for HUH7 (left) and B16F10 (right) cells grown in LLM supplemented with or without aspartate. $N = 11$ HUH7 no aspartate, $n = 9$ B16F10 no aspartate, $n = 10$ HUH7 aspartate, $n = 9$ B16F10 aspartate. Data are presented as mean ± s.d. (*n* indicates independent samples). Unpaired two-tailed *t*-test with Welch correction. Representative images are shown on the right. Scale bar = 250 µm. **d**. Hypusine levels in HUH7 (left) and B16F10 (right) spheroids grown in LLM supplemented with or without aspartate. A representative image of $n = 3$ independent experiments is shown. Quantification of hypusine signal normalized over total eIF5A signal is indicated on top of each lane. **e**. Top: SUnSET assay showing puromycin incorporation in 4T1 and MCF10A HRAS^{V12} spheroids grown in LLM supplemented with or without aspartate. Spheroids were treated with cycloheximide (CHX, 100 nM) or vehicle, followed by puromycin (10 µg/ml). Bottom: Ponceau red staining showing equal protein loading. **f**. Left: GSEA normalized enrichment scores (NES) for the top 15 upregulated gene sets based on total RNA sequencing data for 4T1 spheroids grown in LLM supplemented with aspartate *vs* no aspartate. Dot colors and areas indicate FDR-adjusted *P*-values and gene-set sizes, respectively. Gene sets related to translation are highlighted in bold. Right: Volcano plot based on differential expression analysis of total RNA sequencing data for 4T1 spheroids grown in LLM supplemented with or without aspartate. Genes in Reactome's translation gene set are highlighted in blue. Log_2 Fold Changes (FC) and negative log_{10}-transformed *P*-values are indicated in the x and y axes respectively. Both axes were further subject to inverse hyperbolic sine transformation for improved visualization. The horizontal dashed lines represent (from bottom to top) raw and BH-adjusted *P*-values of 0.05, while the vertical ones represent absolute fold-changes of 1.5. *P*-values based on *fgsea*'s adaptive multilevel splitting Monte Carlo approach, subject to FDR adjustment using the Benjamini-Hochberg (BH) approach. **g**. Hypusine levels in 4T1 (top) and MCF10A HRAS^{V12} (bottom) spheroids silenced for *eIf5a1*, *eIf5a2*, or scramble shRNA, grown in LLM supplemented with or without aspartate. A representative image of $n = 3$ independent experiments is shown. Quantification of hypusine signal normalized over actin signal is indicated on top of each lane. **h**. Total spheroid areas for 4T1 cells silenced for *eIf5a1* ($n = 8$ 4T1 no aspartate, $n = 8$ 4T1 aspartate), *eIf5a2* ($n = 10$ 4T1 no aspartate, $n = 10$ 4T1 aspartate) or scramble shRNA ($n = 9$ 4T1 no aspartate, $n = 10$ 4T1 aspartate), grown in LLM supplemented with or without aspartate. Data are presented as mean ± s.d. (*n* indicates independent samples). Two-way ANOVA with Tukey's multiple-comparison tests. **i**. Total spheroid areas for MCF10A HRAS^{V12} cells silenced for *eIF5a1* ($n = 12$ MCF10A HRAS^{V12} no aspartate, $n = 11$ MCF10A HRAS^{V12} aspartate), *eIF5a2* ($n = 11$ MCF10A HRAS^{V12} no aspartate, $n = 10$ MCF10A HRAS^{V12} aspartate) or scramble shRNA ($n = 10$ MCF10A HRAS^{V12} no aspartate, $n = 11$ MCF10A HRAS^{V12} aspartate), grown in LLM supplemented with or without aspartate. Data are presented as mean ± s.d. (*n* indicates independent samples). Two-way ANOVA with Tukey's multiple-comparison tests. **j**. $^{13}C_4$-labeled fractions for various metabolites downstream of aspartate (included) in 4T1 spheroids ($n = 3$) grown in LLM supplemented with $^{13}C_4$-aspartate. Data are presented as mean ± s.d. A representative graph of $n = 3$ experiments is shown. **k**. Average fractions of total carbon corresponding to ^{13}C isotopes in different metabolites, in 4T1 spheroids ($n = 3$) grown in LLM supplemented with $^{13}C_4$-aspartate. **l**. Histograms of CD44 surface expression in 4T1 spheroids dissociated with Trypsin ($n = 3$) or Accutase ($n = 3$). Data are normalized to mode (y axis is scaled so that the maximum of each curve is at 100) and further smoothed for display purposes. **m**. Intracellular *vs* cell surface levels of ^{13}C-glutamate in 4T1 spheroids silenced for *Grin2d* ($n = 3$) or scramble shRNA ($n = 3$), grown in LLM supplemented with $^{13}C_5$-glutamate. Data are presented as mean ± s.d. (*n* indicates independent samples). Two-way ANOVA with Tukey's multiple-comparison tests. **n**. Total spheroid areas for 4T1 cells grown in LLM supplemented with or without L- or D-aspartate. $N = 15$ no aspartate, $n = 16$ L-aspartate, $n = 13$ D-aspartate. Data are presented as mean ± s.d. (*n* indicates independent samples). One-way ANOVA ($P < 0.001$) with Tukey's multiple-comparison tests. Representative images are shown on the bottom. Scale bar = 250 µm. **o**. Hypusine levels in 4T1 spheroids grown in LLM supplemented with or without L- or D-aspartate. A representative image of $n = 3$ experiments is shown. Quantification of hypusine signal normalized over eIF5A signal is indicated on top of each lane. **p**. Hypusine levels in 4T1 spheroids grown in LLM supplemented with or without aspartate or glutamate. A representative image of $n = 3$ experiments is shown. Quantification of hypusine signal normalized over eIF5A signal is indicated on top of each lane. **q**. Grin2d detected in lung metastases 14 days after i.v. injections with 4T1 cancer cells, in mice pre-treated with daily injections of aspartate (20 mM, i.p., 10 days) or PBS, assessed by multiplex immunohistochemistry. Representative images from $n = 5$ 4T1 sh*Scr* PBS, $n = 5$ 4T1 sh*Scr* aspartate, $n = 5$ 4T1 sh*Grin2d* PBS, $n = 5$ 4T1 sh*Grin2d* aspartate independent mice are shown. Green = membrane marker ATP1A1; Red = Grin2d; Blue = DAPI nuclear staining. Scale bars = 25 µm. Arrows indicate membrane colocalization of Grin2d and ATP1A1. This staining is part of a multiplex staining and only relevant stains are shown. **r**. Relative fractions of *Grin2b* and *Grin2d* copies quantified by droplet digital PCR in 4T1 lung metastases, $n = 3$. Data are presented as mean ± s.d. (*n* indicates independent samples). Unpaired two-tailed *t*-test with Welch correction. **s**. Average ionomycin-normalized calcium response traces in 4T1 cells overexpressing *Grin2b*. The shaded ribbon represents standard error of the mean at each time point, while the grey rectangles indicate sequential addition of aspartate, glutamate and ionomycin at the times indicated by the arrows. A representative experiment ($n = 38$ cells) out of 2 independent experiments is shown. *Grin2b* overexpression stimulated a calcium response following glutamate but not aspartate addition in 4T1 cells. This shows that the NMDA receptor subunit expression determines the agonist to which breast cancer cells respond. **t**. Ionomycin-normalized calcium response upon sequential addition of aspartate and glutamate ($n = 79$ cells). Unpaired two-tailed *t*-test with Welch correction.

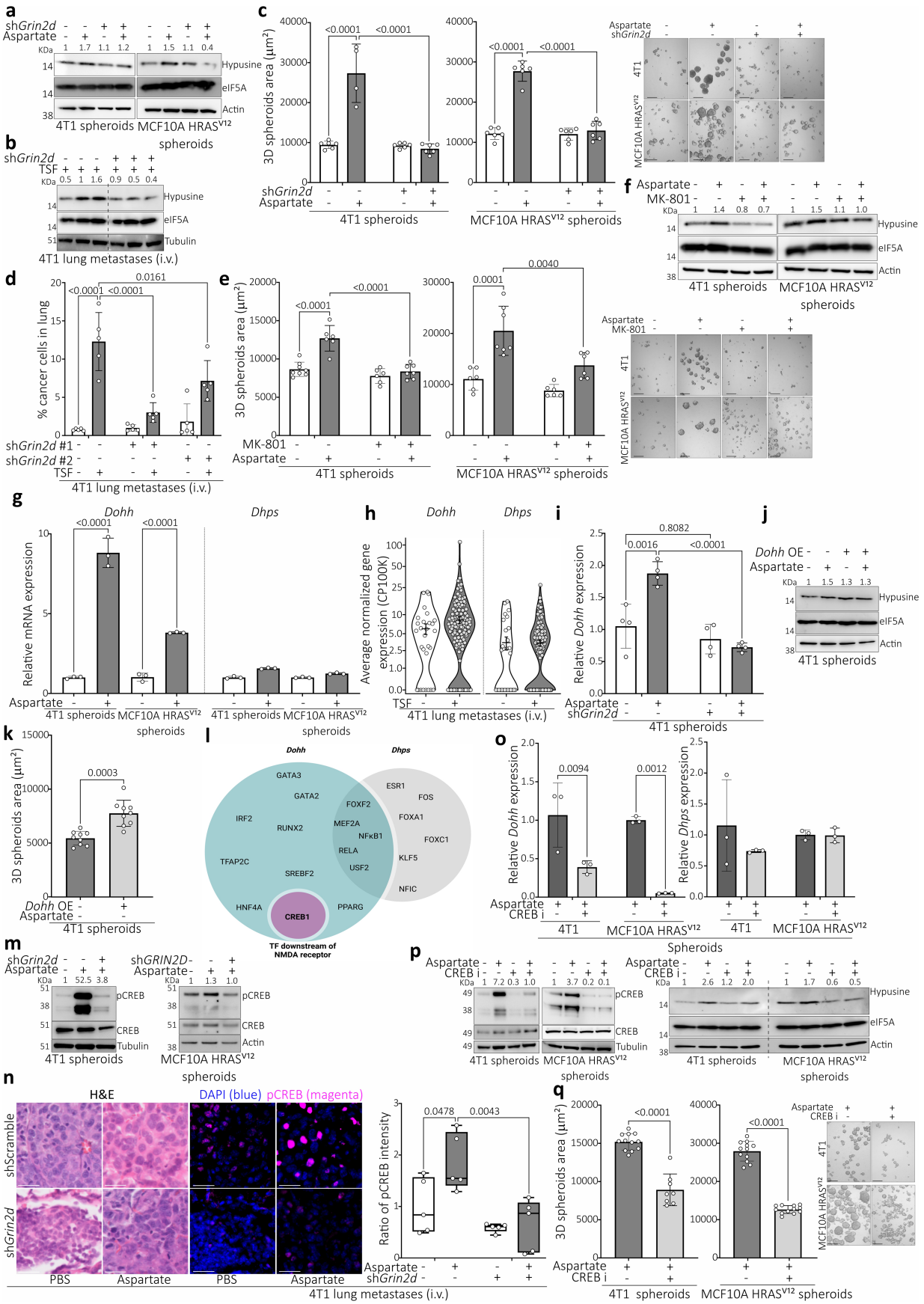

Extended Data Fig. 3 | See next page for caption.

Extended Data Fig. 3 | Aspartate-induced NMDA receptor activity promotes CREB phosphorylation. a. Hypusine levels in 4T1 (left) and MCF10A HRAS^{V12} (right) spheroids silenced for *Grin2d* or scramble shRNA, grown in lung-like medium (LLM) supplemented with or without aspartate. A representative image of $n = 3$ experiments is shown. Quantification of hypusine signal normalized over total eIF5A signal is indicated on top of each lane. **b**. Hypusine levels in 4T1 lung metastases silenced for *Grin2d* ($n = 3$) or scramble shRNA ($n = 3$) in mice pre-treated with tumor secreted factors (TSFs). Quantification of hypusine signal normalized over eIF5A signal is indicated on top of each lane. **c**. Total spheroid areas for 4T1 (left) and MCF10A HRAS^{V12} (right) cells silenced for *Grin2d* ($n = 6$ 4T1 no aspartate, $n = 6$ MCF10A HRAS^{V12} no aspartate, $n = 6$ 4T1 aspartate, $n = 6$ MCF10A HRAS^{V12} aspartate) or scramble shRNA ($n = 6$ 4T1 no aspartate, $n = 6$ MCF10A HRAS^{V12} no aspartate, $n = 4$ 4T1 aspartate, $n = 6$ MCF10A HRAS^{V12} aspartate), grown in LLM supplemented with or without aspartate. Data are presented as mean ± s.d. (n indicates independent samples). Two-way ANOVA with Tukey's multiple-comparison tests. Representative images are shown on the right. Scale bar = 250 µm. Data from the scramble group are the same as those in the scramble group from Fig. 2a. **d**. Percentage of cancer cells present in the lung 16 days after i.v. injections with CD90.1^{+} 4T1 cells silenced for *Grin2d* (with two different shRNA sequences) or scramble shRNA in mice pre-treated with TSFs or control medium ($n = 5$ 4T1 sh*Scr* control medium, $n = 5$ 4T1 sh*Scr* TSFs, $n = 5$ 4T1 sh*Grin2d*#1 control medium, $n = 5$ 4T1 sh*Grin2d*#1 TSFs, $n = 5$ 4T1 sh*Grin2d*#2 control medium, $n = 5$ 4T1 sh*Grin2d*#2 TSFs). Data are presented as mean ± sd. Two-way ANOVA with Šídák's multiple-comparison tests. **e**. Total spheroid areas for 4T1 (left) and MCF10A HRAS^{V12} (right) cells grown in LLM supplemented with or without aspartate and treated with or without the NMDA receptor inhibitor MK-801 for 3 days. $N = 8$ 4T1 no aspartate, $n = 6$ 4T1 aspartate, $n = 6$ 4T1 no aspartate with MK-801, $n = 7$ 4T1 aspartate with MK-801, $n = 6$ MCF10A HRAS^{V12} no aspartate, $n = 7$ MCF10A HRAS^{V12} aspartate, $n = 6$ MCF10A HRAS^{V12} no aspartate with MK-801, $n = 6$ MCF10A HRAS^{V12} aspartate with MK-801. Data are presented as mean ± s.d. (n indicates independent samples). Representative images are shown on the right. Scale bar = 250 µm. Two-way ANOVA with Tukey's multiple-comparison tests. **f**. Hypusine levels in 4T1 (left) and MCF10A HRAS^{V12} (right) spheroids grown in LLM supplemented with or without aspartate and treated with or without the NMDA receptor inhibitor MK-801 for 3 days. A representative image of $n = 3$ independent experiments is shown. Quantification of hypusine signal normalized over eIF5A signal is indicated on top of each lane. **g**. Relative mRNA expression of *Dohh* and *Dhps* in 4T1 and MCF10A HRAS^{V12} spheroids grown in LLM supplemented with or without aspartate. Data for each gene and cell line are normalized relative to the average of the respective control (no aspartate) condition. Bars represent averages, and single dots individual replicates. Error bars represent ± s.d. ($n = 3$ independent replicates). Three-way ANOVA with Tukey's multiple-comparison tests. **h**. *Dohh* and *Dhps* mRNA expression levels based on scRNA-seq data for cancer cells in 4T1 lung metastases from mice pre-treated with TSFs ($n = 139$ cells) or control medium ($n = 29$ cells). Data are normalized as counts per 100k reads (CP100K). Crossbars represent mean ± s.e.m. **i**. Relative mRNA expression of *Dohh* in 4T1 spheroids silenced for *Grin2d* or scramble shRNA, grown in LLM supplemented with or without aspartate. Data are normalized relative to the average of the respective control (scramble no aspartate) condition. Bars represent averages, and single dots individual replicates. Error bars represent ± s.d. ($n = 4$ independent replicates). Two-way ANOVA with Šídák's multiple-comparison tests. **j**. Hypusine levels in 4T1 spheroids overexpressing *Dohh* or an empty vector, grown in LLM supplemented with or without aspartate. A representative image of $n = 3$ experiments is shown. Quantification of hypusine signal normalized over total eIF5A signal is indicated on top of each lane. **k**. Total spheroid areas for 4T1 cells overexpressing *Dohh* ($n = 9$) or an empty vector ($n = 9$), grown in LLM supplemented without aspartate for 3 days. Data are presented as mean ± s.d. (n indicates independent samples). Unpaired two-tailed t-test with Welch correction. **l**. Venn diagram depicting the intersection between transcription factors downstream of NMDA receptor and predicted to bind to *Dohh* or *Dhps*. Prediction was based on the JASPAR Predicted Transcription Factor Targets from the Harmonizome database (maayanlab.cloud/Harmonizome/dataset). **m**. Phosphorylated CREB levels in 4T1 (left) and MCF10A HRAS^{V12} (right) spheroids silenced for *Grin2d* or scramble shRNA, grown in LLM supplemented with or without aspartate. A representative image of $n = 3$ experiments is shown. Quantification of phosphorylated CREB signal normalized over total CREB signal is indicated on top of each lane. **n**. Left: representative H&E staining for 4T1 lung metastases represented in Fig. 3a, Fig. 4a,c, Extended Data Fig. 3n. Middle: phosphorylated CREB detected in lung metastases 14 days after i.v. injection with 4T1 cancer cells, in mice pre-treated with daily injections of aspartate (20 mM, i.p., 10 days) or PBS, assessed by multiplex immunohistochemistry. Representative images from $n = 5$ 4T1 sh*Scr* PBS, $n = 5$ 4T1 sh*Scr* aspartate, $n = 5$ 4T1 sh*Grin2d* PBS, $n = 5$ 4T1 sh*Grin2d* aspartate independent mice are shown. Blue = DAPI nuclear staining; magenta = pCREB. Scale bars = 25 µm. Right: ratio of pCREB intensity normalized on 4T1 sh*Scr* PBS. Box hinges indicate the 1st/3rd quartiles of the corresponding data, while box mid-lines represent medians, and whiskers span the range of the data. Individual data points are indicated by the white dots. Two-way ANOVA with Tukey's multiple-comparison tests. This staining is part of a multiplex staining and only relevant stains are shown. Stainings for H&E and pCREB orginate from consecutive cuts. The same metastatic regions are also used in Fig. 3a and Fig. 4a,c. **o**. Relative mRNA expression of *Dohh* (left) and *Dhps* (right) in 4T1 and MCF10A HRAS^{V12} spheroids grown in LLM supplemented with aspartate and treated with or without the CREB inhibitor Compound3i. Data for each gene are normalized relative to the average of the respective control (no CREB inhibitor) condition. Bars represent averages, and single dots individual replicates. Error bars represent ± s.d. ($n = 3$ independent replicates). Two-way ANOVA with Šídák's multiple-comparison tests. **p**. Phosphorylated CREB (left) and hypusine (right) levels in 4T1 and MCF10A HRAS^{V12} spheroids grown in LLM supplemented with aspartate and treated with or without the CREB inhibitor Compound3i. A representative image of $n = 3$ experiments is shown. Quantification of phosphorylated CREB signal normalized over total CREB signal or hypusine signal normalized over total eIF5A signal is indicated on top of each lane. **q**. Total spheroid areas for 4T1 (left) and MCF10A HRAS^{V12} (right) cells grown in LLM supplemented with aspartate and treated with or without the CREB inhibitor Compound3i. $N = 12$ 4T1 aspartate, $n = 8$ 4T1 aspartate with CREB inhibitor, $n = 12$ MCF10A HRAS^{V12} aspartate, $n = 12$ MCF10A HRAS^{V12} aspartate with CREB inhibitor. Data are presented as mean ± s.d. (n indicates independent samples). Unpaired two-tailed t-test with Welch correction. Representative images are shown on the right. Scale bar = 250 µm.

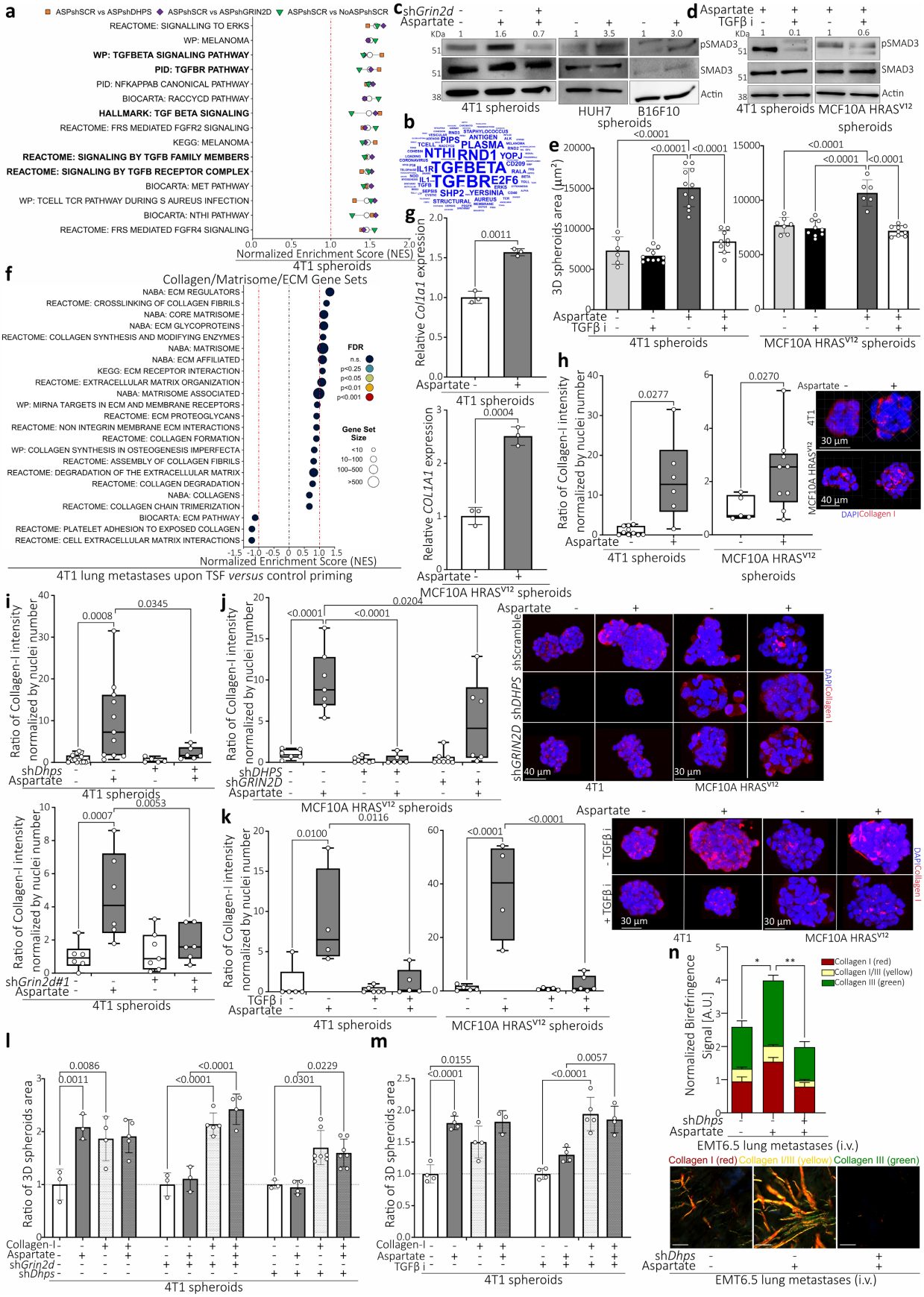

Extended Data Fig. 4 | See next page for caption.

Extended Data Fig. 4 | eIF5A hypusination results in TGFβ-mediated collagen synthesis. a. GSEA normalized enrichment scores (NES) for the top 15 gene sets commonly upregulated in translation based on changes in the ratio of Polysomal to Subpolysomal RNA levels, between 4T1 spheroids silenced for scramble shRNA grown in lung-like medium (LLM) supplemented with aspartate and 4T1 spheroids silenced for (i) *Dhps* (orange symbols) or (ii) *Grin2d* (purple symbols) grown in LLM supplemented with aspartate, or (iii) 4T1 spheroids silenced for scramble shRNA grown in LLM without aspartate (green symbols). White dots represent the average NES over all three comparisons. Gene sets related to TGFβ signaling are highlighted in bold. **b**. Word cloud highlighting the top 100 most frequently found terms among enriched gene sets, based on GSEA results analogous to those used to generate Extended Data Fig. 4a, but considering all three comparisons simultaneously (see Methods). **c**. Phosphorylated SMAD3 levels in 4T1 spheroids silenced for *Grin2d* or scramble shRNA (left), HUH7 (middle) and B16F10 (right) spheroids, grown in LLM supplemented with or without aspartate. A representative image of $n = 3$ experiments is shown. Quantification of phosphorylated SMAD3 signal normalized over total SMAD3 signal is indicated on top of each lane. **d**. Phosphorylated SMAD3 levels in 4T1 (left) and MCF10A $HRAS^{V12}$ (right) spheroids grown in LLM supplemented with aspartate and treated with or without a TGFβ inhibitor. A representative image of $n = 3$ experiments is shown. Quantification of phosphorylated SMAD3 signal normalized over total SMAD3 signal is indicated on top of each lane. **e**. Total spheroid areas for 4T1 (left) and MCF10A $HRAS^{V12}$ (right) cells grown in LLM supplemented with or without aspartate and treated with or without the TGFβ inhibitor for 5 (4T1) or 3 days (MCF10A $HRAS^{V12}$). $N = 6$ 4T1 no aspartate, $n = 11$ 4T1 no aspartate with TGFβ inhibitor, $n = 11$ 4T1 aspartate, $n = 9$ aspartate with TGFβ inhibitor; $n = 7$ MCF10A $HRAS^{V12}$ no aspartate, $n = 6$ MCF10A $HRAS^{V12}$ aspartate, $n = 9$ MCF10A $HRAS^{V12}$ no aspartate with TGFβ inhibitor, $n = 9$ MCF10A $HRAS^{V12}$ aspartate with TGFβ inhibitor. Data are presented as mean ± s.d. (*n* indicates independent samples). Two-way ANOVA with Tukey's multiple-comparison tests. **f**. GSEA normalized enrichment scores (NES) for gene sets containing either of the terms COLLAGEN, MATRISOME, ECM, and EXTRACELLULAR_MATRIX found on cancer cells based on scRNA-seq comparing 4T1 lung metastases from mice pre-treated with control medium or TSFs. Dot colors and areas indicate FDR-adjusted *P*-values and gene-set sized, respectively. *P*-values based on *fgsea*'s adaptive multilevel splitting Monte Carlo approach, subject to FDR adjustment using the Benjamini-Hochberg (BH) approach. **g**. Relative mRNA expression of *Col1a1* in 4T1 (top) and MCF10A $HRAS^{V12}$ (bottom) spheroids grown in LLM supplemented with or without aspartate. Data for each gene and cell line are normalized relative to the average of the respective control (no aspartate) condition. Bars represent averages, and single dots individual replicates. Error bars represent ± s.d. ($n = 3$ independent replicates). Unpaired two-tailed *t*-test with Welch correction. **h**. Box and whisker plots of relative abundance of collagen I in 4T1 (left) and MCF10A $HRAS^{V12}$ (right) spheroids grown in LLM supplemented with or without aspartate, measured by immunofluorescence. $N = 10$ 4T1 no aspartate, $n = 6$ 4T1 aspartate, and $n = 5$ MCF10A $HRAS^{V12}$ no aspartate and $n = 9$ MCF10A $HRAS^{V12}$ aspartate. The total fluorescence intensity was normalized over the number of DAPI-stained nuclei. Relative fluorescence intensities per cell are depicted, normalized to the mean intensity for the control condition. Box hinges indicate the $1^{st}/3^{rd}$ quartiles of the corresponding data, while box mid-lines represent medians, and whiskers span the range of the data. Individual data points are indicated by the white dots. Unpaired two-tailed *t*-test with Welch correction. Representative three-dimensional representation are depicted on the right. Blue, DAPI-stained nuclei; red, collagen I. **i**. Box and whisker plots of relative abundance of collagen I in 4T1 spheroids silenced for *Dhps* (top) or *Grin2d* (bottom) or scramble shRNA, grown in LLM supplemented with or without aspartate, measured by immunofluorescence. Top: $n = 15$ no aspartate scramble, $n = 11$ aspartate scramble, $n = 5$ no aspartate sh*Dhps*, $n = 6$ aspartate sh*Dhps*. Bottom: $n = 6$ no aspartate scramble, $n = 6$ aspartate scramble, $n = 7$ no aspartate sh*Grin2d*, $n = 6$ aspartate sh*Grin2d*. The total fluorescence intensity was normalized over the number of DAPI-stained nuclei. Relative fluorescence intensities per cell are depicted, normalized to the mean intensity for the control condition. Box hinges indicate the $1^{st}/3^{rd}$ quartiles of the corresponding data, while box mid-lines represent medians, and whiskers span the range of the data. Individual data points are indicated by the white dots. Two-way ANOVA with Tukey's multiple-comparison tests. Representative three-dimensional representation are depicted in Extended Data Fig. 4j. **j**. Box and whisker plots of relative abundance of collagen I in MCF10A $HRAS^{V12}$ spheroids silenced for *DHPS, GRIN2D* or scramble shRNA, grown in LLM supplemented with or without aspartate, measured by immunofluorescence. $N = 6$ no aspartate scramble, $n = 7$ aspartate scramble, $n = 8$ no aspartate sh*DHPS*, $n = 6$ aspartate sh*DHPS*, $n = 8$ no aspartate sh*GRIN2D*, $n = 6$ aspartate sh*GRIN2D*. The total fluorescence intensity was normalized over the number of DAPI-stained nuclei. Relative fluorescence intensities per cell are depicted, normalized to the mean intensity for the control condition. Box hinges indicate the $1^{st}/3^{rd}$ quartiles of the corresponding data, while box mid-lines represent medians, and whiskers span the range of the data. Individual data points are indicated by the white dots. Two-way ANOVA with Tukey's multiple-comparison tests. Representative three-dimensional representation are depicted on the right and include samples shown in Extended Data Fig. 4i. Blue, DAPI-stained nuclei; red, collagen I. **k**. Box and whisker plots of relative abundance of collagen I in 4T1 (left) and MCF10A $HRAS^{V12}$ (right) spheroids grown in LLM supplemented with or without aspartate and treated with or without the TGFβ inhibitor, measured by immunofluorescence. $N = 5$ 4T1 no aspartate, $n = 4$ 4T1 aspartate, $n = 6$ 4T1 no aspartate with TGFβ inhibitor, $n = 5$ 4T1 no aspartate with TGFβ inhibitor, and $n = 5$ MCF10A $HRAS^{V12}$ no aspartate, $n = 4$ MCF10A $HRAS^{V12}$ aspartate, $n = 5$ MCF10A $HRAS^{V12}$ no aspartate with TGFβ inhibitor, $n = 6$ MCF10A $HRAS^{V12}$ aspartate with TGFβ inhibitor. The total fluorescence intensity was normalized over the number of DAPI-stained nuclei. Relative fluorescence intensities per cell are depicted, normalized to the mean intensity for the control condition. Box hinges indicate the $1^{st}/3^{rd}$ quartiles of the corresponding data, while box mid-lines represent medians, and whiskers span the range of the data. Individual data points are indicated by the white dots. Two-way ANOVA with Šídák's multiple-comparison tests. Representative three-dimensional representation are depicted on the right. Blue, DAPI-stained nuclei; red, collagen I. **l**. Relative spheroid areas for 4T1 cells silenced for *Grin2d*, *Dhps* or scramble shRNA grown in LLM with 1.5% Matrigel, supplemented with or without aspartate and with or without 1.5% Collagen-I. $N = 3$ no aspartate scramble, $n = 3$ aspartate scramble, $n = 4$ no aspartate scramble with Collagen-I, $n = 5$ aspartate scramble with Collagen-I; $n = 3$ no aspartate sh*Dhps*, $n = 3$ aspartate sh*Dhps*, $n = 5$ no aspartate sh*Dhps* with Collagen-I, $n = 4$ aspartate sh*Dhps* with Collagen-I; $n = 3$ no aspartate sh*Grin2d*, $n = 4$ aspartate sh*Grin2d*, $n = 7$ no aspartate sh*Grin2d* with Collagen-I, $n = 7$ aspartate sh*Grin2d* with Collagen-I. Data are presented as mean ± s.d, normalized to the mean spheroid areas for the respective no aspartate conditions (*n* indicates independent samples). Two-way ANOVA with Tukey's multiple-comparison tests. **m**. Relative spheroid areas for 4T1 cells grown in LLM with 1.5% Matrigel, supplemented with or without aspartate and with or without 1.5% Collagen-I and treated with or without the TGFβ inhibitor. $N = 4$ no aspartate, $n = 4$ aspartate, $n = 4$ no aspartate with Collagen-I, $n = 4$ aspartate with Collagen-I; $n = 4$ no aspartate with TGFβ inhibitor, $n = 4$ aspartate with TGFβ inhibitor, $n = 5$ no aspartate with TGFβ inhibitor and Collagen-I, $n = 4$ aspartate with TGFβ inhibitor and Collagen-I. Data are presented as mean ± s.d, normalized to the mean spheroid area for the respective no aspartate conditions (*n* indicates independent samples). Two-way ANOVA with Tukey's multiple-comparison tests. **n**. Top: Quantification of linearized collagen based on Picrosirius Red staining and polarized light microscopy detected in EMT6.5 lung metastases silenced for *Dhps* or scramble shRNA in mice pre-treated with daily injections of aspartate (20 mM, i.p., 10 days) or PBS. Significant collagen red/yellow/green increase (*) 0.0023/0.1758/0.0042 EMT6.5 aspartate scramble, $n = 5$ PBS and $n = 5$ aspartate. Significant collagen red/yellow/green decrease (**) < 0.0001/ < 0.0001/ < 0.0001 (EMT6.5 sh*Dhps*), $n = 5$ PBS scramble, $n = 5$ aspartate scramble and $n = 5$ aspartate sh*Dhps*. Data are normalized by metastasis area (megapixel) and expressed as mean ± SEM. Two-way ANOVA with Šídák's multiple-comparison tests. Bottom: representative images of linearized collagen based on Picrosirius Red staining and polarized light microscopy detected in EMT6.5 lung metastases. Red color mostly indicates thick collagen I fibers and green color mostly indicates thin collagen III fibers. A representative image of $n = 5$ EMT6.5 PBS scramble, $n = 5$ EMT6.5 aspartate scramble, $n = 5$ EMT6.5 aspartate sh*Dhps* lung metastases is shown. Scale bars = 20 μm.

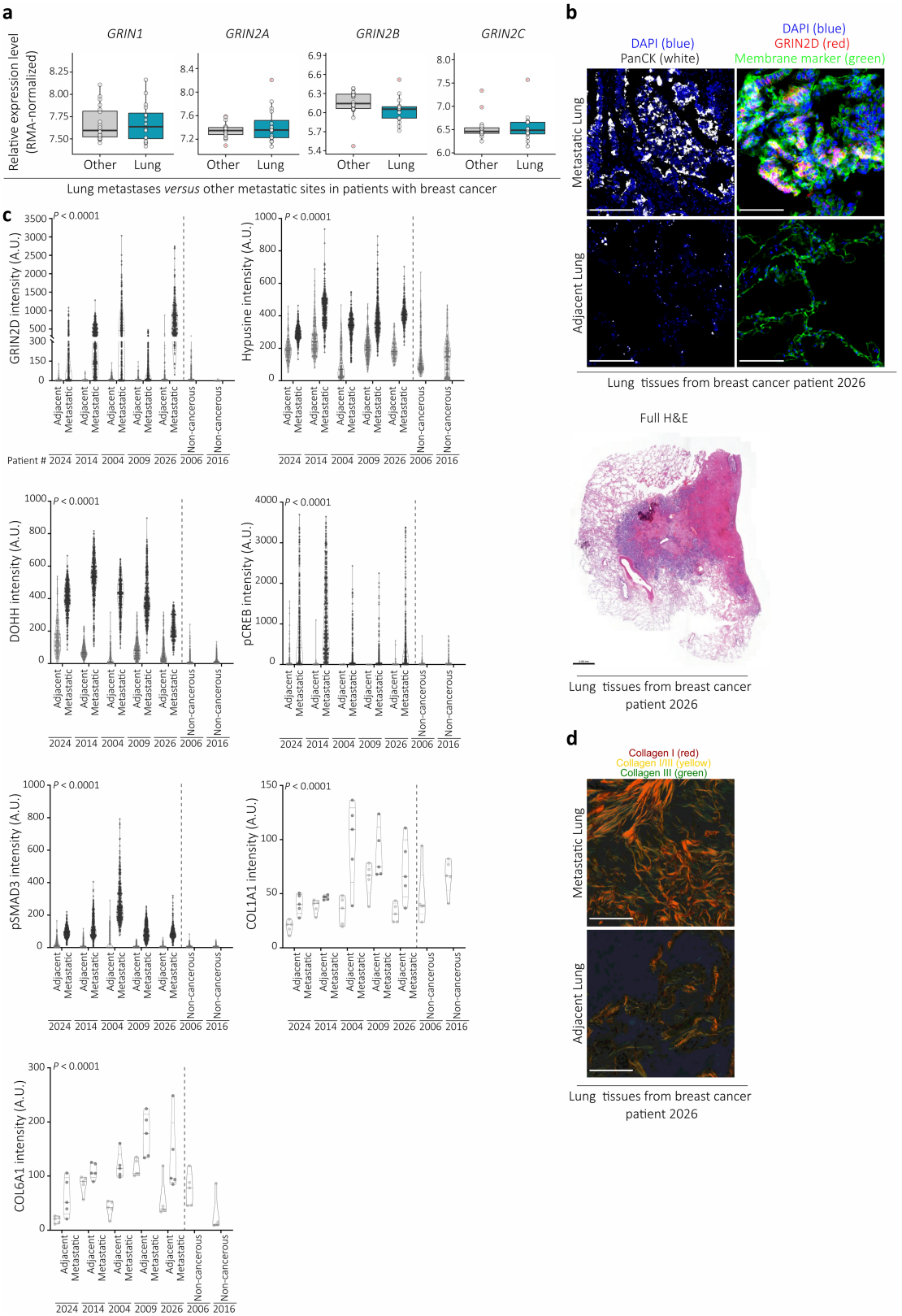

Extended Data Fig. 5 | See next page for caption.

Extended Data Fig. 5 | Expression of NMDA receptor subunits and staining of proteins indicative of aspartate signaling in patients with breast cancer. **a**. RMA-normalized mRNA expression levels of *NMDA*-receptor-related genes in breast cancer-derived lung metastases *vs* breast cancer-derived bone/brain/liver metastases, based on patient biopsies (GSE14018). $N = 16$ lung metastases and $n = 20$ non-lung metastases samples ($n = 8$ bone metastases, $n = 7$ brain metastases, $n = 5$ liver metastases). Box hinges indicate the $1^{st}/3^{rd}$ quartiles of the corresponding data, while box mid-lines represent medians, and whiskers span the range of the data excluding outliers (data points more than 1.5 x IQR away from the $1^{st}/3^{rd}$ quartiles, where IQR = inter-quartile range), with the latter indicated in red. Individual data points are indicated by the white dots. Statistics show *P*-values based on differential expression analysis with *limma*. **b**. Top: DAPI and PanCK (left), GRIN2D and membrane marker (right) detected in metastatic and adjacent lungs from the UPTIDER breast cancer patient 2026 shown in Fig. 5e, assessed by multiplex immunohistochemistry. Blue = DAPI nuclear staining, red = GRIN2D, green = membrane marker ATP1A1 (scale bars = 100 µm). Membrane marker has been added to identify surface localization of GRIN2D, the same exact representative image was used in Fig. 5e. Bottom: representative image of H&E staining of the whole lung from patient 2026, scale bar = 2 mm. H&E and multiplex immunohistochemistry stainings originate from non-consecutive cuts. **c**. Quantification of GRIN2D, Hypusine, DOHH, nuclear pCREB, nuclear pSMAD3, COL1A1 and COL6A1 intensities in tissues derived from the UPTIDER breast cancer patients. For GRIN2D, Hypusine and DOHH, fluorescence intensity values per single cell are depicted, across 5 independent regions. For pCREB and pSMAD3, fluorescence intensity values per nucleus are depicted, across 5 independent regions. For COL1A1 and COL6A1, mean fluorescence intensities per unit area are depicted, across 5 independent regions. Two-way ANOVA, with *P* values for the tissue type (metastatic *vs* adjacent) factor shown above the graphs. All single comparisons per patients were significant based on unpaired two-tailed *t*-test with Welch correction, except for COL1A1 and COL6A1, for which single comparisons per patients were significant in 7 out of 10 measurements based on unpaired two-tailed *t*-test with Welch correction. Representative images are shown in Fig. 5e and Extended Data Fig. 6. **d**. Representative images of linearized collagen based on Picrosirius Red staining and polarized light microscopy detected in metastatic and adjacent lungs from the UPTIDER breast cancer patient 2026, quantified in Fig. 5f. Red color mostly indicates thick collagen I fibers and green color mostly indicates thin collagen III fibers. A representative image of $n = 5$ patients is shown. Scale bars = 1 mm.

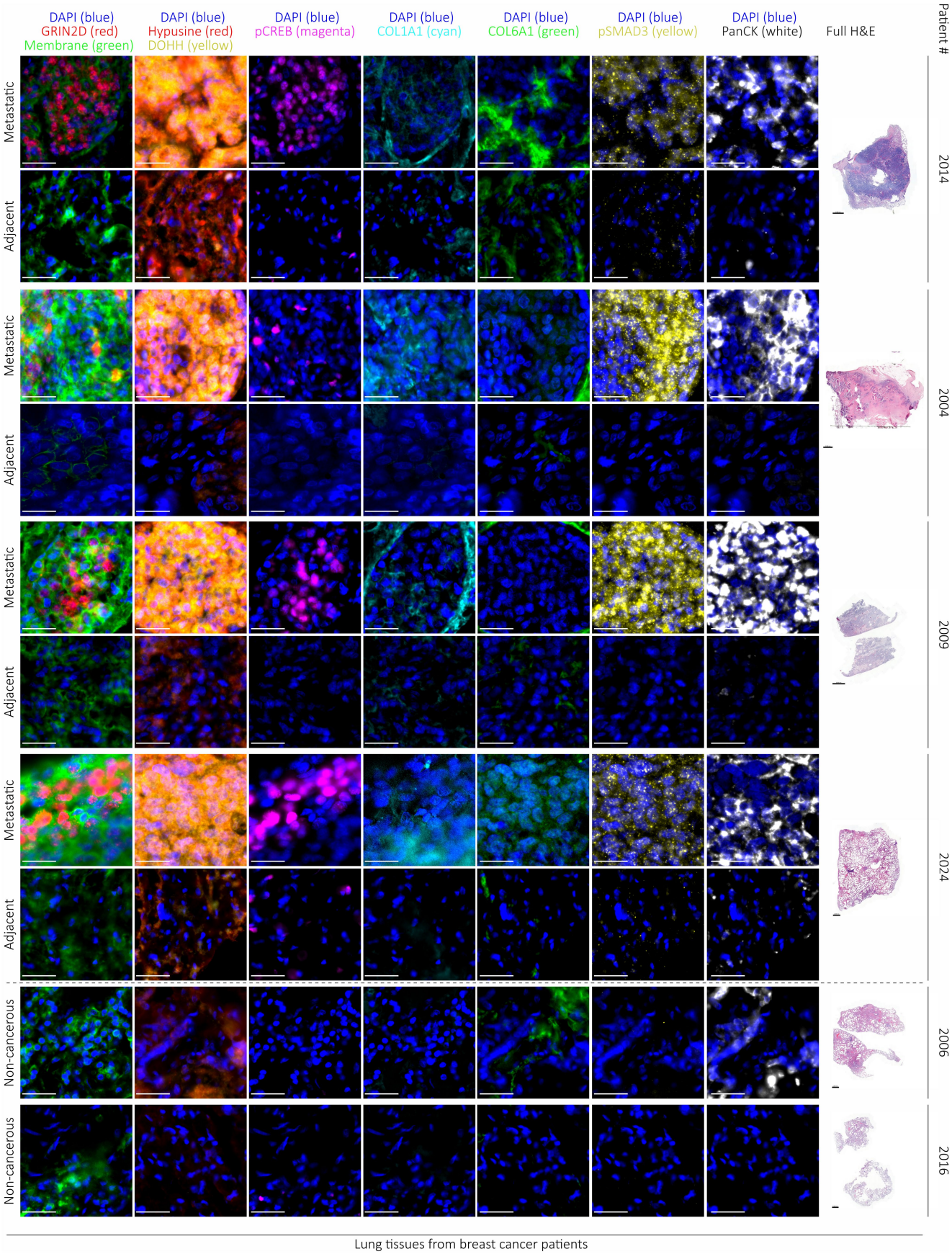

Extended Data Fig. 6 | See next page for caption.

Extended Data Fig. 6 | Representative images of IHC performed in breast cancer patients. Left: GRIN2D, Hypusine, DOHH, phosphorylated CREB, COL1A1, COL6A1, phosphorylated SMAD3 and PanCK detected in metastatic and adjacent lungs from the UPTIDER breast cancer patients ($n = 7$), assessed by multiplex immunohistochemistry. Blue = DAPI nuclear staining, green = membrane marker ATP1A1; red = Hypusine, yellow = DOHH; magenta = phosphorylated CREB; cyan = COL1A1; green = COL6A1; yellow = phosphorylated SMAD3; white = PanCK. Scale bars = 50 µm. Membrane marker ATP1A1 has been added to identify surface localization of GRIN2D. Quantification for all patients, $n = 7$ (for a total of 5 regions per patient) is shown on Extended Data Fig. 5c. Right: Representative images of H&E stainings of the whole lungs for each patient, scale bars = 2 mm. H&E and multiplex immunohistochemistry stainings originate from non-consecutive cuts.

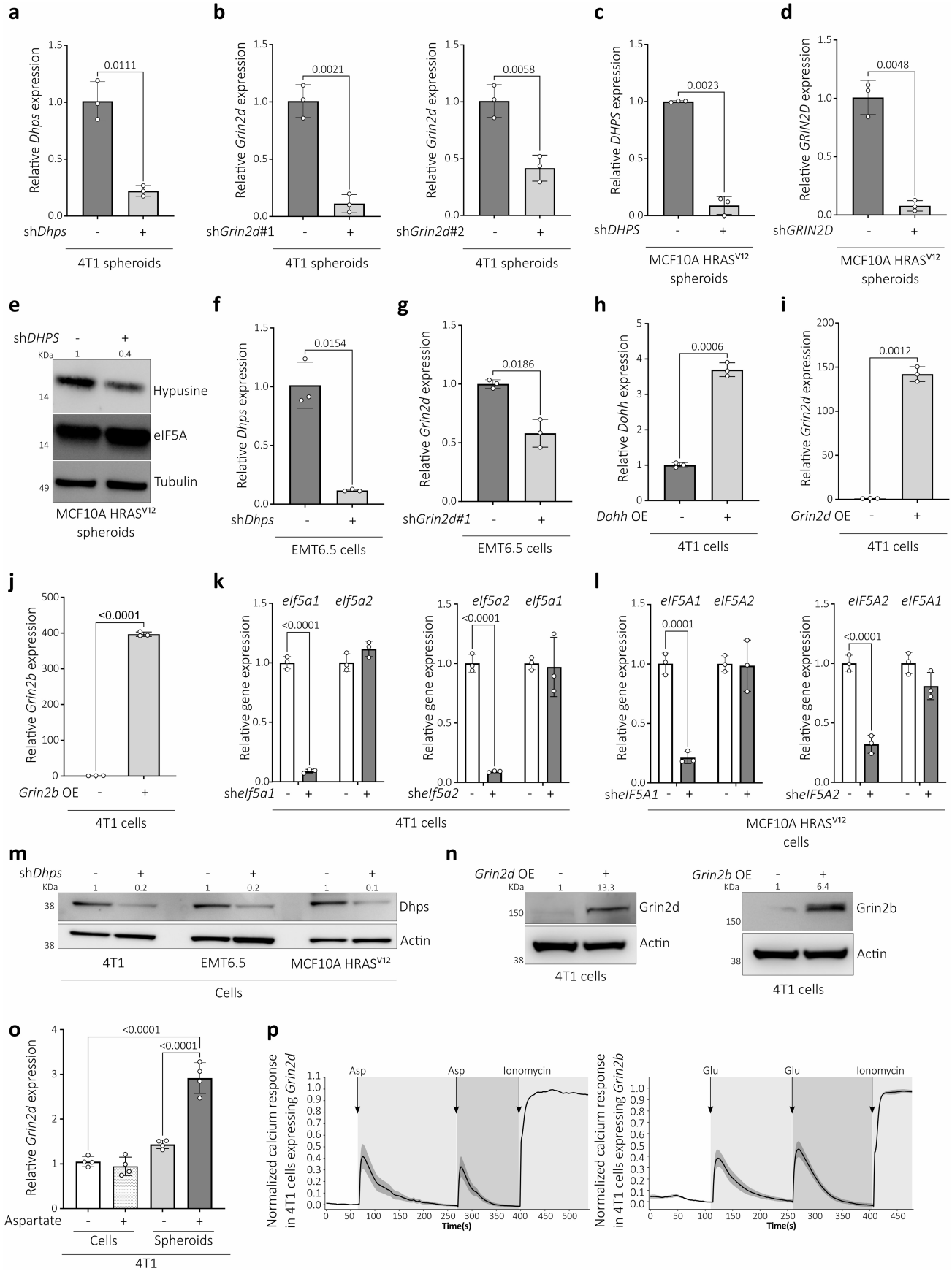

Extended Data Fig. 7 | See next page for caption.

Extended Data Fig. 7 | Protein and mRNA expression of genetically modified breast cancer cells and method validation. a. Relative mRNA expression levels of *Dhps* in 4T1 spheroids silenced for *Dhps* or scramble shRNA. Data are normalized relative to the average of the control (shRNA against scramble sequence) condition. Bars represent averages, and single dots individual replicates. Error bars represent ± s.d ($n = 3$ independent replicates). Unpaired two-tailed *t*-test with Welch correction. **b**. Relative mRNA expression levels of *Grin2d* in 4T1 spheroids silenced for *Grin2d* or scramble shRNA. Data are normalized relative to the average of the control (shRNA against scramble sequence) condition. Bars represent averages, and single dots individual replicates ($n = 3$ independent replicates). Unpaired two-tailed *t*-test with Welch correction. **c**. Relative mRNA expression levels of *DHPS* in MCF10A HRAS^{V12} spheroids silenced for *DHPS* or scramble shRNA. Data are normalized relative to the average of the control (shRNA against scramble sequence) condition. Bars represent averages, and single dots individual replicates ($n = 3$ independent replicates). Unpaired two-tailed *t*-test with Welch correction. **d**. Relative mRNA expression levels of *GRIN2D* in MCF10A HRAS^{V12} spheroids silenced for *GRIN2D* or scramble shRNA. Data are normalized relative to the average of the control (shRNA against scramble sequence) condition. Bars represent averages, and single dots individual replicates ($n = 3$ independent replicates). Unpaired two-tailed *t*-test with Welch correction. **e**. Hypusine levels in MCF10A HRAS^{V12} cells silenced for *DHPS* or scramble shRNA. Quantification of hypusine signal normalized over total eIF5A signal is indicated on top of each lane. **f**. Relative mRNA expression levels of *Dhps* in EMT6.5 cells silenced for *Dhps* or scramble shRNA. Data are normalized relative to the average of the control (shRNA against scramble sequence) condition. Bars represent averages, and single dots individual replicates ($n = 3$ independent replicates). Unpaired two-tailed *t*-test with Welch correction. **g**. Relative mRNA expression levels of *Grin2d* in EMT6.5 cells silenced for *Grin2d* or scramble shRNA. Data are normalized relative to the average of the control (shRNA against scramble sequence) condition. Bars represent averages, and single dots individual replicates ($n = 3$ independent replicates). Unpaired two-tailed *t*-test with Welch correction. **h**. Relative mRNA expression levels of *Dohh* in 4T1 cells expressing an overexpression vector for *Dohh* or an empty vector. Data are normalized relative to the average of the control (empty vector) condition. Bars represent averages, and single dots individual replicates ($n = 3$ independent replicates). OE = overexpression. Unpaired two-tailed *t*-test with Welch correction. **i**. Relative mRNA expression levels of *Grin2d* in 4T1 cells expressing an overexpression vector for *Grin2d* or an empty vector. Data are normalized relative to the average of the control (empty vector) condition. Bars represent averages, and single dots individual replicates ($n = 3$ independent replicates). Unpaired two-tailed *t*-test with Welch correction. **j**. Relative mRNA expression levels of *Grin2b* in 4T1 cells expressing an overexpression vector for *Grin2b* or an empty vector. Data are normalized relative to the average of the control (empty vector) condition. Bars represent averages, and single dots individual replicates ($n = 3$ independent replicates). Unpaired two-tailed *t*-test with Welch correction. **k**. Relative mRNA expression levels of *eIf5a1* and *eIf5a2* in 4T1 cells silenced for *eIf5a1 or eIf5a2* or scramble shRNA. Data are normalized relative to the average of the control (shRNA against scramble sequence) condition. Bars represent averages, and single dots individual replicates. Error bars represent ± s.d ($n = 3$ independent replicates). Two-way ANOVA with Šídák's multiple-comparison tests. **l**. Relative mRNA expression levels of *eIF5A1* and *eIF5A2* in MCF10A HRAS^{V12} cells silenced for *eIF5A1 or eIF5A2* or scramble shRNA. Data are normalized relative to the average of the control (shRNA against scramble sequence) condition. Bars represent averages, and single dots individual replicates. Error bars represent ± s.d ($n = 3$ independent replicates). Two-way ANOVA with Šídák's multiple-comparison tests. **m**. Dhps levels in 4T1, EMT6.5 and MCF10A HRAS^{V12} cells silenced for *DHPS* or scramble shRNA. Quantification of Dhps signal normalized over actin signal is indicated on top of each lane. **n**. Left: Grin2d levels in 4T1 cells expressing an overexpression vector for *Grin2d* or an empty vector. Quantification of Grin2d signal normalized over actin signal is indicated on top of each lane. Right: Grin2b detected in 4T1 cells expressing an overexpression vector for *Grin2b* or an empty vector. Quantification of Grin2b signal normalized over actin signal is indicated on top of each lane. **o**. Relative mRNA expression levels of *Grin2d* in 4T1 cells or spheroids cultured as a 2D monolayer in RPMI (left) or as 3D spheroids in lung-like medium (right) with or without aspartate. Data are normalized relative to the average of the control (2D no aspartate) condition. Bars represent averages, and single dots individual replicates ($n = 4$ independent replicates). One-way ANOVA ($P < 0.0001$) with Tukey's multiple-comparison tests. **p**. Average ionomycin-normalized calcium response traces in 4T1 cells overexpressing *Grin2d* (left) or *Grin2b* (right). The shaded ribbons represent standard errors of the mean at each time point in each sample, while the grey rectangles indicate sequential additions of aspartate (left) or glutamate (right) plus ionomycin at the times indicated by the arrow. A representative experiment ($n = 14$ cells for *Grin2d* OE and $n = 15$ cells *Grin2b* OE) out of 2 independent experiments is shown.

nature portfolio

Corresponding author(s): Sarah-Maria Fendt

Last updated by author(s): Sep 25, 2024

Reporting Summary

Nature Portfolio wishes to improve the reproducibility of the work that we publish. This form provides structure for consistency and transparency in reporting. For further information on Nature Portfolio policies, see our Editorial Policies and the Editorial Policy Checklist.

Statistics

For all statistical analyses, confirm that the following items are present in the figure legend, table legend, main text, or Methods section.

n/a	Confirmed
☐	☒ The exact sample size (*n*) for each experimental group/condition, given as a discrete number and unit of measurement
☐	☒ A statement on whether measurements were taken from distinct samples or whether the same sample was measured repeatedly
☐	☒ The statistical test(s) used AND whether they are one- or two-sided *Only common tests should be described solely by name; describe more complex techniques in the Methods section.*
☒	☐ A description of all covariates tested
☒	☐ A description of any assumptions or corrections, such as tests of normality and adjustment for multiple comparisons
☐	☒ A full description of the statistical parameters including central tendency (e.g. means) or other basic estimates (e.g. regression coefficient) AND variation (e.g. standard deviation) or associated estimates of uncertainty (e.g. confidence intervals)
☐	☒ For null hypothesis testing, the test statistic (e.g. *F*, *t*, *r*) with confidence intervals, effect sizes, degrees of freedom and *P* value noted *Give P values as exact values whenever suitable.*
☒	☐ For Bayesian analysis, information on the choice of priors and Markov chain Monte Carlo settings
☒	☐ For hierarchical and complex designs, identification of the appropriate level for tests and full reporting of outcomes
☒	☐ Estimates of effect sizes (e.g. Cohen's *d*, Pearson's *r*), indicating how they were calculated

Our web collection on statistics for biologists contains articles on many of the points above.

Software and code

Policy information about availability of computer code

Data collection	GC-MS data were collected using MSD Chemstation Data Analysis software (F.01.03.2357). LC-MS data were collected using the MassHunter Workstation LC/MS Data Acquisition v.10.1 software. H&E stainings and immunohistochemistry on tissue samples were acquired using ZEN v.3.4 software (Zeiss). Calcium influx data were collected with a Nikon Eclipse Ti2 inverted fluorescence microscope. Western blot imaging acquisition was performed using ImageQuant LAS 4000 (GE Healthcare). Microscopy images were acquired using Motic Images Plus v.2.0 software (Motic). Flow cytometry data were acquired using the BD FACS Diva software v9.0 (BD Biosciences). Confocal images were acquired using a Leica TCS SP8 X confocal microscope equipped with a White Light Laser LAS X software (Leica). Sequencing data were obtained on Illumina NovaSeq 6000 system (Illumina).
Data analysis	H&E stainings and immunofluorescences on tissue slides were done using ZEN Blue software (Zeiss) and QuPath software. Picro-Sirius red stainings, calcium influx analysis and spheroid area were analyzed with the FIJI distribution of ImageJ 1.53f51. Fluorescence quantification analysis on confocal images were performed with the Imaris Image Analysis Software 9 X (Bitplane). Flow cytometry data were analyzed using FlowJo (v10.8.1). For Droplet digital PCR, analysis was performed using a QuantaSoft v.1.7.4.0917 software. For mass spectrometry analysis, mass isotopomer abundances and isotopologue distributions were extracted from the raw ion chromatograms using Matlab (R2021b). GNU Image Manipulation Program (GIMP, built 2.10.30) was used for image cropping and editing. All statistical analyses were performed in GraphPad Prism v.9 or v.10 or within the R/Bioconductor framework. For polysome sequencing and total RNA sequencing analysis, sequenced reads were trimmed for adaptors and low-quality base calls using Trim Galore! (v0.6.6), after which quality control was performed with FastQC (v0.11.9). High-quality reads were then mapped to the mm39 reference mouse genome (GRCm39) using STAR (v2.6.1) and quantified using Salmon (v1.4.0). Gene counts for matched polysomal/sub-polysomal sample pairs (for polysome sequencing) or for individual total RNA samples (for total RNA sequencing) collected under all conditions of interest were processed simultaneously within the DESeq2 (v1.34.0) framework. Pre-ranked gene-set enrichment analysis (GSEA) was performed on the output of DESeq2 using the R package fgsea (v1.20.0), considering a collection of mouse gene sets obtained via

the R package msigdbr (v7.4.1) and by querying KEGG's REST API.
For single-cell RNA-sequencing analysis, sequenced reads were mapped to a customized version of the mm10 mouse genome (mm10 build GRCm38.p6, including an extra chromosome with the sequence for CD90.1), using the Cell Ranger v5.0.1 software (10x Genomics). The resulting single-cell gene expression data were analyzed within the R/Bioconductor framework. Raw UMI count matrices for all samples were first imported using Seurat (v4.1.0) and subject to ambient RNA correction using a customized version of SoupX (v1.6.2). Ambient-corrected count matrices for all individual samples were then merged and converted for further processing with Monocle3-alpha (v2.99.3). Low-quality cells were then filtered out based on standard quality-control metrics, and size-factor and variance-stabilizing normalization were then applied to the filtered data set. Highly variable genes (HVGs) were identified based on their departure from the average normalized dispersion versus expression trend observed among all genes, and principal component analysis (PCA) was then performed on the size factor-normalized and variance-stabilized count matrix restricted to these HVGs, followed by 2D UMAP dimensional reduction. After that, cells were clustered in the UMAP plane by applying the Louvain graph-based algorithm at high resolution. The resulting fine-grained clusters were then manually annotated to specific cell types, based on evaluating the expression profiles of several cell type-specific markers. This annotation was further refined based on subsequent sub-clustering applied to each of the preliminarily annotated cell types, concomitantly with doublet removal guided by the output of scDblFinder (v1.8.0). Specifically, cancer cells could be unambiguously identified based on CD90.1 expression.
Differential expression analysis, based on comparing cancer cells under tumor-secreted factors or control medium pre-treatment at 16 days of metastatic colonization only, was performed within the Seurat framework, using the function FindMarkers. Pre-ranked gene-set enrichment analysis (GSEA) was performed on the output of FindMarkers using the R package fgsea (v1.20.0), considering a collection of mouse gene sets obtained via the R package msigdbr (v7.4.1) and by querying KEGG's REST API.
The publicly available microarray-based patient-metastasis data set GSE1401882 was downloaded from the Gene Expression Omnibus (GEO) using the R package GEOquery (v2.62.2). Data for probes with undefined gene symbols or with ambiguous gene assignments were filtered out before further analysis. Among the remaining probes, those presenting duplicated gene symbols were further collapsed into single probes, by preserving only those probes with the highest overall expression levels for each duplicated gene symbol. Differential expression analysis was performed based on the RMA-normalized expression levels for the remaining probes using the R package limma (v3.50.1), comparing expression levels in lung vs all other metastatic sites available in the data set. Pre-ranked gene-set enrichment analysis (GSEA) was performed on the output of limma using the R package fgsea (v1.20.0), considering a collection of human gene sets obtained via the R package msigdbr (v7.4.1) and by querying KEGG's REST API.

For manuscripts utilizing custom algorithms or software that are central to the research but not yet described in published literature, software must be made available to editors and reviewers. We strongly encourage code deposition in a community repository (e.g. GitHub). See the Nature Portfolio guidelines for submitting code & software for further information.

Data

Policy information about availability of data

All manuscripts must include a data availability statement. This statement should provide the following information, where applicable:

- Accession codes, unique identifiers, or web links for publicly available datasets
- A description of any restrictions on data availability
- For clinical datasets or third party data, please ensure that the statement adheres to our policy

The authors declare that all the other data supporting the findings of this study are available within the paper and its supplementary information files, and from the corresponding author upon reasonable request. Gel source images are available in Supplementary Figure 1. Mouse single-cell RNA-sequencing data and polysome/total RNA sequencing data have been deposited in the Gene Expression Omnibus (GEO) under accession code GSE236087. The publicly available microarray-based patient-metastasis data set GSE1401882 can be downloaded from the Gene Expression Omnibus (GEO) https://www.ncbi.nlm.nih.gov/geo/query/acc.cgi?acc=GSE14018. No original softwares and/or algorithms were developed in the present study; however, code used for data analysis can be provided upon request. Any additional information required to reanalyze the data reported in this paper is available from the corresponding author upon request. All other data supporting the findings of this study are available within the Article and the Supplementary Information, and from the corresponding author on reasonable request.

Research involving human participants, their data, or biological material

Policy information about studies with human participants or human data. See also policy information about sex, gender (identity/presentation), and sexual orientation and race, ethnicity and racism.

Reporting on sex and gender	Tissue from female breast cancer patients or from male or female patients without cancer were analyzed in this study, gender was not provided or used in the selection of patient tissue analyzed in this manuscript.
Reporting on race, ethnicity, or other socially relevant groupings	na
Population characteristics	UPTIDER: Metastatic breast cancer, or hereditary cancer syndrome with a moderate to high lifetime risk of breast cancer, for which the patient is treated/followed in UZ Leuven. Age ≥ 18 years. Healthy lung tissue human participants: Human 'normal' lung tissue was collected from patients who underwent lung surgery for emphysematous lung volume reduction.
Recruitment	UPTIDER: female patients (≥ 18 years) with metastatic breast cancer that consent to participate undergo a rapid research autopsy in the first 12 hours after death. Healthy lung tissue human participants: patients who underwent lung surgery for emphysematous lung volume reduction and consented to donate resected tissue.
Ethics oversight	UZ/KU Leuven Program for Post-mortem Tissue Donation to Enhance Research (UPTIDER), NCT04531696, protocol S64410 and UZ/KU Leuven, protocol S57123.

Note that full information on the approval of the study protocol must also be provided in the manuscript.

Field-specific reporting

Please select the one below that is the best fit for your research. If you are not sure, read the appropriate sections before making your selection.

☒ Life sciences ☐ Behavioural & social sciences ☐ Ecological, evolutionary & environmental sciences

For a reference copy of the document with all sections, see nature.com/documents/nr-reporting-summary-flat.pdf

Life sciences study design

All studies must disclose on these points even when the disclosure is negative.

Sample size	In vitro sample sizes were based on previous similar studies that have given statistically significant results (doi: 10.1016/j.molcel.2020.11.027, doi: 10.1038/s41586-019-0977-x, doi: 10.1038/s41586-022-04758-2, doi:10.1038/s43018-023-00513-2). For in vivo experiments, sample size was determined using power calculations with B=0.8 and P<0.05, based on preliminary data and previous studies, and respects the limited use of animal models in line with the 3R recommendations: Replacement, Reduction, Refinement.
Data exclusions	Identifying and removing outliers was made using the ROUT or Grubbs method of regression (Prism) with coefficient Q = 1% or alpha = 0.05%
Replication	All experiments were performed at least in triplicate. All attempts at replication were successful.
Randomization	Mice were randomized before tumor-secreted factors/control media injections, aspartate/PBS injections or injection with the different cell lines. For in vitro studies, samples were randomized, when possible, prior data acquisition.
Blinding	Mice were given a unique number prior to data collection and analysis. Data was collected and analyzed blindly, and subsequently grouped in the corresponding cohorts for statistical analysis. For in vitro experiments, investigators were blinded to group allocation during data collection and/or analysis by giving an unique identifier other than the sample name. Data was grouped for statistical analysis as indicated in the figures.

Reporting for specific materials, systems and methods

We require information from authors about some types of materials, experimental systems and methods used in many studies. Here, indicate whether each material, system or method listed is relevant to your study. If you are not sure if a list item applies to your research, read the appropriate section before selecting a response.

Materials & experimental systems

n/a	Involved in the study
☐	☒ Antibodies
☐	☒ Eukaryotic cell lines
☒	☐ Palaeontology and archaeology
☐	☒ Animals and other organisms
☒	☐ Clinical data
☒	☐ Dual use research of concern
☒	☐ Plants

Methods

n/a	Involved in the study
☒	☐ ChIP-seq
☐	☒ Flow cytometry
☒	☐ MRI-based neuroimaging

Antibodies

Antibodies used

For western blot experiments, the following antibodies were used: hypusine (EMD Millipore, ABS1064, 1:2,000 dilution), eIF5A (BD Biosciences, 611976, 1:1,000 dilution), phosphorylated CREB (Ser133) (Cell Signaling Technologies, 9198S, 1:1,000 dilution), CREB (Cell Signaling Technologies, 9104S, 1:1,000 dilution), phosphorylated SMAD3 (S423+S425) (Abcam, EP823Y, 1:1,000 dilution), SMAD3 (Cell Signaling Technologies, 9513S, 1:1,000 dilution), phosphorylated eIF2α (Cell Signaling Technologies 9721S, 1:1,000 dilution), ATF4 (Cell Signaling Technologies, 11815S, 1:500 dilution), Grin2d (Novus Biological, NBP2-94573, 1:500 dilution), Grin2b (Abcam, Ab93610, 1:1000 dilution), Dhps (Santa Cruz Biotechnology, sc-365077, 1:500), puromycin (Merck Sigma, MABE343), β-Actin (Merck Sigma, A5441, 1:10,000 dilution), β-Tubulin (Cell Signaling Technologies, 2146S, 1:1,000 dilution), Grin2d (Novus Biological, NBP2-94573, 1:300 dilution), HRP-linked anti-rabbit secondary antibody (Cell Signaling Technologies, 7074S, 1:5,000 dilution), HRP-linked anti-mouse secondary antibody(Cell Signaling Technologies, 7076S, 1:5,000 dilution).
For immunofluorescence experiments, the following antibodies were used: Collagen I (Abcam, Ab34710, 1:500 dilution), DAPI (Sigma Altrich, D9542, 6 µM). For immunohistochemistry stainings, the following antibodies were used; hypusine (EMD Millipore, ABS1064, 1:50 dilution for mouse tissues, 1:75 dilution for human tissues), phosphorylated SMAD3 (S423+S425) (Abcam, EP823Y, 1:100 dilution), DOHH (Sigma-Aldrich, HPA041953, 1:300), PanCK (Dako, M3515 1:200 dilution), EpCAM (Abcam, Ab71916, 1:1,000 dilution), Collagen VI (Abcam, Ab182744, 1:1,000 dilution), Collagen I (Cell Signaling Technologies, E8F4L XP® 1:300), ATP1A1 (Proteintech, 14418-1-ap 1:200 dilution), Wheat Germ Agglutinin, HRP Coniugate (Biotium, Inc, 29073, 1µg/mL).
For flow cytometry experiments, the following antibodies were used: CD16/CD32 (BD Bioscience, 553142, 1:25 dilution), CD45 (BD Bioscience, 550994, 1:200 dilution), PDPN (BioLegend, 127409, 1:200 dilution), CD90.1 (BioLegend, 202505, 1:400 dilution), Viability efluor780 (ThermoFisher, 65-0865-14, 1:800 dilution), CD44 (BioLegend, 103011, 1:500 dilution), Viability efluor450 (ThermoFisher,

65-0863-14, 1:500 dilution).

Validation

For western blot, immunofluorescence and flow cytometry, antibodies were used as recommended in the respective data sheets and validated for immunocytofluorescence and western blot analysis and react with human and murine samples, as stated in the manufacturer's website. Additional validation was performed by using knockdown cell lines and/or pharmacologic inhibitors when possible. Specifically, Dhps, Grin2d and Grin2b, hypusine and eIF5A antibodies were validated in Extended Data Figure 7m, Extended Data Figure 7n, Extended Data Figure 2q and Extended Data Figure 2g. ATF4, phosphorylated eIF2α, phosphorylated CREB, phosphorylated SMAD3 and puromycin were validated respectively in Extended Data Figure 1g, Extended Data Figure 3p, Extended Data Figure 4d and Extended Data Figure 2e.

Eukaryotic cell lines

Policy information about cell lines and Sex and Gender in Research

Cell line source(s)	Human HEK293T epithelial cells, human MCF10A, breast epithelial cells, murine 4T1 mammary gland cancer cells and human HUH7 hepatocellular carcinoma cells were purchased from ATCC. Murine EMT6.5 mammary gland cancer cell line is a single-cell clone from the EMT6 cell line available from ATCC and kindly provided by Professor Robin L. Anderson (Peter MacCallum Cancer Centre). Murine 4T07 cells were generated by Dr. F.R. Miller (https://doi.org/10.1038/bjc.1987.242) and kindly provided by Prof. A. P. Gomes (H Lee Moffitt Cancer Center). Murine B16F10 melanoma cells available from ATCC were kindly provided by Prof. Ilaria Elia (KU Leuven).
Authentication	None of the cell lines used were authenticated
Mycoplasma contamination	All cell lines were confirmed to be mycoplasma-free by routine screening with the MycoAlert Mycoplasma Detection Kit (Lonza) and the MycoStrip Mycoplasma Detection Kit (InvivoGen).
Commonly misidentified lines (See ICLAC register)	No commonly misidentified cell lines were used.

Animals and other research organisms

Policy information about studies involving animals; ARRIVE guidelines recommended for reporting animal research, and Sex and Gender in Research

Laboratory animals	6-8-week old female Balb/c mice were used for cancer cell or treatment injections. All mice were housed under a regimen of 12 h light/12 h dark cycles and under conventional conditions.
Wild animals	No wild animals were used
Reporting on sex	Findings apply to female sex, as results apply to female breast cancer.
Field-collected samples	No field-collected samples were used.
Ethics oversight	For experiments involving orthotopic and experimental metastatic mouse models, housing and experimental animal procedures were approved by the Institutional Animal Care and Research Advisory Committee of KU Leuven, Belgium, under the ECD number ECD P025/2020. All animal studies comply with ethical regulations. For all experiments, the maximum permitted tumor volume was 1.8 cm3 and this limit was not exceeded in any experiment. Humane endpoints were determined using a scoring sheet to determine the condition of the mouse as follows: tumor size of 1.8 cm3, loss of ability to ambulate, labored respiration, surgical infection, or weight loss over 10% of initial body weight. Mice were monitored and upon detection of one of the previously mentioned symptoms, the animal was euthanized.

Note that full information on the approval of the study protocol must also be provided in the manuscript.

Plants

Seed stocks	*Report on the source of all seed stocks or other plant material used. If applicable, state the seed stock centre and catalogue number. If plant specimens were collected from the field, describe the collection location, date and sampling procedures.*
Novel plant genotypes	*Describe the methods by which all novel plant genotypes were produced. This includes those generated by transgenic approaches, gene editing, chemical/radiation-based mutagenesis and hybridization. For transgenic lines, describe the transformation method, the number of independent lines analyzed and the generation upon which experiments were performed. For gene-edited lines, describe the editor used, the endogenous sequence targeted for editing, the targeting guide RNA sequence (if applicable) and how the editor was applied.*
Authentication	*Describe any authentication procedures for each seed stock used or novel genotype generated. Describe any experiments used to assess the effect of a mutation and, where applicable, how potential secondary effects (e.g. second site T-DNA insertions, mosiacism, off-target gene editing) were examined.*

Flow Cytometry

Plots

Confirm that:

☒ The axis labels state the marker and fluorochrome used (e.g. CD4-FITC).

☒ The axis scales are clearly visible. Include numbers along axes only for bottom left plot of group (a 'group' is an analysis of identical markers).

☒ All plots are contour plots with outliers or pseudocolor plots.

☒ A numerical value for number of cells or percentage (with statistics) is provided.

Methodology

Sample preparation	Lungs and livers were extracted and the tissue was washed in blood bank saline, dry and minced for >2min using blades. Tissues were incubated with Liberase (Roche) (0.3 mg/mL) and DNAse1 (1 µg/mL) during 45 min at 37°C with occasional vortex. The reaction was quenched with 3% FBS:PBS + 2mM EDTA and filtered through a 70 µm cell strainer. Cell pellet was washed, incubated with Red Blood Lysis buffer (Merck) and transferred through a 40 µm cell strainer. Single-cells suspension was counted and 20x106 cells/mL were stained for flow cytometry analysis.
Instrument	BD FACS Canto II, BD FACS Diva Fortessa, BD FACS Diva Symphony
Software	BD FACSDiva and FlowJo
Cell population abundance	For lung or liver metastasis analysis: All cells (>80%). All cells/Single Cells (>97%). All cells/Single Cells /Alive (>85%). All cells/Single Cells/Alive/CD45- (40-75%). For cell surface marker expression analysis: All cells (>94%). All cells/Single Cells (>97%). All cells/Single Cells /Alive (>25%).
Gating strategy	For CD90.1 labeled cancer cells from single cell lung suspensions, gating on positive for viability marker for live cells, CD45 negative, Podoplanin negative (4T1 model) or Podoplanin positive (EMT6.5 model) and CD90.1 positive. Details on gating strategy is provided on Supplementary Figure 2. For CD44 stained colonies, gating on positive for viability marker for live cells and CD44 positive.

☒ Tick this box to confirm that a figure exemplifying the gating strategy is provided in the Supplementary Information.